DESIGN, MANUFACTURE AND PERFORMANCE EVALUATION OF WASTE HEAT RECOVERY UNIT IN A GASIFICATION PLANT

University of Fort Hare
Together in Excellence

A Thesis submitted in fulfillment of the requirements for the degree of

DOCTOR OF PHILOSOPHY

IN PHYSICS

By

NWABUNWANNE LILIAN NWOKOLO

In the Faculty of Science and Agriculture at the University of Fort Hare

Supervisor: Prof Sampson Mamphweli

Co-Supervisor: Prof Golden Makaka

December: 2016

DECLARATION

I certify that I am the sole author of this PhD thesis and that it has not been submitted in part or whole for a degree in any other university or institution.

The work was done under the supervision of Prof Sampson Mamphweli at the Institute of technology University of Fort Hare.

Signature of student : _____

Name of Student : _____

Date : _____

DEDICATION

All my praise belongs to you God for successful completion of my PhD study. I dedicate this thesis to my family for their love, affection and dedicated support I received in my PhD adventure

ACKNOWLEDGEMENT

Lord I sincerely acknowledge and thank you for the immense wisdom and good health you gave me throughout my PhD study. I sincerely thank my supervisor Prof Sampson Mamphweli who played not only the role of a supervisor but also a fatherly role. I acknowledge your professional guidance, input and support in the completion of this study. There were pleasurable moments and un-pleasurable moment but they all added up to give this thesis its beauty. I'm glad you are my supervisor. I have learned both academic and life lessons working with you. I acknowledge the guidance of my Co-supervisor in better structuring of the mathematical models of the study.

My family was a great pillar of support I had, I specially thank Dad, Mum, Dr Chinyere, Obinna, Ugochukwu, Chisom, Obuneme and Echezona. Obuneme and Echee thanks very much for the days you accompanied me for data collection and gave up your time. It remains significant to me till tomorrow. I love you all. I sincerely thank my mentor and friend Dr Nnadigadi Chigor who was the first to take the bull by the horn and beckoned on me to come along. To my friend Chika Oyeagu, I specially thank you for your constant care, calls and follow-up on my work progress truly that kept me on the go.

To my prayer partners Dr Evelyn Fatokun, Godwin Nebo and Dr Ikechi Agugba you people rock because as our prayers were going up, it was coming down with divine wisdom and all goodies from God. To my colleague Kechrist Obileke I sincerely thank you, despite your own research

work; you dedicated your time for mine. To the rest of my colleague Anukam Anthony, Avewi Melapi and the rest I thank you all. My sincere thanks go to all the staff of Fort Hare Institute of Technology and particularly to the administrator.

Lastly I acknowledge and thank the Energy and Water Sector Education and Training Authority (EWSETA) for financing my study.

SUMMARY

Johansson biomass gasification system is a standalone power generation system as it utilizes the syngas produced from the downdraft gasifier in an internal combustion gas engine for power generation. The syngas exiting the gasifier and entering the cyclone dissipates heat on the body of the cyclone due to the high temperature at which it exit. In addition this same syngas undergoes some cooling process at the gas scrubber before reaching the gas engine. As the gas engine drives the synchronous generator for power generation, some of the un-combusted gases exit through the exhaust pipe at high temperatures. All these add-up as waste heat within the gasification system, hence there is a significant opportunity for waste heat recovery in Johansson biomass gasification system.

Syngas cleanup prior to its utilization in downstream application is a necessity due to the presence of contaminants such as carbon particles. The cleanup of syngas depends on the composition of syngas, further application requirement and economic consideration. Hence the choice and the design of a syngas cleaning process should be influenced by economic and energetic cost. Cold gas cleanup which is usually carried out at low temperature is considered as a conventional approach in syngas cleanup due to proven reliability and efficient removal of contaminants. However, cold gas cleanup result in significant loss of heat in the form of waste heat.

Therefore the aim of this study is to design and construct a waste heat recovery unit (WHRU) so as to harness the heat dissipated on the body of the cyclone for water heating. But prior to the actual construction of the waste heat recovery unit, a feasibility study was conducted so as to ascertain the quality as well as the quantity of heat to be recovered. The feasibility study involved experimental measurements of syngas temperature and cyclone surface temperature during gasification of pinewood in Johansson biomass downdraft gasifier. The syngas temperature was observed to be within a temperature range of 450 ºC-500 ºC while the two surface temperatures for the cylindrical and conical section of the cyclone ranged from about 150 ºC-220 ºC. From these measured temperatures the potential recoverable waste heat potential was determined. In addition the WHRU was modeled and simulated using computational fluid dynamic software. The modelled waste heat recovery unit (WHRU) employs an indirect contact heat transfer process, as there is a dividing wall between the syngas (heat source) and the water (heat sink). Hence heat is transferred from the syngas to the water through the dividing wall (cyclone surface) in a transient manner. The choice of an indirect contact waste heat recovery unit was due to the presence of carbon particles as contaminants in the syngas.

The WHRU was then constructed using hot rolled (HR) sheet commercial quality of dimensions 3 x 2,500 x 1,225 mm and angle equal commercial quality of dimension 30 x 30 x 2.5 mm. The experimental performance of the WHRU was conducted at difference conditions and discussed. Result showed that the temperature of water in the WHRU could be raised from 20 °C to 78 °C without water withdrawal. Furthermore a maximum of 65 °C was recorded for water withdrawal at a rate of 4 litre/min or 0.07 kg/sec. More also the standing loss realized at this maximum temperature was approximately 2.11 kW/h. A maximum temperature of about 130 °C was

recorded at the engine exhaust pipe which represents a significant opportunity for heat recovery with a thermoelectric generator.

Table of Contents

LIST OF FIGURES

LIST OF TABLES

CHAPTER ONE

BACKGROUND OF STUDY

1.1 INTRODUCTION

The projected rise (715 EJ) in global energy demand by 2030 will increase the importance of syngas for process heat, electric power generation, chemicals and liquid fuel production. The use of syngas dates back to 1812 when it was first used by London gas, light and coke company. Syngas is a technical term for a mixture of gases that result from gasification of carbonaceous feedstock [Woolcock, 2013]. Some of the gases are combustible in nature which is attributed to the partial combustion of the carbon and the hydrogen present in carbonaceous feedstock (biomass materials). The partial combustion of carbonaceous feedstock is due to the use of sub-stoichiometric amount of oxidizing agent unlike in complete combustion where full amount is utilized. The combustible components of syngas include carbon monoxide (CO), methane (CH_4) and hydrogen (H_2). However, some other components of syngas still exist such as carbon dioxide (CO_2), nitrogen (N_2), hydrocarbons such as ethylene (C_2H_4) and ethane (C_2H_6) [Martinez *et al*, 2012].

Gasification is a thermochemical process in which carbonaceous feedstock is heated in sub-stoichiometric amount of oxidizing agent to produce syngas. The oxidizing agent could be air, steam, oxygen, carbon dioxide or a mixture of two or more of it. The choice of any is determined by the desired quality of the syngas to be produced and efficiency of the process [Mondal *et al*, 2011]. Studies show that the use of oxygen and steam or their mixture result in

syngas with medium to high heating values of 12-18 MJ/Nm^3 while, the use of air leads to low heating values of 4-7 MJ/Nm^3 [Herguido, *et al*, 1992, Narvaez *et al*, 1996, Javier *et al*, 1999, Laurence and Ashenafi, 2012, Couto *et al*, 2013]. In terms of operating cost, the use of air is more economical compared to using steam or oxygen. In addition, the ratio of oxidizing agent to feedstock (air/feedstock ratio) is an important parameter of interest during gasification as it influences the amount of carbon particles that are produced alongside with syngas.

A variety of gasifiers have been used for gasification of biomass in order to generate syngas. They are primarily classified into three main categories; fixed bed, fluidized bed and entrained flow gasifier. Fixed bed is mostly used for small scale gasification and is further divided into downdraft, updraft and cross draft. Downdraft gasifier offers the advantage of high conversion efficiency along with low generation of particulates and tolerable tar concentration. They are known to give the least amount of tar among other gasifier types. Low concentration of tar in syngas produced from downdraft gasifier is due to the passing of syngas through a high temperature combustion zone which aids in tar cracking. This is in agreement with a tar concentration of 10-100g/m^3 obtained during biomass gasification in a downdraft gasifier [Bhattacharya *et al*, 2001]. Downdraft gasifier produces syngas that are very suitable for internal combustion (IC) engine due to some additional advantages such as high char conversion and low ash carry over. Downdraft gasifier is considered to be a mature technology nevertheless; it still has some disadvantages such as ash fusion and the need for feedstock (biomass materials) with low moisture content [Martinez *et al*, 2012].

Gasifiers usually operate at high temperatures which allows for thermal degradation of feedstock and series of chemical reactions to take place. For entrained flow gasifier, the operating temperature range from 1200 °C - 1600 °C while that of fluidized bed is 1000 °C - 1200 °C. This explains why they are both preferred for industrial/large scale applications [Damartzis and Zabaniotou, 2011]. Entrained flows are more suitable for coal gasification rather than biomass gasification due to the stringent uniform particle size requirement and high operating temperature. Fluidized bed is characterized by uniform temperature distribution and is suitable for feedstocks with low ash fusion temperature. Fixed bed operating temperature varies within the range of 800 °C– 1000 °C. These operating temperatures effectively influence the temperature of the syngas at the outlet of the gasifier.

The temperature of syngas leaving a gasifier system can range from as low as 200 °C to as high as 1500 °C, depending on the type of gasifier used, air/feedstock ratio, and feedstock properties (such as moisture content). For instance, in Ma *et al* [2015] study in which the use of waste heat from a downdraft gasifier was examined, the temperature of the syngas at the gasifier outlet was about 623 °C - 773 °C. In a dual fluidized bed, a syngas temperature of 850 °C was recorded before the syngas was sent to heat recovery and steam generation (HRSG) unit to recover the sensible heat [Chen *et al,* 2016]. A report on the analysis of two installations of coal gasification using pressurized entrained flow gasifier and pressurized fluidized bed gasifier showed the temperature of syngas leaving the gasifiers to be 1460.9 °C and 900 °C respectively [Zie˛bik *et al*, 2015]. Hence, in order to attain high process efficiency during gasification, it becomes essential to recover heat from high temperature syngas leaving gasifier.

It is also important to highlight that carbon particles also referred to as particulate matter usually emanate with syngas during biomass gasification. The presence of these carbon particles in syngas and other contaminates such as tar are what necessitates the cleaning of syngas prior to their utilization. Although the presence of carbon particles in the syngas does not affect the quality and quantity of heat contained in the product gas, it does influence the heat recovery process and materials used in the recovery. Hence there is need for characterization of these carbon particles to ascertain their chemical compositions, thermal properties and morphological features.

1.2 PROBLEM STATEMENT

Johansson biomass gasification system is a standalone power generation system because it utilizes the syngas produced from the downdraft gasifier in an internal combustion gas engine for power generation. The syngas exiting the gasifier and entering the cyclone dissipates heat on the body of the cyclone due to the high temperature at which the syngas exit. In addition this same syngas undergoes some cooling process at the gas scrubber before reaching the gas engine. As the gas engine drives the synchronous generator for power generation, some of the un-combusted gases exit through the exhaust pipe at high temperatures. All these add-up as waste heat within the gasification system, hence there is a significant opportunity for waste heat recovery in Johansson biomass gasification system. The present study was motivated to breach the gap found with regards to recovery of waste heat from the cyclone section of gasification system so as to enhance the thermal efficiency of the system. The presence of carbon particles in the syngas does influence the heat recovery process as well as the material of recovery hence

characterization of these carbon particles is of necessity. The presence of alkali and alkaline earth metals in the carbon particles could lead to formation of deposits on heat recovery equipment surface when used in direct contact heat transfer mechanism. This could result in heat inhibition due to additional layers the deposits would create. In addition to these alkali and alkaline earth metals, chlorine is also identified as an important fouling facilitator on heat transfer surfaces.

1.3 RESEARCH AIMS AND OBJECTIVES

The main aim of this study is to harness the waste heat energy through the integration of waste heat recovery unit (WHRU) around the cyclone dust collector attached to the biomass downdraft gasifier system.

OBJECTIVES

1. To determine how much heat energy that could be possibly recovered from the surface of the cyclone dust collector.
2. To evaluate the characteristic features of carbon particles recovered from the syngas stream during gas cleaning at the cyclone dust collector.
3. To conduct a computer simulation for the gasification of pine wood in a downdraft gasifier system.
4. To simulate the performance of the waste heat recovery unit using computational fluid dynamics.
5. To design and construct a waste heat recovery unit that will be integrated around the cyclone dust collector of the gasifier system.

6. To monitor the performance of the constructed heat recovery unit.

1.4 RESEARCH QUESTION

The following questions were answered by this study

1. What is the possible quantity of heat energy that can be recovered from the surface of the cyclone dust collector?
2. What are the characteristic features of the carbon particles that are recovered at the cyclone dust collector?
3. How do you predict the composition of syngas from gasification of pine wood in a downdraft gasifier system?
4. What information can be drawn from computational fluid dynamic simulation of the envisaged waste heat recovery unit?
5. What choice of design and construction method is appropriate for the waste heat recovery unit?
6. How does the waste heat recovery unit perform at steady state and varying mass flow rate?

1.5 RESEARCH METHODOLOGY

In order to achieve the aim and objectives of this study, the methodology employed is divided into five stages as represented in the flow diagram: Figure 1.1

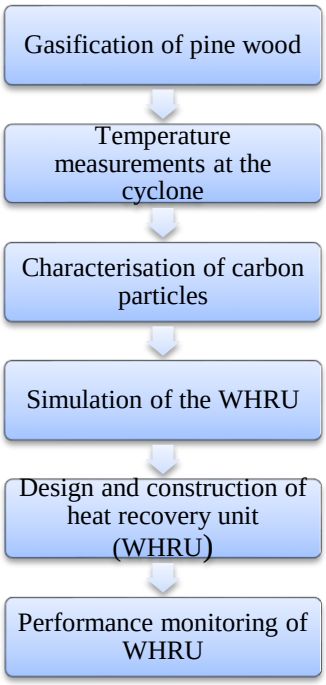

Figure 2.1: Methodology Stages

Pine wood off cuts were sourced from a nearby sawmill and were gasified in an air blow downdraft gasifier. During the gasification process, the temperature of the syngas and surface temperature of the cyclone were measured. This is to ascertain their degree of hotness which aided in estimating the quantity of heat that could be recovered. Secondly, the carbon particles were collected at the cyclone collection chamber after system shut down for the purpose of characterization. Thirdly a computational fluid dynamic simulation of the WHRU was done before the actual construction. The actual construction of the waste heat recovery unit was

carried out using mild steel sheet and this was followed by its integration around the cyclone section of the downdraft gasifier system. Lastly the performance of the WHRU was monitored while operating the biomass downdraft gasifier.

1.6 DELINEATION AND LIMITATION

The present study encompassed an investigation into the feasibility of recovering heat energy at a biomass gasification system and the actual recovery of some portion of the heat energy contained in the syngas using a custom built waste heat recovery unit. The actual gasification of pine wood was conducted in Johansson biomass downdraft gasifier located at Melani village in Eastern Cape Province of South Africa. But the further utilization of the syngas in a gas engine for power generation was not considered as this was outside the scope of the study. In addition the electrical performance of the 150 KVA generator attached to the gasification system was not considered as this is outside the scope of the present study.

1.7 ASSUMPTIONS

Gasification is a high temperature process for conversion of biomass into a gaseous product known as syngas. Hence the generated syngas is assumed to exit at high temperature making syngas a high energy carrier. The quality and quantity of heat energy that could be recovered from hot syngas is believed to depend on temperature. Heat quality is a measure of the heat

energy usefulness and heat quantity is a measure of how much energy is contained in the syngas. The feasibility of recovering heat form hot syngas is as well dependent on temperature. It is also assumed that for heat recovery to be possible heat source temperature must be greater than the heat sink temperature. The greater the difference between heat source temperature and heat sink temperature, the more quantity of heat energy that can be recovered.

1.8 SIGNIFICANCE/RATIONAL

This study first investigated the possibility of recovering heat from the surface of a cyclone dust collector attached to a downdraft gasifier system. From the temperature profiles obtained for the syngas and cyclone surface it was evident that there were potentials for heat recovery. The waste heat recovery unit integrated around the cyclone showed that hot water can be released through indirect heat transfer from the syngas. More also the study has shown that cyclone dust collector can serve dual purpose namely syngas purification and heat transfer medium hence enhancing its usage. In addition the study have successfully proved that the existing Johansson biomass gasifier system which current generates power using an internal combustion engine powered by syngas can also meet some heat application need such as water heating as proven and biomass drying as suggested. This approach will effectively improve the overall efficiency of the biomass gasification system.

1.9 DEFINITION OF TERMS

Biomass – is a term used in describing organic material or matter derived from plants, vegetables and animals [Coronado *et al*, 2011].

Biomass Gasification - is a thermochemical process of converting solid biomass fuel to high calorific gas product [Santhanam *et al*, 2016].

Syngas - is a term given to the mixture of gases produced from partial combustion of biomass in gasifiers or reactors [Pandey *et al*, 2013].

Cyclone – is a piece of equipment that makes use of centrifugal and gravitational field to separate particles on gaseous stream [Sevvel *et al*, 2015].

Waste heat recovery unit - is a piece of equipment that is capable of transferring heat from the surface of the cyclone to the water contained in it.

CHAPTER TWO

REVIEW OF LITERATURE

2.1 INTRODUCTION

Gasification is a thermochemical process through which biomass materials are converted to gaseous product called syngas. The generated syngas can be used in gas engines, turbines and fuel cell for power generation. More also syngas are used for heat generation, combined heat and power production and chemical production. The wide spread availability of biomass material and its renewable nature makes it suitable for gasification purposes. In addition, the low content of nitrogen and sulfur in biomass material results in reduced nitrogen oxides (NO_x) and sulfur dioxide (SO_2) emission during gasification [Kuo and Wu, 2015]. Syngas when produced is first cooled or cleaned prior to its utilization in gas engines so as to remove particles and tar. The cooling process results in heat dissipation in the form of waste heat.

The term waste heat is described as unused thermal energy which is generated as a product or by-product of a process [US DOE, 2008]. Waste heat is mostly unavoidable in industrial applications that require transformation of materials into a more useful product or conversion of energy from one form to another. Biomass gasification is not an exception as it involves transformation of energy stored in wood to gaseous form. Some waste heat sources include, hot gasification gas cooled during gas cleaning, hot combustion or flue gas dumped to the environment, hot equipment surfaces and heated products from industrial processes. Recovery of waste heat offers both direct and indirect benefits, the direct benefit include reduction in

consumption of primary fuel and process cost. The indirect advantages include minimization in pollution, minimization in equipment size, and minimization in energy consumption [Jadhao and Thombare, 2013]. Two major factors influence the choice of a heat recovery mechanism namely: temperature of the waste heat and economic value. Temperature determines the usefulness (quality) of the waste heat stream and the feasibility of the recovery. Waste heat is recoverable at low temperatures such as chilled cooling water as well as at high temperatures such as hot syngas. The high operating temperature of gasifiers where gasification takes place is what leads to generation of hot syngas.

2.2 PRINCIPLES OF BIOMASS GASIFICATION

Biomass is a term used in referring to plant derived matter, animal waste, agricultural waste and industrial waste which can be utilized for energy production. Some biomasses suitable for energy production include wood, rice husk, rice straw, sugarcane bagasse, corn cob, corn stalk, bean straw and municipal solid waste. Typically the energy density (calorific value) of most biomass is around 18 MJ/kg on dry basis which is equivalent to half the energy density of coal. However this energy density is still sufficient for conversion into a more versatile form. Hence biomass is considered a good feedstock for gasification purposes since they can be converted into a more marketable fuel or product through gasification [Puig-Arnavat *et al*, 2010]. Gasification is an efficient conversion process with a wide variety of application. Gasification has a long history that dates back to 19^{th} and 20^{th} century when it was applied in town gas. This was followed by revival of small-scale gasification due to shortage of liquid fuel during World

War II. Gasification gained more interest recently due to oil crises that occurred in 1970. Since then significant research, development and demonstration has being ongoing [Kirkels and Verbong, 2011].

2.2.1 Gasification Process

Gasification product results from a complex chemical mechanism involving a phase transition from solid to gas. The chemical equation summing up reactants and products that result from gasification of biomass in limited supply of air is given as follows [Arafat and Jijakli, 2013].

$$C_nH_xO_yN_z + m\left(O_2 + 3.76N_2\right) \rightarrow x_1H_2 + x_2CO + x_3CO_2 + x_4H_2O + x_5CH_4 + x_6C + \left(z/2 + 3.76m\right)N_2 \quad (2.1)$$

Where n, x, y and z are the atomic ratio of carbon, hydrogen, oxygen and nitrogen, m, x_1, x_2, x_3, x_4, x_5 and x_6 are the stoichiometric quantity of air, hydrogen, carbon monoxide, carbon dioxide, water vapour, methane, free carbon and nitrogen. Free carbon represents the unconverted fraction of carbon at the end of the gasification process. Nitrogen is very much abundant in the air and exceeds the concentration of oxygen in air [Arafat and Jijakli, 2013].

Gasification occurs at high temperature in a gasifier also known as the reactor and in the presence of limited supply of oxidizing agents. This oxidizing agent could be air, pure oxygen, steam, carbon monoxide or a combination of two or more. The chemistry of gasification is quite

complex but four basic stages are identified to be involved. These four stages are drying, pyrolysis, oxidation and reduction [Couto *et al*, 2013].

Drying – during the drying process the biomass material does not undergo any thermal degradation due to the prevailing low temperature at this stage. Basically the moisture content of the feedstock is driven off in the form of steam at a temperature about 100 °C - 200°C as represented in the accompanying equation (2.2). As this steam emanates it flows downwards along side with the gas stream and some of them end up as hydrogen in water-gas reaction [Chawdhury and Mahkamov, 2011]. The moisture content of biomass material typically ranges from 5%-35% [Puig-Arnauat *et al*, 2010].

$$Wet\ feedstock\ +\ Heat\ \rightarrow Dry\ feedstock\ +\ H_2O \qquad (2.2)$$

Drying the biomass prior to entering the gasifier is of necessity for biomass of high moisture content. Preferably, moisture content within the range of 10%-15% is accepted for downdraft gasification but higher percentage is equally acceptable in updraft gasifier [Basu and Ruiz, 2013].

Pyrolysis – this process is also referred to as devolatilization because it involves the releases of volatiles as a result of the breaking down of complex compounds that resides within the feedstock (for example wood). Pyrolysis process results in about 70% weight loss of biomass [Bhavanam and Sastry, 2011] and is represented as shown in equation (2.3):

$$Wood + Heat \rightarrow Char\ (C) + Volatiles\ (CO,\ CO_2,\ H_2,\ H_2O,\ CH_4) + Tar\ Vapour \quad (2.3)$$

Equation 2.3 shows that pyrolysis degrades biomass into solid, gaseous and liquid fractions. The release of volatile starts at a temperature of 250°C and about 80% to 95% of the original mass of the material is converted into liquid and gases while 5% to 20% is converted to char [Jayah, 2002]. Pyrolysis in itself is a standalone thermochemical process that is divided into three sub-classes: slow pyrolysis, fast pyrolysis and flash pyrolysis [Shafie *et al*, 2012].

Oxidation – at this stage the char descending from the pyrolysis zone gets oxidized. The oxidation of char causes a rapid rise in temperature between 800°C-1100°C hence char oxidation is considered an exothermic reaction process. The heat generated at this stage is utilized in the other processes [Jayah, 2002]. The dominating reaction at this zone is shown in equations (2.4) and (2.5) [Chawdhury and Mahkamov, 2011].

$$C + O_2 \rightarrow CO_2 \quad (\text{-}394\ kJ / kg\ mol) \quad (2.4)$$

$$2H_2 + O_2 \rightarrow 2H_2O \quad (\text{-}242\ kJ / kg\ mol) \quad (2.5)$$

Reduction – the reduction zone lies at the bottom of the gasifier and the reaction that occurs at this stage are considered to be endothermic since they cause a reduction in temperature from about 1100°C to 700°C. The reaction that occurs at this stage is between the surrounding gases (that is carbon dioxide and water vapor) and hot bed of char particles at the surface. This

involves absorption of gases and some surface reaction which is then followed by desorption of the product gases as shown in equations (2.6) and (2.7) [Jayah, 2002].

$$C + CO_2 \leftrightarrow 2CO \quad (+172.5\ kJ/mol) \tag{2.6}$$

$$C + H_2O \leftrightarrow CO + H_2 \quad (+131.3\ kJ/mol) \tag{2.7}$$

2.2.2 Gasification technologies

Gasification technologies are classified according to various criteria which include reactor type, oxidizing agent (air, oxygen, steam or carbon dioxide), energy supply (allothermal or auto thermal) and working pressure (atmospheric or pressurized) [Tremel *et al*, 2013]. Different reactor types with variation in the direction of flow of biomass and oxidizing agents have been developed. According to reactor type, gasification technologies are basically classified into three with sub-divisions within each category. Table 2.1 shows the classifications of these reactors/gasifiers and the direction of flow of biomass and oxidizing agent [Couto *et al*, 2013].

Table 2.1: Reactor Classifications [Couto *et al*, 2013]

Types	Subdivision	Fuel flow	Oxidant flow
Fixed bed	• Downdraft	• Descending	• Descending
	• Updraft	• Descending	• Ascending
	• Cross draft	• Descending	• Descending
Fluidized bed	• Bubbling	• Descending	• Ascending
	• Circulating	• Descending	• Ascending
Entrained flow	• Coaxial	• Descending	• Descending
	• Opposed Jet	• Descending	• Descending

Fixed bed gasifiers are more suitable for small to medium power generations that are below 1MW power. They are the traditional gasifers used for gasification processes. From Table 2.1, fixed bed gasifiers are classified into downdraft, updraft and cross-draft. The updraft gasifier has a clearly defined zone for the four processes of gasification explained earlier. It achieves high thermal efficiency and it also accepts feedstock with high moisture content of up to 50%. The major drawback in the use of updraft gasifier is due to high production of tar in the syngas and poor loading capacity [Mamphweli and Meyer, 2012]. The schematic diagrams of these gasifiers are also shown in figures 2.1 and 2.2.

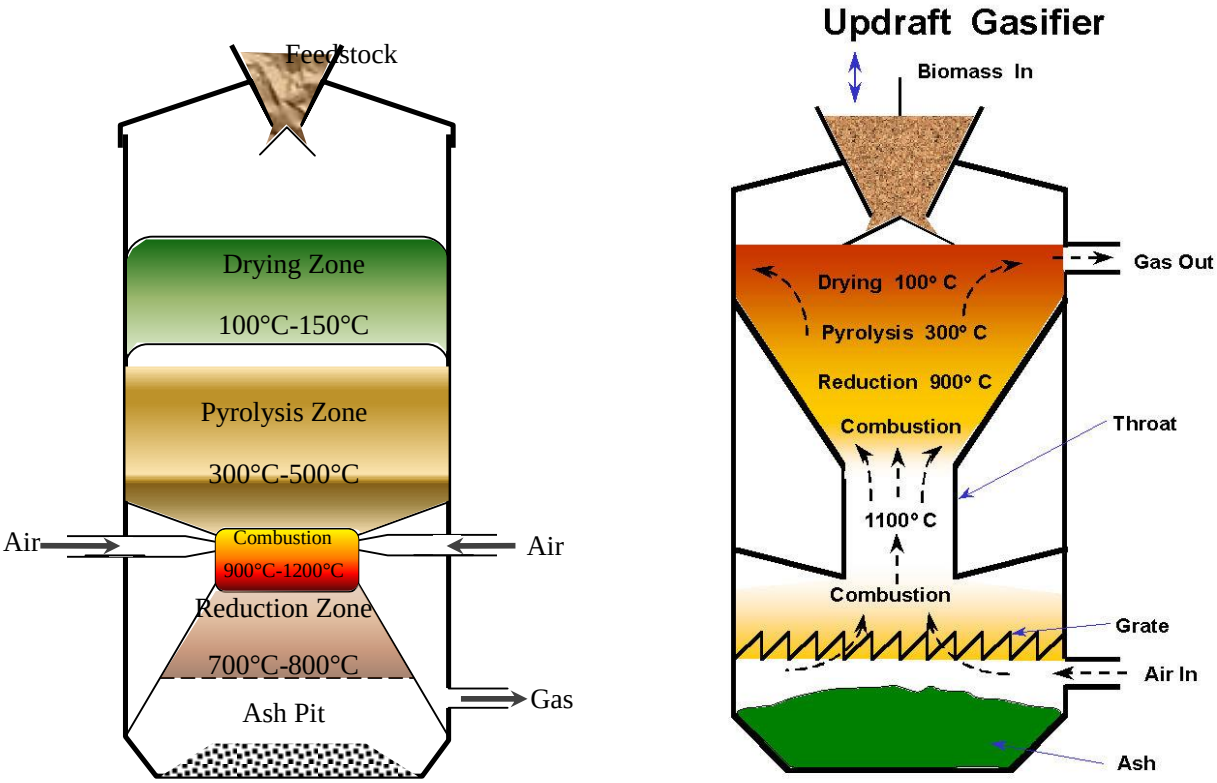

Figure 2.1: Fixed bed gasifier types (left) downdraft gasifier, (right) updraft gasifier

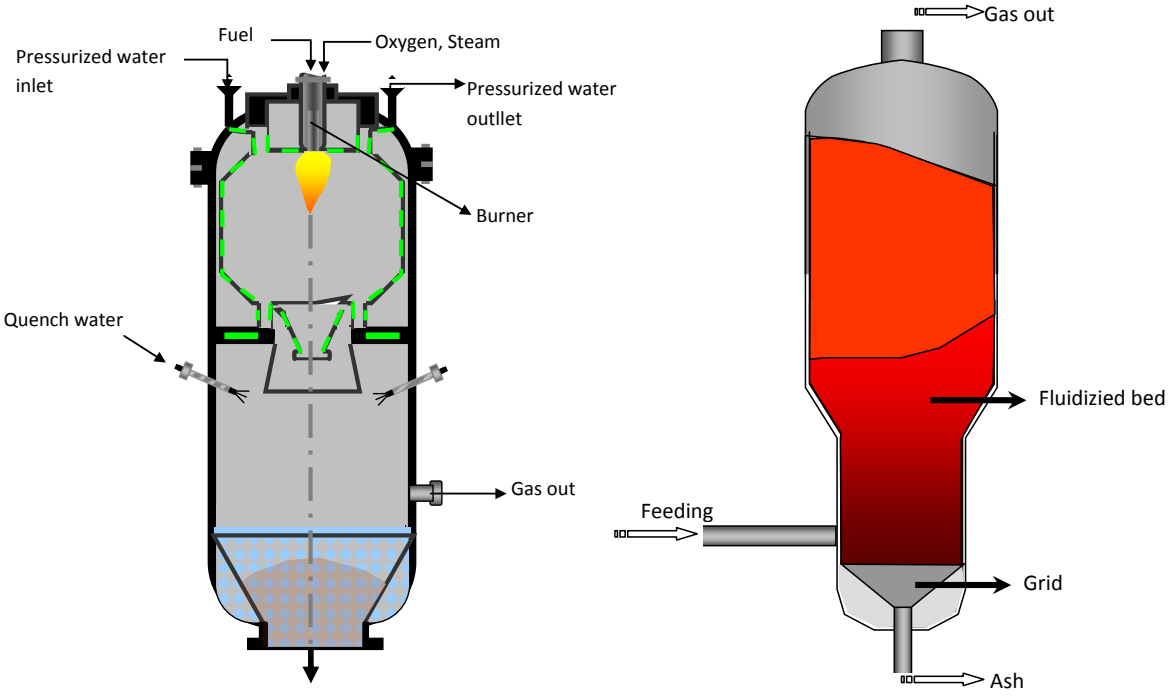

Figure 2.2: Entrained flow (left) and Fluidized bed (right)

The downdraft gasifier is known for its simplicity and suitability for engine application, which is attributed to low concentration of tar in the syngas produced. Some other advantages include higher fuel conversion rate, less environmental objection and flexible adaptation of gas production to load. However the downdraft gasifier also possess some limitations which lie mostly in its inability to operate on a number of unprocessed fuels, particularly fuel with high moisture content, fluffy and low density fuels [Chawdhury and Mahkamov, 2011].

In the downdraft gasifier the solid fuel and oxidizing agent move cocurrently downwards and the syngas is withdrawn from the bottom. Due to the downward movement of both fuel and oxidants, the products from the pyrolysis zone go through a glowing bed of hot charcoal and get converted to gases. More also tar is consumed in the process and the extent to which it is consumed is dependent on the temperature of the hot zone and the residence time [Couto *et al*, 2013]. The cracking of tars lessens the intensive cleaning of gas as is applicable in updraft gasifier. Investigations show that downdraft gasifier has been used by many authors in gasification of different biomass species with varying objectives.

Zainal *et al* [2002] investigated the effect of equivalence ratio on gas composition, calorific value of gas and gas production rate in a downdraft gasifier using furniture wood and wood chips. The study observed that the calorific value of producer gas increased with increase in equivalence ratio but made a downward turn after attaining its peak at an equivalence ratio of 0.388. In addition complete conversion of carbon to gas did not happen even at optimum equivalence ratio. Dogru *et al* [2004] successfully gasified briquetted leather residue with bulk density of 537.30 kg/m^3 in a 10 kW throated downdraft gasifier. Bridges were occasionally formed at the throated part of the gasifier and temperatures of the different zones were measured

in the study. An exploratory downdraft gasifier was designed with an internal separate combustion section where turbulent, swirling high-temperature combustion flows are generated. From the series of experiment carried out using this gasifier and wood shaving as feedstock, the maximum tar cracking temperature was found to be above 1100 °C. Carbon monoxide and hydrogen volumetric concentration release were 22% and 11% respectively [Patil *et al*, 2011]. A modeling and experimental study were combined to study a downdraft gasifier and gas engine fuel with industrial olive oil waste (olive pits, leaves and branches). The calorific values of 5.1 MJ/Nm^3 obtained for the olive pit producer gas showed that olive pit is potentially viable for combined heat and power. The leaves and branches resulted in a producer gas with a calorific value of 3.7 MJ/Nm^3 showing its unsuitability for gasification [Vera *et al*, 2013]. Prasad *et al*, [2014] gasified pelletized de oiled cake in a downdraft gasifier and obtained a gasification efficiency of 65% lower than 84% recorded for wood gasification. Both theoretical and experimental studies were carried out on a 50 kW_{th} downdraft gasifier with the blends of coconut shell and rubber seed shell. The maximum values for the performance parameters were found at an equivalence ratio of about 0.2-0.3. Coconut shell showed better conversion efficiency when compared with rubber seed shell [Jeya Singh and Sekhar, 2016].

Entrained flow gasifiers are the most widely used which could be attributed to its versatility in terms of fuel type flexibility. Both solid and liquid fuel can be used in entrained flow gasifiers. In entrained flow solid fuels are gasified at high pressures (2.94-3.43 Mpa) and high temperature of up to 1500ºC. The solid fuel reacts with the gasifying agent in a suspended fluid flow mode. Entrained flows usually require crushed/grinded feedstock which can be injected in a dry or slurry state. Entrained flow gasifier requires the use of expensive materials for construction and

high temperature heat exchangers for gas cooling due to high operating temperature [Mondal *et al*, 2011]. Entrained flow is also considered appropriate for production of second generation biofuels [Hernández *et al*, 2012].

Fluidized beds were mostly used for coal gasification and are known for its uniform temperature distribution. The uniform temperature is mostly achieved by introducing air into a bed of fine grained materials. Fluidized bed is divided into circulating and bubbling fluidized bed. In circulating fluidized bed, the bed material is circulated between the reaction vessel and a cyclone separator while in bubbling the moving bed material is above the grate [McKendry, 2002]. Some basic features or characteristics of the three major classifications of gasifiers has been reported and summarized as shown in Table 2.2 [Damartzis and Zabaniotou, 2011, Hernández *et al*, 2010, Bahng *et al*, 2009].

Table 2.2: Summary of characteristics of gasifiers

Gasifier type	**Characteristics**
Fixed bed	Proven for fuel with a relative uniform size
	Simple, reliable and cheap
	Large tar production with exception of downdraft
	Long residence time
Entrained flow	Operates at high temperature (1200°C - 1500°C) and high heating rate
	Requires finely graded fuel for high level of fuel conversion
	Low formation of tar due to high operating temperature
	Available on large scale
	Short but narrowly distributed residence time

Fluidized bed	Uniform temperature distribution
	Potential for slagging of bed material due to biomass ash content
	Not suitable for biomass with high ash content
	High operating temperature (1000ºC -1200ºC)

2.3 DOWNSTREAM PROCESSING OF SYNGAS

Gasification of biomass fuels, ideally result in production of carbon monoxides and hydrogen. However, this gaseous product (syngas) also consists of carbon dioxide, methane, water and small quantities of hydrocarbon which are either condensable or non-condensable. Some impurities such as particulate matter, alkali compound, sulfur compound, nitrogen compound and tar contaminate the syngas that exit the gasifier to a certain degree. The degree of contamination can be dependent on the nature of biomass feedstock, the type of oxidizing agent (oxygen, air and steam), process operating condition and the design of gasifier used. For instance, when steam is used as oxidizing agent the syngas produced contains a smaller quantity of nitrogen (about 3%) as compared to about 41% when air is used [Ahrenfeld, 2007]. Although the use of air is economically viable it also compromises the quality of gas produced.

The presence of impurities such as tar causes fouling of process equipments such as fuel lines or the piping system, filters, heat exchangers, engines and turbines. This happens when tar condenses or polymerizes to more complex structures. Tars are formed at a temperature above 230°C during the pyrolysis stage when other components such as solid char are formed. Tars are defined as hydrocarbons with higher molecular weight than benzene [Maniatisa & Beenackers,

2000]. They have physical properties that are dependent on temperature and heat rate. Tar formation is much higher in counter-current gasifier (as shown in Table 2.3) which is why it is not usually considered for internal combustion (IC) engine application.

Table 2.3: Tar concentration in gasifiers [Laurence and Ashenafi, 2012]

Tar Concentration	Fixed bed		Fluidized bed	
	Co-current	Counter-Current	Circulating	Bubbling
Tar range (mg/Nm^3)	0.01-6	10-150	1-30	1-23
Mean tar (mg/Nm^3)	0.5	50	8	12

The maximum tolerable tar content in the syngas used in IC engine is of the order 100 mg/Nm^3. As observed from Table 2.3, co-current gasifier (downdraft) results in a minimal concentration of tar which is because of the passage of the gas through a hot temperature combustion zone. This will end in tar cracking hence tar removal is not of utmost consideration in downdraft gasifier. However, particulate matter still poses as a challenge in downdraft gasifier. The bulk of particulate matter from gasification of biomass in a downdraft gasifier is constituted by solid carbon particles.

These carbon particles vary in their compositions as well as sizes from less than 1 µm to over 100 µm [Hoffmann and Stein, 2008]. Based on this sizes also referred as particle diameter, carbon particles are divided into fine and coarse particles. Particle diameter (d_p) is a significant parameter used in describing the properties and behavior of particles. However defining the

diameter of particles is difficult in some cases due to irregularities in shapes of some particles. Two descriptions of particle diameter that stands out are Stokes diameter and aerodynamic diameter. Stokes diameter defines the diameter of a particle with similar terminal settling velocity and density while aerodynamic diameter has similar terminal settling velocity and a particle density of 1 g/cm^3 [Hinds, 1999]. The two diameters, aerodynamic and Stokes are related by equation (2.8)

$$d_{ae} = d_s \times \sqrt{\frac{\rho_p(d_s)}{\rho_0(d_{ae})}} \tag{2.8}$$

where d_{ae} is aerodynamic diameter, d_s is stokes diameter, ρ_p is particle density, ρ_0 is standard density (1 g/cm^3) and C_c is Cunningham slip correction factor [Morgalla *et al*, 2015]. The formation of particles during biomass gasification differ from that of combustion and the mechanism of formation for combustion is well known and studied compared to that of gasification. In addition, the particle formation mechanism of fine and coarse-mode particle are said to be different. Fine particles are formed through chemical reactions and homogeneous condensation, nucleation while coarse particles are formed through mechanical processes. Their elemental compositions are also reported to differ. Potassium, sulphur and chlorine are mostly present in fine particle while coarse particles are rich in calcium, aluminum, potassium, silicon, [Joller *et al*, 2005]. This is in agreement with the statement that particles having different origin and generated via different routes usually vary in chemical compositions and physical properties.

Three particle formation route were identified in San Miguel *et al*, [2012] study, firstly particles formed as result of progressive wearing down of carbonaceous biomass particle due to

mechanical interactions inside the gasifier. Secondly, carbon particles are formed through condensation of gaseous organic molecules and are accompanied with coagulation, agglomeration and aggregation of primary particles into larger solid particles. The third formation mechanism is the emanation of inorganic components after complete gasification of carbonaceous fraction. Due to generation of particles along side with syngas during gasification, syngas undergoes some cleaning processes before their subsequent use for energy, heat or chemical applications. The extraction of heat from hot syngas requires the use of heat recovery devices hence, the presence of carbon parricles in the syngas is a concern.

Syngas cleaning forms a crucial step in the downstream processes for an internal combustion (IC) engine integrated biomass gasification systems [Pande and Bhaskarwar, 2012]. However the final application (end use) of the syngas determines the cleaning technique or technology to adopt. More also syngas composition, economic consideration and gas flow rate (depending on gasifier size) are other factors of consideration in the choice of a cleaning technology. Removal of impurities, particularly, particulate matter from biomass gasification product gas usually involves an integrated multi-step approach.

2.4 SYNGAS PURIFICATION

Particulate emission can cause abrasion to downstream equipment or worst still present emission problem. Particulates consist of inorganic ash and unconverted biomass referred to as char. The

current technologies for removing particulates are summarized below [Laurence and Ashenafi, 2012]:

a. Dry gas cleaning or collector

i. Cyclone separator

ii. Barrier filters

iii. Electrostatic precipitator

b. Wet gas cleaning

i. Spray scrubber

ii. Venturi scrubbers

iii. Cyclone spray scrubber

iv. Packedbed scrubber

2.4.1 Dry Gas Cleaning

Dry gas cleaning also referred to as hot gas cleaning involves a gas cleaning process that occurs within a temperature range of 400°C -1300°C. Syngas when cleaned at an elevated temperature offers thermal benefit for many syngas applications. Some other benefits are improved efficiency and improved syngas conversion with fewer byproducts. Dry gas cleaning can be achieved through inertial separation, barrier filtration and electrostatic interaction.

Inertial separation employs mass and acceleration principle in separating solid particles from gaseous stream of which a good example is a cyclone. In barrier filtration, raw gas is made to pass through a porous monolithic solid or around fibers or granules. Some good examples are

rigid filters, fabric filters, fixed and moving bed granular filter. Electrostatic interaction involves the charging of particles by a strong electric field which in turn creates a difference in the dielectric properties of the particles and the gas molecules [Woolcock and Brown, 2013].

2.4.1.1 Cyclonic Separation

Cyclonic separation is a means of removing particulate matter from syngas, air or liquid streams. In addition cyclone can be employed when separating fine droplets of liquid from gaseous streams. Cyclone comprises of an upper cylindrical part referred to as barrel and a lower conical part. To remove particulates from syngas stream exiting a gasifier system, the syngas stream is made to enter in a tangential manner into the cyclone. The tangential entry ends up in a spiral flow of syngas, beginning at the barrel part of the cyclone to the conical part. At the conical section the clean syngas reverses and exits in a straight stream through the center of the cyclone, whereas the particulates collides with the outer wall and fall to the bottom (collection chamber). It is important to mention here that the rotational radius of the syngas stream is reduced at the narrower end (conical section) of the cyclone. The downward movement of particulates is as a result of centrifugal force, inertia and its denser nature [Wang, 2004]. Figure 2.3 shows the schematic flow pattern of syngas stream within a cyclone.

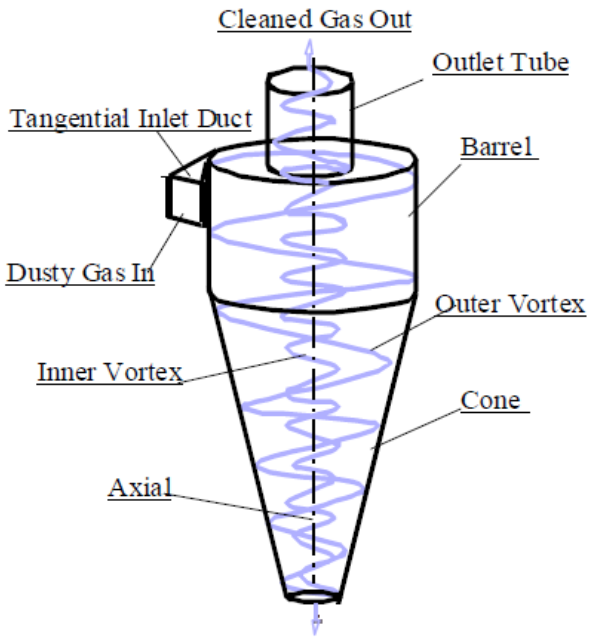

Figure 2.3: Schematic flow diagram of a cyclone [Wang, 2004]

Cyclone is widely used in industries due to its low capital cost, low maintenance requirement and ability to operate at high temperature. Some of the industrial applications are summarized below:

- Power production – separating gas from particulates in a gasifier
- Sawmill – removal of sawdust from extracted air
- Oil refineries – separating oil and gas
- Cement industry – serve as components of kiln Preheaters
- Food industry – recovering freeze-dried coffee
- Petroleum refineries – recovering and recycling certain catalyst

Cyclone in some cases serves as pre-cleaners for more expensive final control devices such as electrostatic precipitators. They are likewise used for pollution control, although they don't meet the strict air pollution regulation. Cyclone comes in three categories: High efficiency, conventional and high throughput. High throughput has the lowest efficiency followed by conventional. Figure 2.4 depicts a typical efficiency curve for the three categories of the cyclone.

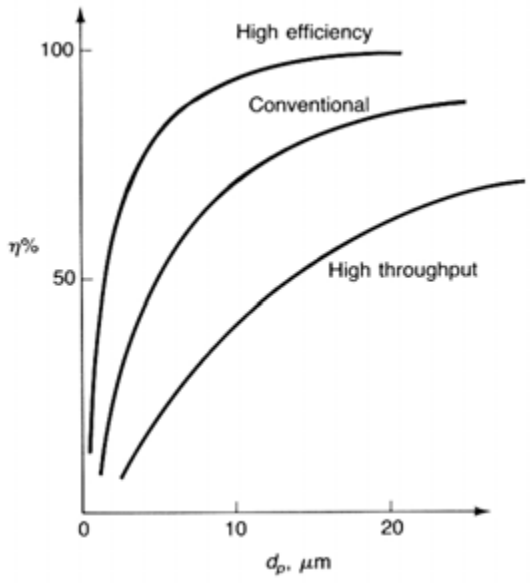

Figure 2.4: Efficiency Curve for the three Categories of Cyclone [Nazaroff and Alvarez-Cohen]

Cyclone efficiency is dependent on particle size and cyclone design as observed from Figure 2.4. Increasing efficiency incurs additional operating cost because higher efficiency requires higher inflow pressure.

Particle Collection Theory

The number of turns or revolutions (N) the gas stream spins in the outer vortex of the cyclone is determined using Lapple model as shown in equation (2.9) [Wang, 2004]:

$$N = \frac{1}{H}\left[L_b + \frac{L_c}{2} \right] \tag{2.9}$$

where N is number of turns inside the device, H is height of inlet duct (m), L_b is length of cyclone body (m), L_c is length of cyclone cone in (m).

The number of turns the gas stream spins is directly proportional to the collection efficiency of the cyclone. The syngas residence time in the outer vortex of the cyclone and syngas inlet velocity is calculated respectively as shown in equation (2.10) and (2.11) [Nazaroff and Alvarez-Cohen, 2000].

$$t = \frac{\pi D N}{V_i} \tag{2.10}$$

$$V_i = \frac{Q}{WH} \tag{2.11}$$

where D is cyclone body diameter (m), V_i is gas inlet velocity (m/s), Q is volumetric inflow (m^3/s), H is height of inlet (m) and W is width of inlet (m).

Particle drift velocity is the terminal velocity (V_t) that will allow a particle that was at a distance of 'W' away from the wall to be collected at specific time. It is determined as shown in equation (2.12) [Nazaroff and Alvarez-Cohen, 2000]:

$$V_t = \frac{W}{t} = \frac{WV_i}{\pi DN} \tag{2.12}$$

In addition, terminal velocity can also be determined in terms of particle size or particle diameter. This is achieved by assuming stokes flow (drag force = $3\pi\mu d_p V_t$) and spherical particle subjected to centrifugal force to be = mv^2/r, where m represents the mass of particle in excess of mass of gas displaced, $v = V_i$ and $r = D/2$. Hence the terminal velocity can be obtained as shown in equation (2.13) [Nazaroff and Alvarez-Cohen, 2000]:

$$V_t = \frac{\left(\rho_p - \rho_g\right) d_p{}^2 \, V_i^2}{9 \, \mu \, D} \tag{2.13}$$

where V_t is terminal velocity (m/s), d_p is diameter of the particle or particle size (m), ρ_p is particle density (kg/m^3), ρ_g is syngas density (kg/m^3) and μ is syngas viscosity (kg/ms).

In solving for particle diameter it is assumed that the particle terminal velocity was obtained when the opposing drag force equaled the centrifugal force. Hence equating the two terminal velocities will result in the determination of particle diameter as [Wang, 2004]:

$$d_p = \left[\frac{9\mu W}{\pi N V_i \left(\rho_p - \rho_g\right)}\right]^{1/2} \tag{2.14}$$

Note that d_p is the smallest size of particle that could be collected if the syngas spinning starts at the inside edge of the inlet duct. As a result all particles of this size or greater could be separated at an efficiency of 100% theoretically. In summary, cyclone is one of the oldest technology and most used for solid particulate removal.

2.4.2 Wet Gas Cleaning

Wet gas cleaning as the name implies, is a wet process that involves the purification of gas by means of a liquid scrubbing agent. The heat exchange that occurs between the scrubbing agent and the syngas during the cleaning process, impacts on the overall plant efficiency, particularly on the thermal efficiency. Treating the scrubbing medium so as to meet the environmental standard incurs additional cost. These are some shortcomings with wet gas cleaning; nevertheless it still remains an important gas cleaning technology due to its reliability, simplicity and effectiveness [Woolcock and Brown, 2013]. Wet gas cleaning technologies are mostly classified according to their operating techniques.

Spray scrubber **-** comes either in the form of a spray tower or spray chamber made of an empty cylindrical or rectangular chamber and spray nozzle. During the cleaning process the spray nozzle disperses liquid droplets which come in contact with the gas stream in concurrent or counter current-manner. The contact power of the two streams is derived from a combination of liquid pressure and flow rate. A collection efficiency of 90% can be achieved for particles larger that 5µm and 40% for submicron particles using a spray scrubber [Woolcock and Brown, 2013]. The physical absorption process is dependent on the density, viscosity of the gas stream and

liquid solvent and specific characteristics of the contaminant such as diffusivity and equilibrium solubility.

Venturi scrubber **–** is mostly used for removal of submicron particles within the range of 0.5-5μm. This type of scrubber accelerates the scrubbing liquid together with the gas stream to high velocity and turbulence so as to improve gas-liquid contact. Based on the design features scrubbing liquid is introduced to the upstream of the throat or directly into the throat. In so doing the scrubbing liquid atomizes into small droplets due to the turbulence in the throat, hence increasing the particle interaction. Once the particles are captured by the liquid, the wet particulate matter and excess liquid droplets then separate from the gas stream by an entrainment section which usually consists of a cyclonic separator and/or a mist eliminator [EPA, 1998; Corbitt, 1990].

Cyclone Spray Scrubber - Cyclone scrubber was developed in order to enhance the particle removal efficiency of conventional cyclones by adding the wet scrubbing effect. The principle of cyclone spray scrubber is similar to that of a conventional cyclone with additional water spray at the inlet area [Park and Lee, 2009].

2.5 GASIFICATION MODELS AND SIMULATION

The growing interest in the field of gasification has led to the development of several models so as to explain and optimize the process of gasification. Models generally aid in developing a better scientific understanding of a process such as gasification or a system such as gasifier.

More also it aids in testing the impact of different operating conditions and parameters prior to actual experimentation. Simulation on the other hand is an important aspect of research and very crucial particularly at the developmental stage of a work. Simulation models for gasifiers are classified into thermodynamic equilibrium model, kinetic model, computational fluid dynamics (CFD) model and artificial neural network. These models use different approaches in their prediction of real process application and have different limitations [Patra *et al*, 2016].

Some basic gasification reactions usually considered during gasification modeling include Boudouard reaction shown in equation (2.6), water gas reactions shown in equation (2.7), methane formation, steam reforming reaction and water gas shift reaction shown in equation (2.15), (2.16) and (2.17) respectively [Melgar *et al*, 2007].

$$C + 2H_2 \leftrightarrow CH_4 \tag{2.15}$$

$$CH_4 + H_2O \rightarrow H_2 + CO_2 \tag{2.16}$$

$$CO + H_2O \leftrightarrow CO_2 + H_2 \tag{2.17}$$

The goal of these models is to study the thermochemical processes that occur during gasification as well as to evaluate the influence of input parameters such as feedstock properties, air fuel ratio, moisture content, temperature and pressure. Some models only consider the final

composition of the product while others put into consideration the different processes along the gasifier [Puig-Arnauat *et al*, 2010].

2.5.1 Thermodynamic equilibrium model

Thermodynamic equilibrium models have two ways in which it can be approached: stoichiometric and nonstoichiometric approach. In stoichiometric approach all the chemical reactions and their species are clearly defined. It involves the selection of species with the lowest value of free energy of formation. According to Prins *et al*. [2003] and Desrosiers [1976] the only species present at concentration above 10^{-4} mol% and gasification temperatures between 600 °C - 1500 °C are CO, N_2, CO_2, H_2, CH_4, H_2O and solid carbon. Non-stoichiometric equilibrium model does not require specification of reaction mechanism but involves minimization of Gibbs free energy in the system [Mathieu and Dubuisson, 2002]. The required input parameters for non-stoichiometric model are the elemental compositions of the feedstock which can be obtained readily from ultimate analysis hence they are particularly suitable for feedstock such as biomass [Basu, 2010].

Thermodynamic equilibrium models are independent of gasifier designs and are based on some general assumptions that are in agreement with specific reactor types. Some of these assumptions include consideration of reactors as implicitly zero dimensional, as perfectly insulated, fast gasification reaction rates, long enough residence time that allows attainment of equilibrium state, perfect mixing and uniform temperature [Prins *et al*, 2003]. Based on these

assumptions, that differ from reality thermodynamic equilibrium models usually disagree with some circumstances. Typical examples are overestimation of H_2 and CO yields and the underestimation of CO_2, CH_4, tars and char at low gasification temperature [Villanueva, 2008]. For this reason equilibrium models have undergone modifications and corrections. Some studies based on this are summarized.

Pandey *et al* [2013] presented a report on the prediction of syngas composition from biomass gasification using thermodynamics equilibrium model. In Barman *et al* [2012] study an equilibrium model was used in a non-equilibrium condition by multiplying coefficients with equilibrium constant to predict gas exit temperature and gas composition. In addition variation in performance of the studied gasifier was predicted for different air fuel ratio and moisture content. Melgar *et al* [2007] formulated equilibrium models for downdraft gasifiers by combining the laws of conservation of atomic species, laws of energy conservation and laws of chemical equilibrium. Jarungthammachote and Dutta [2007] developed an equilibrium model for predicting the composition of the syngas released in a downdraft gasifier. The study improved the model by correcting equilibrium constant of the methane reaction (equation 2.8) and water–gas shift reaction (equation 2.10). Zainal *et al* [2001] predicted the syngas composition of different biomass materials using stoichiometric thermodynamic equilibrium.

2.5.2 Kinetic model

The inability of equilibrium model to correlate gasifier design parameter with final composition of syngas necessitated the use of kinetic model. Kinectic model allows detailed description of biomass gasification while considering the behavior of the gasifier. It predicts gas yield, product composition after finite residence time in finite volume and temperature inside the gasifier [Basu, 2010]. Although kinetic models are more accurate and detailed they incur longer computational time, thus making it intensive. They provide kinetic mechanism information needed in gasifier designing and evaluation. In biomass gasification modeling most kinetic models separates the process into sub-models that correspond to gasifier zones. The division into sub-models simplifies the model and provides better understanding of the gasifier particularly in downdraft gasifier [Sharma, 2008]. These sub-models include sub-model of pyrolysis, sub-model of oxidation and sub-model of reduction.

Kinetic sub-model of pyrolysis unlike equilibrium model uses cellulose, hemicelluose and lignin composition as feed input parameter. They are described using one-stage global single reaction, one-stage multiple reactions and two-stage semi global reaction [Várhegyi, 1997]. In sub-model of oxidation zone, pyrolysis products are oxidized in non-stoichiometric supply of oxygen. Some reaction may not reach equilibrium state at the oxidation due to variation in reactivity of pyrolysis product and difference in their reaction time [Sharma, 2011]. Sub-model of reduction zone include major reactions such as Boudouard reaction, water gas reaction, methane formation reaction, steam reforming reaction and water gas shift reaction. The reaction rates here are dependent on Arrhenius type temperature [Giltrap *et al*, 2003]. Both oxidation and reduction zone sub-models are suitable for downdraft gasifier.

Giltrap *et al* [2003] predicted the composition of syngas under steady state condition using a reduction zone model for downdraft gasifier they developed. The model is based on the assumption that all the oxygen from the inlet air is combusted to CO_2 and all pyrolysis products are completely cracked. Giltrap's model was modified by Babu and Sheth [2006] in bid to predict the temperature profile in the reduction zone. A linear and exponential increase was recorded for the char reactivity factor along the length of the reduction bed. The model was simulated using a finite difference method and was compared with Jayah *et al* [2003] experimental data.

Jayah *et al* [2003] model is a modification of Chen's model and consist of two sub-models which were aimed at calculating the composition of product gases entering the gasification zone. They also described the physical and chemical processes as well as conservation principles. Furthermore a mathematical model consisting of three separate sub-models was developed to predict the steady state performance of a biomass downdraft gasifier/spark ignition engine power system. These sub-models described the processes in the drying-pyrolysis zone, oxidation zone and reduction zone. The reduction zone was described using chemical kinetics principles in order to do away with the assumptions associated with achieving thermo-chemical equilibrium state during operation. The model predicted the molar concentration of different species in syngas as well as the temperature profile along the height of the gasifier [Centeno *et al*, 2012]. Chaurasia [2016] proposed a new kinetic scheme that incorporates the effects of the pyrolyisis fraction and char reactivity factor in its simulation. The model examined the influence of gasification zone length, air flow rate, initial gas temperature and mole fraction of oxygen in primary air on product composition. A dynamic multiphase model combining global kinetics of

pyrolysis, combustion kinetics of gaseous and solid species, homogenous and heterogeneous reduction kinetics and diffusion controlled moisture evaporation was developed. In simulation of the model variables such as biomass consumption rate, producer gas flow rate and composition were predicted [Patra *et al*, 2016].

2.6 COMPUTATIONAL FLUID DYNAMICS MODELING

Computational fluid dynamics is a simulation technique (CFD) that mathematically simulates fluid flow and heat transfer. CFD uses numerical techniques and algorithm in solving governing equations of continuity, momentum and energy for fluid flow [Blocken, 2004, Hesham, 2014]. Generally fluid flows are ruled by partial differential equations (PDE) that characterize laws of conservation of mass, momentum and energy. These PDE systems are substituted using set of algebraic equations and are solved with CFD techniques. CFD supplements theoretical and experimental fluid dynamics by providing cheaper way of testing fluid flow systems. It provides means of testing conditions that may be difficult or impossible to measure experimentally. Computational fluid dynamics predicts fluid (gas and liquid) flows qualitatively (and often quantitatively) using the following method [Kuzmin, 2013]:

- Mathematical modeling – partial differential equation
- Numerical approach – discretization and solution technique
- The use of Software – solvers, pre-processing and post-processing

Mathematical modeling involves the use of mathematical equations such as sets of partial differential equations in describing the flow of fluid. This is followed by discretization of the mathematical equations so as to produce a numerical analogue of the equations. Next is the division of domain into small grids or element. Lastly the equations are solved by application of initial conditions and boundary conditions that are specific to the fluid problem. Numerical discretization is achieved through four methods namely: finite difference method, finite element method, finite volume method and spectral method. Boundary conditions are sets of inlet and outlet conditions used for simulation purposes [Ashgriz and Mostaghimi, 2012]. CFD has so many applications and recently is applied in the design of internal combustion engine, for biomass gasification although is still uncommon which can be attributed to lack of broad computational resource and varying physical properties of biomass [Pepiot *et al*, 2010]. For instance, Janajreh and Al Shrah [2013] applied CFD model in the study of biomass gasification in downdraft gasifier with a multi-step reactions for CO, CO_2, H_2O, H_2, CH_4 and Char. However, CFD is very much applicable in fluid flow and heat recovery equipments or heat exchangers.

Computational fluid dynamic has been used extensively in studies related to heat transfer and fluid flow. A comparative analysis of a parallel flow heat exchanger and ribbed tube heat exchanger was done using CFD [Melvinraj *et al*, 2014]. Numerical simulation of the heat transfer characteristic of a double pipe heat exchanger with different fin profiles was conducted using CFD. The heat transfer characteristics compared in the study include temperature variation, heat transfer rate, heat transfer coefficient and fin effectiveness [Kumar *et al*, 2015]. A CFD analysis of shell and finned tube heat exchanger for counter flow was conducted , to test the

effect of temperature rise and pressure drop along the length of the finned tube and the shell. In addition the effectiveness of using a stainless steel as outer material was compared with the use of galvanized iron [Kanti *et al*, 2016]. Manickam *et al* [1998] developed a CFD model for a waste heat recovery boiler using a typical plant off-gas. The model was used to estimate the temperatures of char and dust within the boiler and their possible deposition on the boiler wall.

2.7 HEAT RECOVERY IN GASIFICATION

Limited information related to design of waste heat recovery unit for biomass gasifier is available in open literature. However, the few available literature found are summarized as follow. Ma *et al* [2015] studied the use of waste heat from a downdraft biomass gasifier system. The biomass gasifier system in the study was designed such that the catalytic reactor is placed before the water scrubber for more effective use of the waste heat. The recovery of waste heat in this study was carried out by attaching a thermoelectric generator (TEG) system on the surface of the catalytic reactor. The TEG system is made of a heating collector plate, cooling pipe and eight thermoelectric components which were made using a Bi_2Te_3 based material. From experiment conducted, the gasifier outlet temperature was found to be in the range of 623 °C – 773 °C and the surface temperature of the catalytic reactor was found in the range of 473 °C – 633 °C. The catalytic reactor surface temperature matches the operating temperature of the Bi_2Te_3 thermoelectric generator which is why Bi_2Te_3 material was used. In the study, the waste heat recovered using TEG was converted to electrical power with an approximate power output of 2.9 – 6.1W and equivalent power density of 91.5 - 193.1 W/m^2. The thermoelectric generator

conversion efficiency of the waste heat recovery from the gasifier was found to be approximately 5.4% - 7.16%. The study then concluded that the waste heat recovery potential is dependent on syngas temperature and thermoelectric generator size. The study also highlighted that the biomass gasification system and thermoelectric generator system are two independent systems.

In another study an experimental approach was followed in studying a cyclone heat exchanger as heat transfer equipment. The holdup mass of solid particles blown into the cyclone was calculated by varying the size of the solid particle and fixed mass flow rate of solid particles and air. In addition, the effect of particle size on thermal effectiveness of air and solid was also considered. To achieve the aim of the study, hot air from an engine exhaust was supplied to the cyclone at a temperature of 200°C. Furthermore solid particles were fed into the cyclone through a small container provided with a vibratory feeder and an opening at the bottom. The holdup of particles was then measured by simultaneously closing the valve at the inlet and exit of the cyclone, airflow and solid flow. The study then showed that air-solid holdup mass increase with increasing solid feed rate hence, decreasing the inlet air mass flow rate (velocity) and increasing the particle size up to a certain limit. The study also identified, that the performance of a cyclone as heat transfer equipment is dependent on the surface area of holdup mass of the solid particles inside the cyclone [Sevvel *et al*, 2015]. However, the study did not consider the heat recoverable potential of the cyclone heat exchanger in a gasification unit as well as the design of the cyclone heat exchanger. Furthermore, Al-attab and Zainal [2014] studied the performance of a biomass fueled two-stage micro gas turbine (MGT) system with hot air production heat recovery unit. The integrated heat recovery unit is made of a shell and tube heat exchanger designed using ε-NTU method. The heat recovery unit was aimed at recovering about 86% of the micro gas turbine exhaust thermal power. The recovered thermal power was converted into 50 kWth of hot

air for drying. Here a conventional heat exchanger was applied and the heat recovery process was centered on the micro-gas turbine not on the cyclone of a gasification system.

Hari and Hossain [2013] explored a study that involved the recovery of waste heat from diesel engine exhaust. The study identified that diesel engine discharges significant portion of chemical energy of fuel in terms of heat energy through the exhaust gas. To recovery the waste heat, two identical shell and tube heat exchangers (with shell diameter of 76mm, tube diameter of 20mm and length of 1m) were installed into the exhaust system of a 4-stroke, 4-cylinders, and water cooled Toyota 13B diesel engine. the experimental test conducted revealed that the additional power attainable through the recovered heat are 6.72 kW, 1 kW and 0.57 kW at 220rpm, 1800rpm and 1400rpm engine speed respectively. The installed heat exchangers improved the overall efficiency of the engine by 4.4%, 3.7% and 3.1% at 220rpm, 1800rpm and 1400rpm engine speed respectively.

A biomass gasification system utilizing coconut shell as base material with an integrated waste heat recovery unit (WHU) dryer for the purpose of drying pulverized kernel was studied. In the study, the dryer with a WHU was compared with electric and kerosene dryers in terms of drying curve pattern, rate of drying, cost of drying, physical, chemical and microbial quality parameters of dried pulverized kernel. The producer gas from the 60 kW, thermal gasifier was made to go through the cyclone separator first before entering the gas burner where the gas is burnt to generate heat. The generated heat from the gas burner is blown into the drying chamber using an electric blower via a heat exchanger for the drying process. Here the dryer with the waste heat recovery unit is an indirect heated tray type oven and the exit exhaust air temperature was recorded to be 230 °C – 250 °C [Fernandopulle and Amadoru, 2012].

Pavlas *et al* [2010] study dealt with the application of heat pump in a fluidized bed biomass gasification system for a wood processing plant. Process integration methodology was used in the study because many streams requiring heating and cooling were involved in the energy recovery. A recuperative heat exchanger was integrated after the cyclone where the exit temperature of the syngas is about 550 °C for the purpose of air preheating. In addition, a second heat exchanger (conventional type) situated immediately after the recuperative one further cool the syngas to about 300 °C before entering the filter where the coarse particulates are collected. Further cooling of the syngas to a near zero temperature were performed at the scrubber where the cooling medium comes in direct contact with syngas. Finally the heat pump was integrated to utilize the rejected heat from the conventional second heat exchanger, low grade heat from the scrubber and hot water produced in the engine for heating the water for wood drying and for boiler feed water preheating.

As regards to waste heat recovery in biomass gasification system, existing designs of waste heat recovery unit are limited in open literature. From the review of literature conducted it was found that most heat recovery process carried out involved the use of conventional heat recovery equipments such as recuperative heat exchanger, thermoelectric generator, shell and tube exchangers. In addition the recovered waste heat was used mostly for power generation and drying purposes. Furthermore, the reviewed studies showed that the heat recovery units were integrated after the cyclone separators, while some were not directly on the gasification system but on the gas engine or gas turbine. The syngas temperature at the cyclone separator is evidently high based on the feasibility study carried out. This is attributed to the fact that cyclone is the first entry point for the synags as it exits the gasifier. Previous studies have also shown that waste heat recoverable potential is dependent on the temperature of the stream and the recovery

technology or technique. Hence, the recovery point for the waste heat, the recovering technology and end use application of the recovered waste heat are inevitable factors of consideration for efficient waste heat recovery. All these necessitated the need to design and construct a customized waste heat recovery unit and integrate it around the cyclone separator of the Johannson biomass downdraft gasifier. In addition the present study was motivated to breach the gap found with regards to recovery of waste heat from the cyclone section of gasification system so as to enhance the thermal efficiency of the system.

2.8 TECHNOLOGIES FOR WASTE HEAT RECOVERY

The available technologies for conversion of waste heat to valuable form are numerous in number. Waste heat recovery technologies can be divided into active and passive technologies as presented in Figure 2.5. This division stems from whether the waste heat is used at the recovered temperature or transformed to a different temperature.

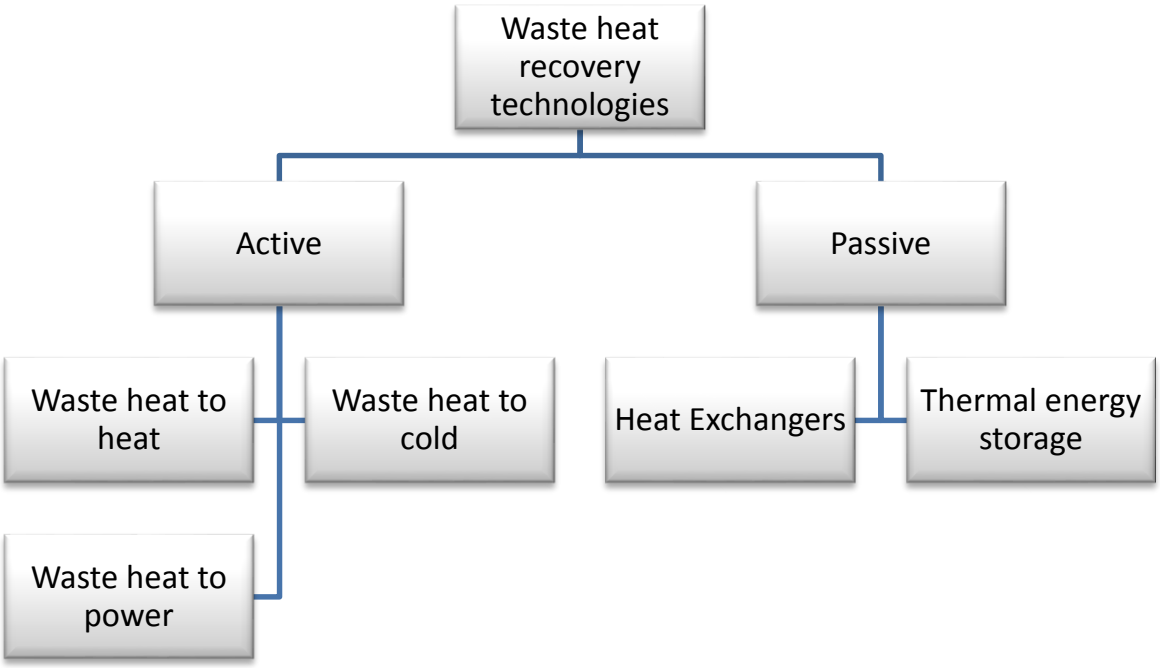

Figure 2.5: Waste heat recovery classifications

Active technologies particularly waste heat to heat (WHTH) and waste heat to cold (WHTC) are termed transformation technologies because they either downgrade or upgrade the temperature of the received waste heat. Alternatively passive technologies re-use waste heat as received for heating or pre heating other processes. The dominant passive technologies are heat exchangers and thermal energy storage. Some of these recovery technologies are already well developed and technically proven while some are still at the growing stage [Brückner *et al*, 2015]. Discussions on these technologies are as follow.

2.8.1 Thermoelectric generator

Thermoelectric generators (TEG) are solid state devices with the capability of transforming waste heat into usable electrical power. They are classified among waste heat to power (WHTP) technologies shown in Figure 2.5. The working principle of a TEG is based not only on Seebeck effect but also on Peltier effect and Thomson effect. Peltier theory is the opposite of Seebeck effect which was first discovered by Thomas Johann Seebeck in 1821. The Seebeck effect occurs when two dissimilar but connected electrical conductors or semiconductors at different temperature produces an electric potential (voltage). Thomson described the heating or cooling of a conductor carrying current with temperature gradient [Ma *et al*, 2015].

A TEG is made of a P-type semiconductor and an N-type semiconductor material that are connected in series electrically and in parallel thermally. At the P-type semiconductor free electrons are transferred from the hot-side to the cold-side while at the N-type the opposite is the case. The flow of heat from the hot-side of the TEG to the cold-side drives both the free electrons and the holes. The potential difference (V) that is created as a result of the flow is proportional to the temperature change (ΔT). This creates a proportionality constant known as Seebeck coefficient (S) as shown in equation (2.18).

$$V = S\Delta T \tag{2.18}$$

Connecting an electron and hole conducting material in series will cause a net voltage to be produced that drive a load. To increase the voltage more thermoelectric modules are connected in series. There are a number of demonstrations of the use of TEG for waste heat recovery in Space applications, vehicle applications such as large truck, exhaust and process heat type of applications. A good example is the generation of a 250 W power from a steel casting line using

TEG [LeBlanc, 2014]. Another study investigated the application of TEG in recovery of medium-high temperature waste heat from a power diesel engine [Haidar and Ghojel, 2001].

Thermoelectric generators are highly reliable, environmentally friendly and easy to maintain because they have no moving parts. However TEG is still faced with the challenge of low conversion efficiency which is presently at 5% but with future capability of 12%. The thermoelectric conversion efficiency is defined as the amount of electrical power generated from a given amount of heat supplied. It is also defined in terms of hot-side (T_h) and cold-side temperature (T_c) of TEG and the figure of merit (ZT) as shown in equation (2.19) [Smith and Thornton, 2009].

$$\eta = \frac{T_h - T_c}{T_h}\left[\frac{\sqrt{1+ZT} - 1}{\sqrt{1+ZT} + T_c/T_h}\right] \tag{2.19}$$

The figure of merit (ZT) is a performance measuring parameter for thermoelectric materials. It is determined from the properties thermoelectric material which includes Seebeck coefficient S, electrical conductivity σ, temperature T and thermal conductivity k of the material and is given as [LeBlanc, 2014].

$$ZT = \frac{S^2\sigma T}{k} \tag{2.20}$$

ZT determines the ability of a material to efficiently produce thermoelectric power. Some thermoelectric materials that are already in use for commercial applications include bismuth telluride, lead telluride and silicon germanium. These materials are classified based on their structures and compositions. Their properties are highly temperature dependent; hence it

impacts on the overall system performance [LeBlanc, 2014]. The use of TEG for waste heat recovery can improve energy efficiency through distributed electricity generation.

2.8.2 Heat Exchanger

Heat exchangers are devices used in transfering thermal energy from one fluid to a second fluid or multiples of fluids, from a solid surface to a fluid and from solid particulates to a fluid. They are used for heating and cooling applications in the industries and domestically. Their common applications are found in thermal power plants and refrigeration systems. Heat exchangers are classified under passive technologies as shown in figure 2.6. There are two major components of a heat exchanger; the heat transfer element such as core or matrix and the fluid distribution elements such as manifolds, tanks, headers, inlet and outlet nozzles. The core contains the heat transfer surface which is the primary wall that separates the fluids undergoing heat exchange. Heat exchangers generally do not have any moving part hence there is reduced risk of break down. However there are some with moving parts such as rotary regenerative exchanger [Shah and Sekulic, 2003]. Heat exchangers come in various types, but according to Shah [1981] they are classified into six namely: according to transfer process, number of fluid, surface compactness, construction features, flow arrangement and heat transfer mechanism.

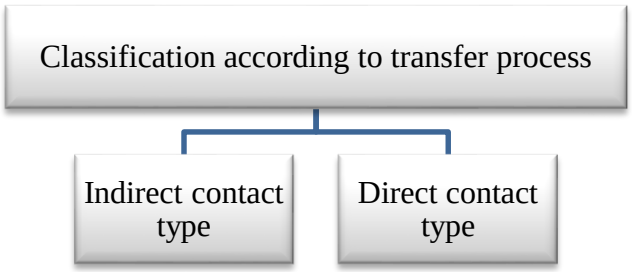

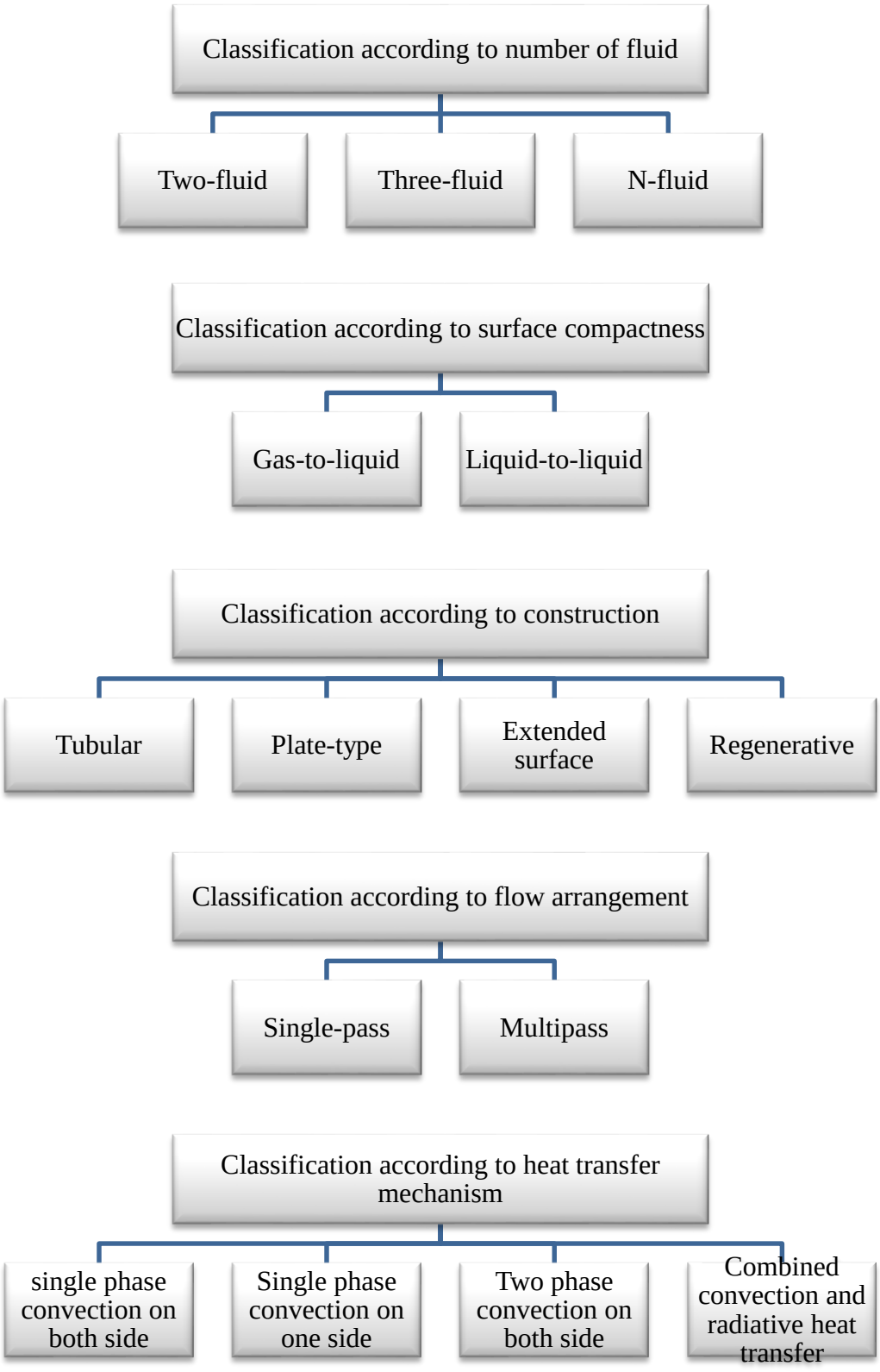

Figure 2.6: Heat exchanger classifications [Shah, 1981]

There is no direct contact between the fluids in mostly all the classifications of heat exchanger shown in figure 2.6. The fluids are separated by a dividing wall which provides some thermal resistance between the fluids. However there are some exceptions the direct contact types in which there are no dividing wall between the fluids. These are mostly applicable with immiscible fluids where the fluids come in contact, exchange heat and then separated. Heat exchange in this case are said to be maximum due to absence of dividing wall thermal resistance. Generally the exchange of heat between the hot and cold stream (fluids) could be continuous or intermittent depending on the nature of the flow. In some case, the dividing walls are extended by addition of appendages called fins. Fins are added mostly to increase the heat transfer area, but they also provide structural strength and thorough mixing of highly viscous liquid [Shah and Sekulic, 2003].

Some common examples of heat exchangers include shell-and-tube, double-pipe, finned tubes, water jacket, pipe coil, plate and frame, boilers, condensers and evaporators. Shell and tube heat exchanger are made from a number of tubes mounted in parallel form and enclosed in a cylindrical shell. Double pipe consist of two concentric circular tubes with one fluid flow through the inner tube and the other through the annulus of the two tubes. A water jacket is a water-filled casing consisting of an inlet and outlet vent. Plate and frame consist of a series of thin rectangular metal plate that are held together in a frame and sealed around the edge with a gasket. In condenser and evaporator change in phase occurs, vapour is converted to liquid in condenser while liquid is converted to vapour in evaporator. Note that a number of flow arrangements are possible in the different types of heat exchanger.

2.8.2.1 Fluid Flow Configuration

In heat exchanger generally, fluids passage can be multi-pass or single-pass. A multi-pass exists when a fluid makes one pass through the full length of a heat exchanger and reverses its flow through another equal length or different length. On the other hand, a heat exchanger is considered single-pass when the fluid makes only one pass without reversing. The flow configuration of fluids in single-pass heat exchangers are basically classified into three namely: counter-flow, parallel flow and cross flow. The choice of any of these flow configurations is dependent on heat exchanger effectiveness, allowable thermal stress, pressure drop, temperature levels, piping and allowable maximum velocities [Shah and Sekulic, 2003].

Counter-flow – In counter flow configuration both the hot fluid and the cold fluid flow opposite to each other in direction. In this arrangement the inlet of hot fluid and outlet of the cold fluid are at one terminal while the hot fluid outlet and cold fluid inlet are at the other terminal. Figure 2.7 illustrates a counter-flow arrangement and its typical temperature distribution. Temperature variations in this arrangement are idealized as one dimensional.

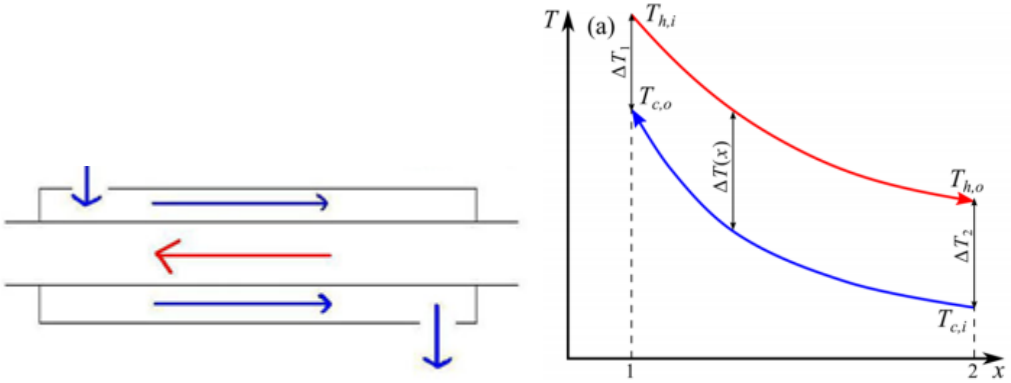

Figure 2.7: Counter-flow pattern and temperature distribution

Counter-flow configuration is reported to produce minimum thermal stress to the dividing wall when compared with other configuration. Hence they are more efficient from heat transfer perspective. This type of flow arrangement is obtained in plate type heat exchanger and double-pipe heat exchanger [Kakac and Liu, 1998].

Parallel flow – In this arrangement or configuration the two fluids enter the heat exchanger through the same nozzle and flow in the same direction parallel to each other and exit together at the other nozzle. Due to the mode of entry a large temperature difference exist between the two fluids at the inlet nozzle and this could result in high thermal stress at the inlet wall. A typical parallel flow pattern and its temperature profile is shown in Figure 2.8

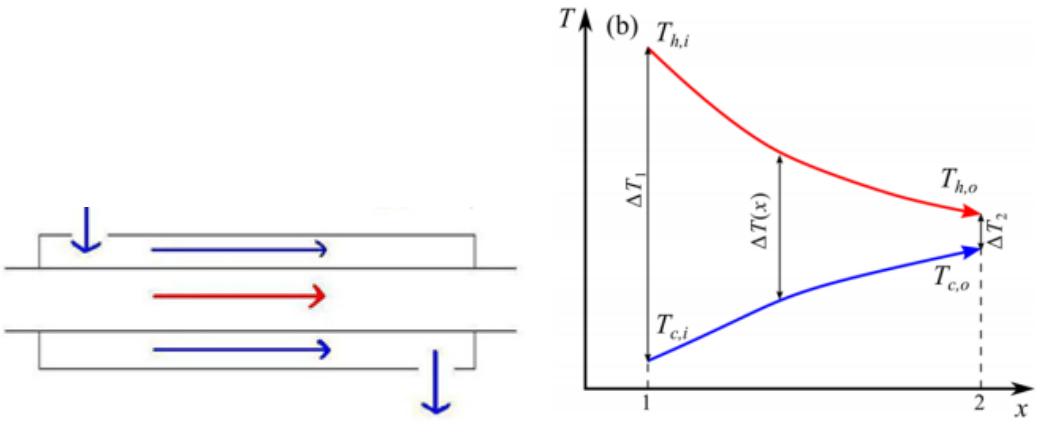

Figure 2.8: Parallel flow pattern and temperature distribution

Parallel flow arrangement is mostly used in applications where the temperatures of the two fluids are desired to exit the outlet nozzle at close to equal temperature. Temperature variations in this case are idealized as one dimensional.

Cross flow – The flow of one fluid in cross flow configuration is perpendicular to the second fluid flow. Typically, the temperature variations in cross flow are said to be two dimensional.

Figure 2.9: Cross flow pattern and temperature distribution

Most shell and tube heat exchangers and extended surface heat exchangers employ a cross flow arrangement. The effectiveness of cross flow arrangement lies between counter-flow and parallel flow configuration. In cross flow arrangement the greatest difference in temperature occurs at the entering point of the two fluids. Mixing of fluid stream does occur sometimes in a cross flow arrangement based on the design. An unmixed fluid stream occurs when the fluid stream flows through the individual channel with no mixture of fluids between the adjacent flow channels. Temperature gradient exists in the transverse plane for unmixed fluid stream while no temperature gradient exists for completely mixed fluid [Shah and Sekulic, 2003].

2.8.2.2 Theory of Heat Exchanger

The theory of heat exchanger describes both the theoretical heat of a fluid and the practical heat that can be transferred. The basic theory of heat exchanger described in this section is focused on the different flow configurations discussed previously. The thermal parameters of heat exchanger define their nature and performance for any given application. The theoretical quantity of heat transferred through the dividing wall of a heat exchanger can be represented using an enthalpy balance of the fluid streams as shown [Kakac and Liu, 1998].

$$Q_h = m_h \left(h_{h1} - h_{h2} \right) \tag{2.21}$$

$$Q_c = m_c \left(h_{c2} - h_{c1} \right) \tag{2.22}$$

where the subscripts h denotes hot fluid and c denotes cold fluid while 1 and 2 denotes inlet and outlet, m represents mass flow rate, h_h and h_c stands for the hot and cold stream enthalpies. For constant specific heat without phase change, equation (2.21 and (2.22) can be written as

$$Q_h = \left(mc_p \right)_h \left(T_{h1} - T_{h2} \right) \tag{2.23}$$

$$Q_c = \left(mc_p \right)_c \left(T_{c2} - T_{c1} \right) \tag{2.24}$$

In the absence of heat loss the quantity of heat the hot fluid emits, is equal to the quantity of heat the cold fluid absorbs. This is in agreement with energy conservation principle, hence the heat transfer rate $Q = Q_h = Q_c$. This heat transfer rate Q can as well be determined in relation to the heat exchanger physical geometry, material composition and fluid condition as given

$$Q = UA\Delta T_{LMTD} \tag{2.25}$$

where U represents the heat transfer overall coefficient, A is the surface area of heat exchanger and ΔT_{LMTD} is log mean temperature difference. ΔT_{LMTD} is used due to the variation in the temperature difference between the hot and cold ($\Delta T = T_h - T_c$) fluid along the length of the heat exchanger. Note that the thermal analysis of heat exchanger under steady state condition is evaluated using equations (2.23) to (2.25).

LMTD heat exchanger analysis method

There are two basic method employed in the analysis of heat exchangers theory namely: Log Mean Temperature difference (LMTD) method and effectiveness-Number of Transfer Unit (e-NTU) method. LMTD is the most common method used in analyzing the thermal capacity of heat exchanger and thermal capacity on the other hand is the ability of a heat exchanger to transfer heat between two fluids at different temperature. The ΔT_{LMTD} in equation 9 is determined by applying the differential forms of equation (2.26) and (2.27) as shown [Kakac and Liu, 1998].

$$dQ = - \left(mc_p\right)_h dT_h = \pm \left(mc_p\right)_c dT_c \qquad (2.26)$$

Where + and – sign denotes parallel and counter flow configuration. For counter flow both dT_h and dT_c will drop over the differential area dA. But in parallel flow only dT_h will drop and dT_c will increase hence assuming a parallel flow we then obtain

$$dT_h = - \frac{dQ}{\left(mc_p\right)_h} \text{ and } dT_c = \frac{dQ}{\left(mc_p\right)_c} \qquad (2.27)$$

Hence, subtracting the cold fluid temperature from the hot fluid temperature

$$dT_h - dT_c = d(T_h - T_c) = - dQ \left[\frac{1}{\left(mc_p\right)_h} + \frac{1}{\left(mc_p\right)_c} \right] \qquad (2.28)$$

Expressing the heat transfer rate dQ across a differential area dA in terms of overall heat transfer coefficient gives

$$dQ = UdA\,(T_h - T_c) \tag{2.29}$$

Substituting dQ into equation (2.28) gives

$$d\left(T_h - T_c\right) = -\,UdA\left(T_h - T_c\right)\left[\frac{1}{\left(mc_p\right)_h} + \frac{1}{\left(mc_p\right)_c}\right] \tag{2.30a}$$

$$\frac{d\left(T_h - T_c\right)}{\left(T_h - T_c\right)} = -\,UdA\left[\frac{1}{\left(mc_p\right)_h} + \frac{1}{\left(mc_p\right)_c}\right] \tag{2.30b}$$

Integrating equation 2.30b along the length of the heat exchanger under the assumption that the right hand side of the equation is a constant

$$\int_1^2 \frac{d\left(T_h - T_c\right)}{\left(T_h - T_c\right)} = -\int_1^2 UdA\left[\frac{1}{\left(mc_p\right)_h} + \frac{1}{\left(mc_p\right)_c}\right] \tag{2.31}$$

$$\ln\left[\frac{\left(T_h - T_c\right)_2}{\left(T_h - T_c\right)_1}\right] = -\,UA\left[\frac{1}{\left(mc_p\right)_h} + \frac{1}{\left(mc_p\right)_c}\right] \tag{2.32}$$

Recalling equation (2.23) and (2.24)

$$Q = \left(mc_p\right)_h\left(T_{h1} - T_{h2}\right) = \left(mc_p\right)_c\left(T_{c2} - T_{c1}\right) \tag{2.33}$$

Solving for reciprocal of (mc_p)

$$\frac{1}{\left(mc_p\right)_h} = \frac{\left(T_{h1} - T_{h2}\right)}{Q} \text{ and } \frac{1}{\left(mc_p\right)_c} = \frac{\left(T_{c2} - T_{c1}\right)}{Q} \tag{2.34}$$

Substituting equation (2.34) into (2.32) gives

$$\ln\left[\frac{\left(T_h - T_c\right)_2}{\left(T_h - T_c\right)_1}\right] = -\,\frac{UA}{Q}\left[\left(T_{h1} - T_{h2}\right) + \left(T_{c2} - T_{c1}\right)\right] \tag{2.35}$$

Solving for Q by rearranging

$$Q = UA\frac{(T_{h2}-T_{c2})-(T_{h1}-T_{c1})}{\ln\left[(T_{h2}-T_{c2})/(T_{h1}-T_{c1})\right]} = UA\Delta T_{LMTD} \quad (2.36)$$

Thus

$$\Delta T_{LMTD} = \frac{(T_{h2}-T_{c2})-(T_{h1}-T_{c1})}{\ln\left[(T_{h2}-T_{c2})\right]/(T_{h1}-T_{c1})} \quad (2.37)$$

Equation 2.37 gives the expression for log mean temperature difference and the symbols are described in Table 2.4. LMTD is a very suitable method to use in thermal analysis of heat exchanger when the inlet and outlet temperature of the hot and cold are known.

Table 2.4: Definition of symbols

Symbols	**Meaning**
T_{h1}, T_{h2}	Inlet and outlet temperature of the hot fluid
T_{c1}, T_{c2}	Inlet and outlet temperature of the cold fluid
$(mc_p)_h$	Mass flow rate and specific heat capacity of the hot fluid
$(mc_p)_c$	Mass flow rate and specific heat capacity of cold fluid
Q	Quantity of heat contained in the hot fluid

The ε-NTU method

The second method of thermal analysis which is number of transfer unit (NTU) is based on the heat exchanger effectiveness concept. This dimensionless parameter known as heat transfer effectiveness upon which NTU method is based is given as

$$\varepsilon = \frac{\dot{Q}}{Q_{max}} = \frac{\text{Actual heat transfer rate}}{\text{Maximum possible heat transfer rate}} \quad (2.38)$$

ε is a performance measuring parameter that designates the efficiency of heat exchangers. It has some thermodynamic significance and values that ranges from 0 to 1. It is important to note that ε is dependent on flow arrangement, number of transfer unit and heat capacity rate ratio (C^*). Hence ε is expressed as a function of the three parameters as shown

$\varepsilon = \left(C^*, \text{NTU, flow arrangement}\right)$. The actual heat transfer rate Q can be expressed in terms of energy released by the hot fluid or energy absorbed by the cold fluid as shown

$$Q = C_h \left(T_{h1} - T_{h2}\right) = C_c \left(T_{c2} - T_{c1}\right) \tag{2.39}$$

While the maximum possible heat transfer rate Q_{max} is given as

$$Q_{max} = C_{min} \left(T_{h1} - T_{c1}\right) \tag{2.40}$$

Where

$$C_{min} = \begin{cases} C_c & \text{if } C_c < C_h \\ C_h & \text{if } C_h < C_c \end{cases}$$

Substituting the expression for actual heat transfer rate (equation 2.39) and maximum possible heat transfer rate (equation 2.40) into equation 2.38 we obtain

$$\varepsilon = \frac{C_h (T_{h1} - T_{h2})}{C_{min} \left(T_{h1} - T_{c1}\right)} = \frac{C_c \left(T_{c1} - T_{c2}\right)}{C_{min} \left(T_{h1} - T_{c1}\right)} \tag{2.41}$$

Equation (2.41) applies for all flow arrangement. Note that the first part of equation is for $C_h = C_{min}$ and the second part is for $C_c = C_{min}$. An alternative expression for ε can be obtained as given

$$\varepsilon = \frac{UA\Delta T_m}{C_{min} \Delta T_{max}} \tag{2.42}$$

where $\Delta T_m = \left(T_{h1} - T_{h2}\right) = \left(T_{c2} - T_{c1}\right)$ and $\Delta T_{max} = \left(T_{h1} - T_{c1}\right)$. The terms C_h and C_c denotes the heat capacities of hot and cold fluid while C_{min} is the heat capacity of the fluid that might go through the maximum temperature difference. Note that heat capacity (C) is the product of mass flow rate and specific heat capacity that is $C = \left(mc_p\right)$. Heat capacity rate ratio is the ratio of the minimum heat capacity to the maximum heat capacity of the fluid streams [Shah and Sekulic, 2003].

$$C^{*}=\frac{C_{min}}{C_{max}}=\frac{(mc_p)_{min}}{(mc_p)_{max}}=\begin{cases}\text{if } C_h = C_{min} & (T_{c2}-T_{c1})/(T_{h1}-T_{h2}) \\ \text{if } C_c = C_{min} & (T_{h1}-T_{h2})/(T_{c2}-T_{c1})\end{cases} \tag{2.43}$$

Where, C_{max} is the heat capacity of the fluid that might go through the minimum temperature change. The value of $C^{*} \leq 1$ but in a case when $C^{*} = 1$, the heat exchanger is said be balanced. Heat capacity rate ratio is regarded as an operating parameter due to its dependence on mass flow rate and temperatures. More also is one of the factors that influence heat exchanger effectiveness. A second factor upon which heat exchanger effectiveness is dependent on is the number of transfer unit (NTU) and is given as [Kakac and Liu, 1998].

$$NTU = \frac{UA}{C_{min}} = \frac{1}{C_{min}}\int_A UdA \tag{2.44}$$

To derive an expression that relates ε, $C^{*} = C_{min}/C_{max}$ and NTU, we first substitute equation 2.44 into equation 2.32 with an assumption that $C_c > C_h$, such that $C_h = C_{min}$ and $C_c = C_{max}$. Hence we obtain

$$T_{h2} - T_{c1} = (T_{h1} - T_{c2})\exp\left[-NTU(\pm 1 - C_{min}/C_{max})\right] \tag{2.45}$$

The positive sign denotes counter flow while the negative sign denotes parallel flow. From equations (2.23), (2.24) and 2.41 an expression can be derived for effectiveness that includes heat capacity rate ratio (C^{*}) and number of transfer unit (NTU). In this expression the output temperatures (T_{h2} and T_{c2}) of both fluids are eliminated and the flow configurations were considered. The expression for counter flow and parallel flow are given in equations (2.46) and (2.47) respectively

$$\varepsilon = \frac{1 - \exp\left[-NTU(1 - C_{min}/C_{max})\right]}{1 - (C_{min}/C_{max})\exp\left[-NTU(1 - C_{min}/C_{max})\right]} \tag{2.46}$$

$$\varepsilon = \frac{1 - \exp\left[-NTU(1 + C_{min}/C_{max})\right]}{1 + (C_{min}/C_{max})} \tag{2.47}$$

The ε-NTU method is very suitable when the outlet temperatures of the fluids are unknown. However LMTD method could be applied in this case but is limited by the trial and error procedure involved.

CHAPTER THREE

RESEARCH METHODOLOGY

3.1 INTRODUCTION

In this chapter the research methodology employed in achieving the aim of the study is described. The main aim of this study is to harness the waste heat energy through the integration of waste heat recovery unit (WHRU) around the cyclone dust collector attached to the biomass downdraft gasifier system. First the Johansson biomass gasifier system is described and this is followed by the description of the purification unit.

3.2 DESCRIPTION OF JOHANSSON GASIFICATION SYSTEM

The Johansson biomass gasifier under study is of a downdraft type, it offers the advantage of producing a tar free gas which makes it suitable for engine application. This system comprises of many components which include the reactor/gasifier, cyclone dust collector, gas scrubber/cooler, saw dust filter, safety filter and gas engine coupled with a generator as shown in Figure 3.1

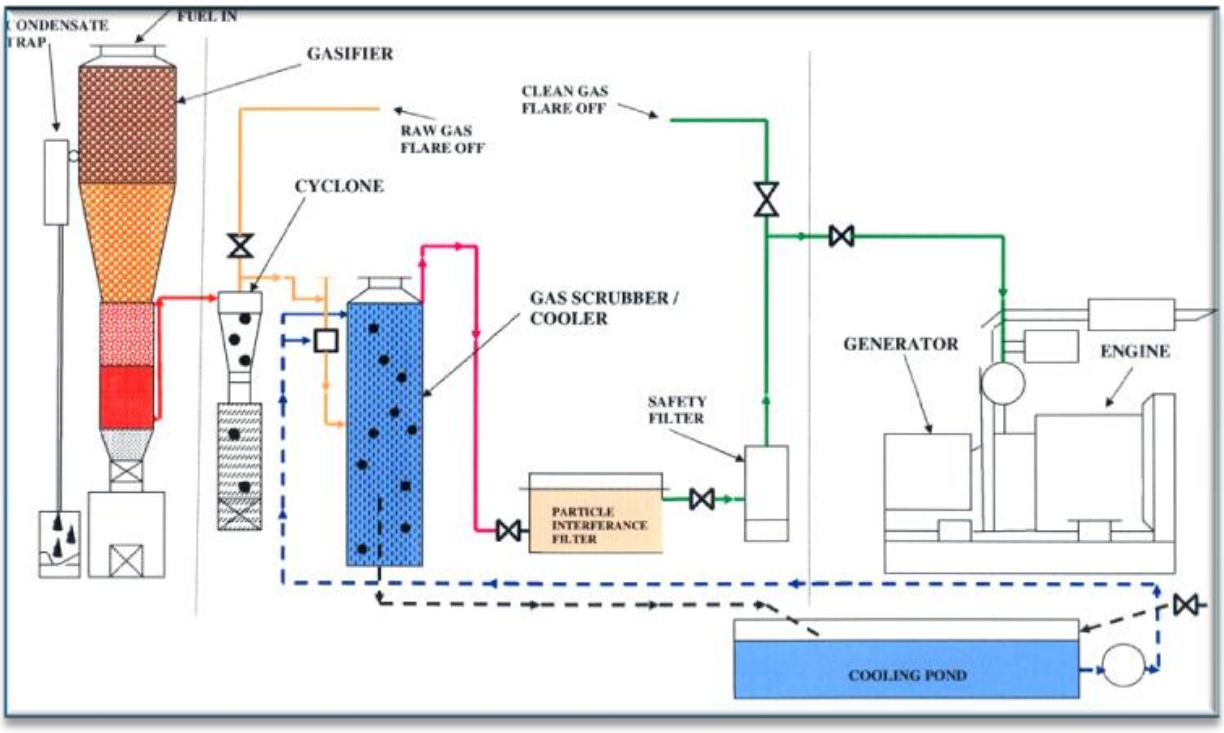

Figure 3.1: Schematic diagram of Johansson biomass gasification system

3.2.1 Gasifier

Gasifier shown in Figure 3.2 is the major component of the system where the gasification process takes place. Chunks of wood sourced from a sawmill were cut into desired sizes using a 254 mm table saw before being loaded in an electrically controlled winch (shown in Figure 3.2) that feeds the wood through the hopper into the gasifier.

Figure 3.2: Gasifier section of the system

After the feeding, the gasifier is ignited and a 2 kW centrifugal blow is then used to supply air through the air nozzle into the combustion zone. The supplied air enhances the combustion process and results in some chemical reactions taking place. The carbon and hydrogen content of the wood reacts with oxygen present in the air to give carbon dioxide and steam as product. These reactions are exothermic in nature and hence provide the heat that drives the processes of drying, pyrolysis and reduction. Some resident moisture in the wood is driven off at the drying zone by the heat from the combustion/oxidation zone. At the reduction zone the endothermic nature of reactions that occur necessitates the need for heat from the combustion zone. This is where the gases that makeup syngas exit from and enter the cyclone which is the first purification unit.

3.2.2 Cyclone dust collector

The cyclone is the first purification unit for the syngas after the gas exits the reactor and before entering the scrubber. The main purpose of the cyclone is to remove the fine carbon particles that exit the reactor with the syngas. Generally cyclone is less prone to explosion; hence it offers a better advantage when compared to fabric filters in high temperature application. The schematic diagram and picture of the cyclone is shown in Figure 3.3.

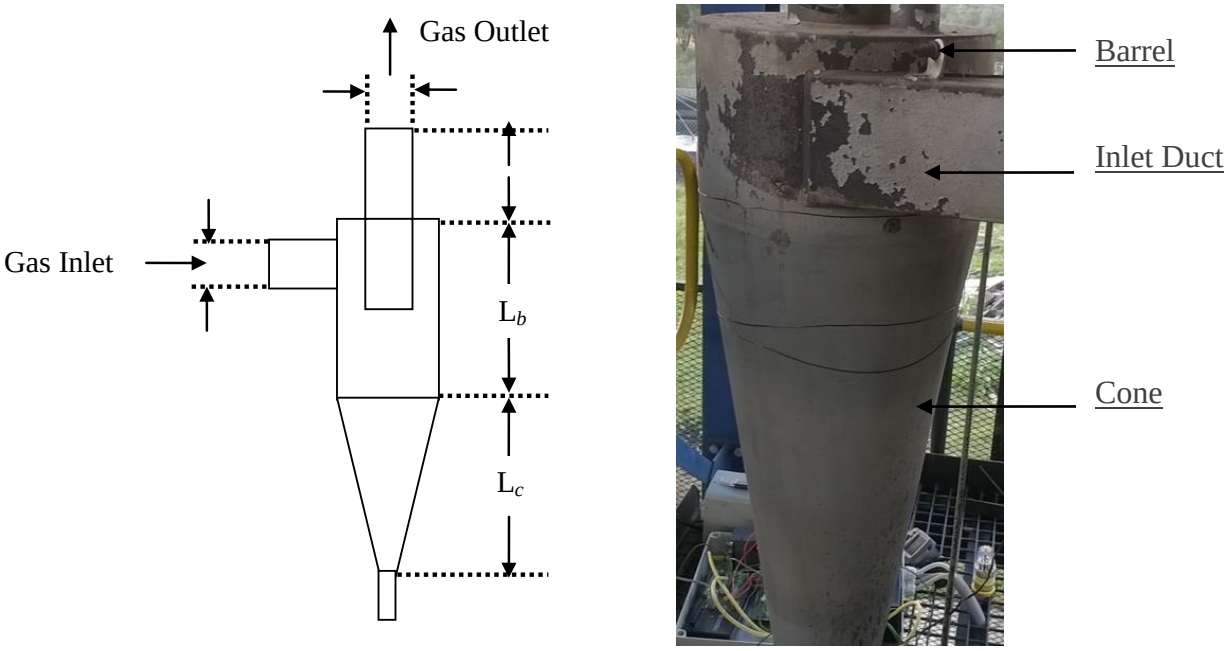

Figure 3.3: Schematic and pictorial view of the cyclone

As the raw gas exits the gasifier it enters the cyclone in a tangential manner. The tangential entry results in a spiral flow of gas beginning at the cylindrical part of the cyclone to the conical part. At the conical section the clean gas reverses and exits in a straight stream through the vortex finder, whereas the particulates collide with the outer wall and fall to the bottom

(collection chamber). About 80% of these particulates are removed when operating at full power and this is equivalent to 4 g/Nm^3. Table 3.1 shows the main dimensions of the cyclone

Table 2.1: Main dimensions of the cyclone

Item	**Dimensions (mm)**
Cyclone cylinder height	220
Cyclone cone height	1010
Cyclone outside diameter	1110
Cyclone inlet duct length	500
Vortex finder length	450

The removal of particulates present in the syngas at the cyclone is enhanced by centrifugal force. The cyclone performance is usually rated in terms of particle cut diameter or cut size and is given mathematically in equation (3.1) as [Wang, 2004]:

$$d_{p50} = \left[\frac{9\mu W}{2\pi N V_i \rho_p} \right]^{1/2} \qquad (3.1)$$

where μ is Gas viscosity (kg/ms), W is Width of inlet duct (m), N is Number of turns inside the cyclone, V_i is Gas inlet velocity (m/s) and ρ_p is Particle density (kg/m^3).

This formular is predicted both for general cyclone and high efficiency cyclone and it represents the particle size that can be separated at 50% efficiency.

3.2.3 Gas scrubber/cooler

At the gas scrubber, the syngas is cooled so as to meet the engine requirement as well as cleaned to remove some fine carbon particles that escaped the cyclone dust collector. Carbon particles less than 0.1 µm are collected by diffusion when water is sprayed from the top of the scrubber while particles greater than 1 µm settle by gravity and are collected gravitationally, by impaction or by centrifugal means. The cooling of syngas at the scrubber involves spraying of water over a scrubbing medium consisting of a low resistance, but porous large surface area. This scrubbing media usually consist of a coarse or even graded charcoal. The water used in the scrubber is recycled through an ambient pond over a long period of time. Figure 3.4 shows the picture of the gas scrubber/cooler.

Figure 3.4: Gas scrubber/cooler

The function of the saw dust filter and engine safety filter are not described in this chapter as is outside the scope of the study. Before the integration of the waste heat recovery unit around the cyclone, the surface temperature of the cyclone was measured as gasification of wood was in progress. Section 3.3 describes the measurement method used.

3.3 CYCLONE SURFACE TEMPERATURE MEASUREMENT

For the cyclone surface temperature measurement both contact (Thermocouples) and non contact (Infrared camera) temperature measuring techniques were used. The setup for the temperature measurement is shown in Figure 3.5.

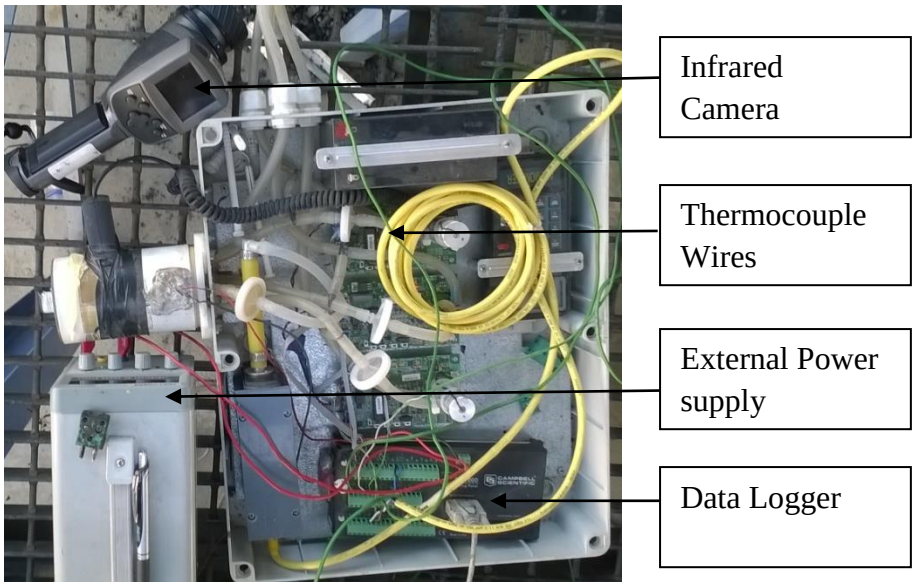

Figure 3.5: Cyclone surface temperature measurement setup

It comprises of thermocouples, CR1000 data logger, external power supply and some gas sensors. Type k thermocouples were used because of its wide operating temperature range (-270 ºC to 1260 ºC). It has a measuring accuracy of $\pm 2.2\ ^{o}C$. Two of the thermocouples were fitted on the body of the cyclone 500 mm apart so as to record the temperature at the upper and lower section of the cyclone. The reduction zone temperature and inlet temperature of synags into the cyclone were measure at this stage. The surface temperature of the cyclone was as well measured with FLIR thermaCAM (infrared camera) with a temperature range of -270 °C to 1260 °C and an accuracy of $\pm 2\ ^{o}C$. FLIR thermaCAM (infrared camera) is a non contact instrument that can visualize the temperature distribution of a surface. This section constitutes the feasibility study conducted before the construction and integration of the WHRU.

3.4 CHARACTERIZATION TECHNIQUES AND INSTRUMENTATION

Some samples of carbon particles were collected at the cyclone collection chamber and were analyzed as described in this section. The morphological surface and elemental composition of the carbon particles were studied using JSM-6390LV scanning electron microscope (SEM) and energy dispersive X-ray spectrometer (EDS). JSM-6390LV is a high performance SEM with high resolution of 3.0 nm. An electron beam from JSM-6390LV SEM was passed through the sample surface at a magnification of 1000 and accelerating voltage of 15 kV to determine the morphological features. The sample was coated with gold for clear visibility of the surface morphology. The mineral constituent was determined using X-ray diffractometer (XRD). The thermo gravimetric analysis of the sample was performed using Perkin-Elmer TGA 7, Norwalk, CT. A sample weight of 10.9 mg was placed in the analysis pan and Nitrogen was used as a

purge gas at a constant purge flow rate of 20 mL/min. The sample was held at 10 °C/min as it was heated from 20 °C to 900 °C and for 1 min at 900 °C. The weight loss by the sample and its derivative rate with respect to time and temperature were recorded as the experiment was ongoing. The heating value of the sample was determined in a previous experiment and was established to be 35.3 MJ/kg [Melapi *et al*, 2015].

3.5 GASIFICATION COMPUTER SIMULATION

3.5.1 Milligan's flaming pyrolysis zone sub-model

The basic equations utilized in the Milligan's flaming pyrolysis zone sub-model are presented in this section. The general equation for reaction of wood in flaming pyrolysis zone sub-model is given by equation (3.2). The equation assumes that 1 mole of CH_yO_z (wood) with a single carbon atom is gasified in limited supply of steam and air.

$$CH_yO_z + wH_2O + m(0.21O_2 + 0.79N_2) \rightarrow x_{char}Char + x_{tar}Tar + x_1CO + x_2H_2 + x_3CO_2 + x_4H_2O + x_5CH_4 + x_6N_2 \quad (3.2)$$

where y and z are the number of atoms for hydrogen and oxygen respectively, while that of carbon is assumed to be 1. w is the amount of water/steam gasified with wood, m is the amount of oxygen and nitrogen per mol of wood, x_{char}, x_{tar}, x_1, x_2, x_3, x_4, x_5 and x_6 are the coefficients of char, tar, hydrogen, carbon monoxide, methane, nitrogen. Note that char is represented as carbon and tar is represented as $CH_{1.03}O_{0.03}$ according to Adams [1980]. A combination of water-gas

reaction and Boudouard reaction which are the major gasification reactions will give the equilibrium equation given by equation (3.3).

$$CO + H_2O \leftrightarrow CO_2 + H_2 \tag{3.3}$$

The corresponding equilibrium constant for equation in (3.3) is given in equation (3.4)

$$K = \frac{x_3 \cdot x_2}{x_1 \cdot x_4} \tag{3.4}$$

Equation (3.5) gives the correlation between the equilibrium constant for the above reactions and temperature (Kelvin) [Gumz, 1950]

$$Log(K) = -36.725 + \frac{3994.704}{T} - 4.462 \times 10^{-3} T + 6.718 \times 10^{-7} T^2 + 12.220 \log(T) \tag{3.5}$$

In order to solve the unknown coefficients of the products in equation (3.2), the following mass balances for carbon, hydrogen, oxygen, nitrogen were formulated as given by equation (3.6) to (3.9)

Carbon balance:

$$1 = x_{char} + x_{tar} + x_1 + x_3 + x_5 \tag{3.6}$$

Hydrogen balance:

$$y + 2w = 1.03x_{tar} + 2x_2 + 2x_4 + 4x_5 \tag{3.7}$$

Oxygen balance:

$$z + w + 0.42m = 0.03x_{tar} + x_1 + x_3 + x_4 \tag{3.8}$$

Nitrogen balance:

$$1.58m = x_6 \tag{3.9}$$

Heat balance in flaming pyrolysis zone is then given by equation (3.10)

$$H_c Wood = H_c Char + H_c Tar + H_c Gas + H_s Char + H_s Tar + H_s Gas + Heat\ Loss \tag{3.10}$$

And *w* which represents the amount of water or steam gasified with the mole of fuel wood is given as

$$w = (12 \times 1 + 1 \times y + 16 \times z) mc_{db} kg \tag{3.11}$$

where mc_{db} is the moisture content of wood on dry basis, x and y are given, heat loss and m are experimentally derived, the values of x_5, x_{char}, and x_{tar} are assumed, x_1, x_2, x_3, x_4, x_6 and T are solved by using the successive approximation method with a Fortran programme. The higher heating value of fuelwood, char and tar are determined from equation (3.12) given by Channiwala [1992] as shown

$$H_{cWood} = 0.349 f_C + 0.178 f_H - 0.103 f_O$$

$$H_{cChar} = 0.349 \times f_{C,char} \qquad (3.12)$$

$$H_{cTar} = 0.349 \times f_{C,tar} + 0.178 f_{H,tar} - 0.103 f_{O,tar}$$

Then the chemical heat content of output gas, sensible heat of char, tar and output gas is determined as follow:

$$H_{CGas} = 241000 x_1 + 283000 x_2 + 802300 x_5$$

$$H_{SChar} = 12.15 \times x_{char} \times (\text{T-300})$$

$$H_{STar} = 21.95 \times x_{tar} \times (T - 300) \qquad (3.13)$$

$$H_{SGas} = (x_1 \times H_{CO}) + (x_2 \times H_{H_2}) + (x_3 \times H_{CO_2}) + (x_4 \times H_{H_2O}) + (x_5 \times H_{CH_4}) + (x_6 \times H_{N_2})$$

The equations were then solved using a successive approximation method and a computer programme formulated using FORTRAN language.

3.5.2 Gasification zone sub-model

In gasification zone sub-model, the output of flaming pyrolysis zone serves as the input values of the first interval. Char is assumed as pure carbon, while nitrogen and ash content of the wood were considered negligible. In addition, particles were assumed to be spherical in shape and that the end of the gasification zone is attained as the carbon particle concentration goes below 5% of the initial char concentration. The modeling of this zone involved following a carbon particle along the axis of the gasifier. Product composition of the zone was calculated using a small time increment approach. It involves the use of a step procedure beginning from the gasification zone and marches through the reactor axially in appropriate time increment [Jayah, 2002].

3.6 COMPUTATIONAL FLUID DYNAMIC MODELING

A rectangular waste heat recovery unit (WHRU) was modeled and simulated with Autodesk simulation computational fluid dynamic (CFD) 2015. The geometry of the WHRU was chosen based on the geometry of the cyclone, which the WHRU is encasing. The model drawing was created in computer aided design (CAD) software before exporting to the CFD software. Figure 3.6 shows the WHRU model.

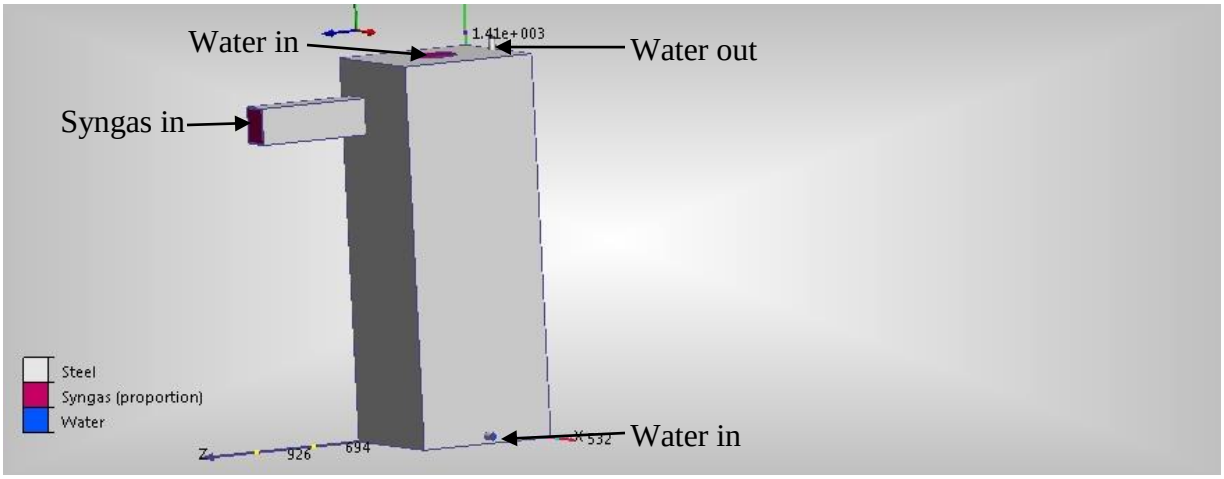

Figure 3.6: Waste heat recovery unit model

The next step was assignment of materials to all parts of the model and definition of material properties which are the foundation of the simulation analysis. One solid and two fluids materials which include steel, syngas and water were assigned to the WHRU. The material properties for the solid (steel) and fluids (syngas and water) materials are defined as shown in Table 3.2.

Table 3.2: Properties of materials used for simulation

NAME	ASSIGNED TO	PROPERTIES	
Steel	Union rectangular water jacket solid 2 in mmFusionCopy:0	X-Direction	Piecewise Linear
		Y-Direction	Same as X-dir.
		Z-Direction	Same as X-dir.
		Density	7850.0 kg/m^3
		Specific heat	510.78 J/kg-K
		Emissivity	0.3
		Transmissivity	0.0
		Electrical	1.6e-07 ohm-m
		Wall roughness	0.0 meter
Syngas	CFDCreatedVolume	Density	9.734e-07 g/mm3
		Viscosity	9.8e-06 Pa-s
		Conductivity	0.0242 W/m-K
		Specific heat	3999.04 J/kg-K
		Compressibility	1.32
		Emissivity	1.0
		Wall roughness	0.0 meter
		Phase	Vapor Pressure
Water	CFDCreatedVolume	Density	Piecewise Linear
		Viscosity	0.001003 Pa-s
		Conductivity	0.6 W/m-K
		Specific heat	4182.0 J/kg-K
		Compressibility	2185650000.0 Pa
		Emissivity	1.0
		Wall roughness	0.0 meter
		Phase	Linked Vapor

The density of water and steel are known but the density of syngas was determined according to equation (3.14)

$$\rho_{syngas} = \frac{\left(\rho_1 v_1 + \rho_2 v_2 + \rho_3 v_3 + \rho_4 v_4 + \rho_5 v_5\right)}{\left(v_1 + v_2 + v_3 + v_4 + v_5\right)} \tag{3.14}$$

where ρ_1, ρ_2, ρ_3, ρ_4 and ρ_5 are the densities of hydrogen (H_2), carbon monoxide (CO), methane (CH_4), carbon dioxide (CO_2) and nitrogen (N_2) respectively, v_1, v_2, v_3, v_4 and v_5 are the percentage volume of these gases.

In the WHRU model, syngas was considered as hot fluid while water is considered as cold fluid. The hot fluid was modeled as a gas with volume flow rate of 100 m^3/h found from the gasifier specification and inlet temperature of 350 °C found from experiment. In addition the cold fluid represented with water had an inlet temperature of 20 °C and a variable volume flow rate. These boundary conditions define the inputs to the simulation model and effectively connect the model with actual experimental design. An automatic mesh setting, mesh enhancement settings were applied prior to running the simulation and the meshed model is as shown in Figure (3.7)

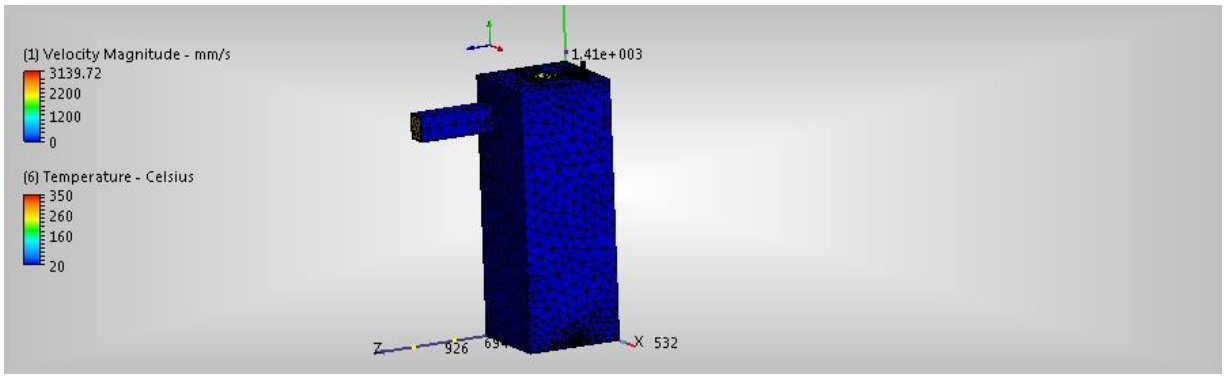

Figure 3.7: Meshed model of the waste heat recovery unit

The meshed model was constructed according to the prescribed element distribution. An element number of 94237 and node number of 26315 were applied. Mesh was created generally to capture the flow and heat transfer gradient. The heat transfer analysis and equation for flow of fluid were then solved using fluent embedded in CFD.

3.6.1 CFD Governing Equation

The equations governing fluid flow and heat transfer analysis are continuity equation, the Navier-Stokes equations and the energy equation. These equations were modified according to conditions of the simulation setup. The continuity equation (3.15) was modified as given in equation (3.16).

$$\frac{\partial \rho}{\partial t} + \frac{\partial (\rho u)}{\partial x} + \frac{\partial (\rho v)}{\partial y} + \frac{\partial (\rho w)}{\partial z} = 0 \tag{3.15}$$

For incompressible fluid, fluid density is constant

$$\frac{\partial u}{\partial x} + \frac{\partial v}{\partial y} + \frac{\partial w}{\partial z} = 0 \tag{3.16}$$

X momentum is:

$$\begin{aligned} &\rho \frac{\partial u}{\partial t} + \rho u \frac{\partial u}{\partial x} + \rho v \frac{\partial u}{\partial y} + \rho w \frac{\partial u}{\partial z} = \\ &\rho g_x - \frac{\partial p}{\partial x} + \frac{\partial}{\partial}\left[2\mu \frac{\partial u}{\partial x} \right] + \frac{\partial}{\partial y}\left[\mu \left(\frac{\partial u}{\partial y} + \frac{\partial v}{\partial x} \right) \right] + \frac{\partial}{\partial z}\left[\mu \left(\frac{\partial u}{\partial z} + \frac{\partial w}{\partial x} \right) \right] + S_\omega + S_{DR} \end{aligned} \tag{3.17}$$

Y momentum is:

$$\rho\frac{\partial v}{\partial t}+\rho u\frac{\partial v}{\partial x}+\rho v\frac{\partial v}{\partial y}+\rho w\frac{\partial v}{\partial z}=$$
$$\rho g_y-\frac{\partial p}{\partial y}+\frac{\partial}{\partial x}\left[\mu\left(\frac{\partial u}{\partial y}+\frac{\partial v}{\partial x}\right)\right]+\frac{\partial}{\partial y}\left[2\mu\frac{\partial v}{\partial y}\right]+\frac{\partial}{\partial z}\left[\mu\left(\frac{\partial v}{\partial z}+\frac{\partial w}{\partial y}\right)\right]+S_\omega+S_{DR} \quad (3.18)$$

And Z momentum is :

$$\rho\frac{\partial w}{\partial t}+\rho u\frac{\partial w}{\partial x}+\rho v\frac{\partial w}{\partial y}+\rho w\frac{\partial w}{\partial z}=$$
$$\rho g_z-\frac{\partial p}{\partial z}+\frac{\partial}{\partial x}\left[\mu\left(\frac{\partial u}{\partial z}+\frac{\partial w}{\partial x}\right)\right]+\frac{\partial}{\partial y}\left[\mu\left(\frac{\partial v}{\partial z}+\frac{\partial w}{\partial y}\right)\right]+\frac{\partial}{\partial z}\left[2\mu\frac{\partial w}{\partial z}\right]+S_\omega+S_{DR} \quad (3.19)$$

The two source terms S_ω and S_{DR} in the momentum equations are for rotating coordinates and distributed resistances respectively. For incompressible flow the energy equation used is shown

$$\rho C_p\left[\frac{\partial T}{\partial t}+u\frac{\partial T}{\partial x}+v\frac{\partial T}{\partial y}+w\frac{\partial T}{\partial z}\right]=\frac{\partial}{\partial x}\left[k\frac{\partial T}{\partial x}\right]+\frac{\partial}{\partial y}\left[k\frac{\partial T}{\partial y}\right]+\frac{\partial}{\partial z}\left[k\frac{\partial T}{\partial z}\right] \quad (3.20)$$

where the variables in the equation are described in Table 3.3

Table 3.3: Definition of variables

Symbols	Meaning
C_p	Specific heat capacity at constant pressure
g_x, g_y, g_z	Gravitational acceleration in x, y, z direction
K	Thermal conductivity
P	Pressure
T	Temperature
T	Time
U	Velocity component in x-direction
V	Velocity component in y-direction
W	Velocity component in z-direction
μ	Viscosity
ρ	Density

3.7 WASTE HEAT RECOVERY UNIT DESIGN AND CONSTRUCTION

3.7.1 Dimensional view of WHRU

The side views, three dimensional view, top and bottom view of the waste heat recovery unit (WHRU) along with their respective dimensions are shown in Figure 3.8. The design was made using an inventor based on the specifications of the cyclone dust collector.

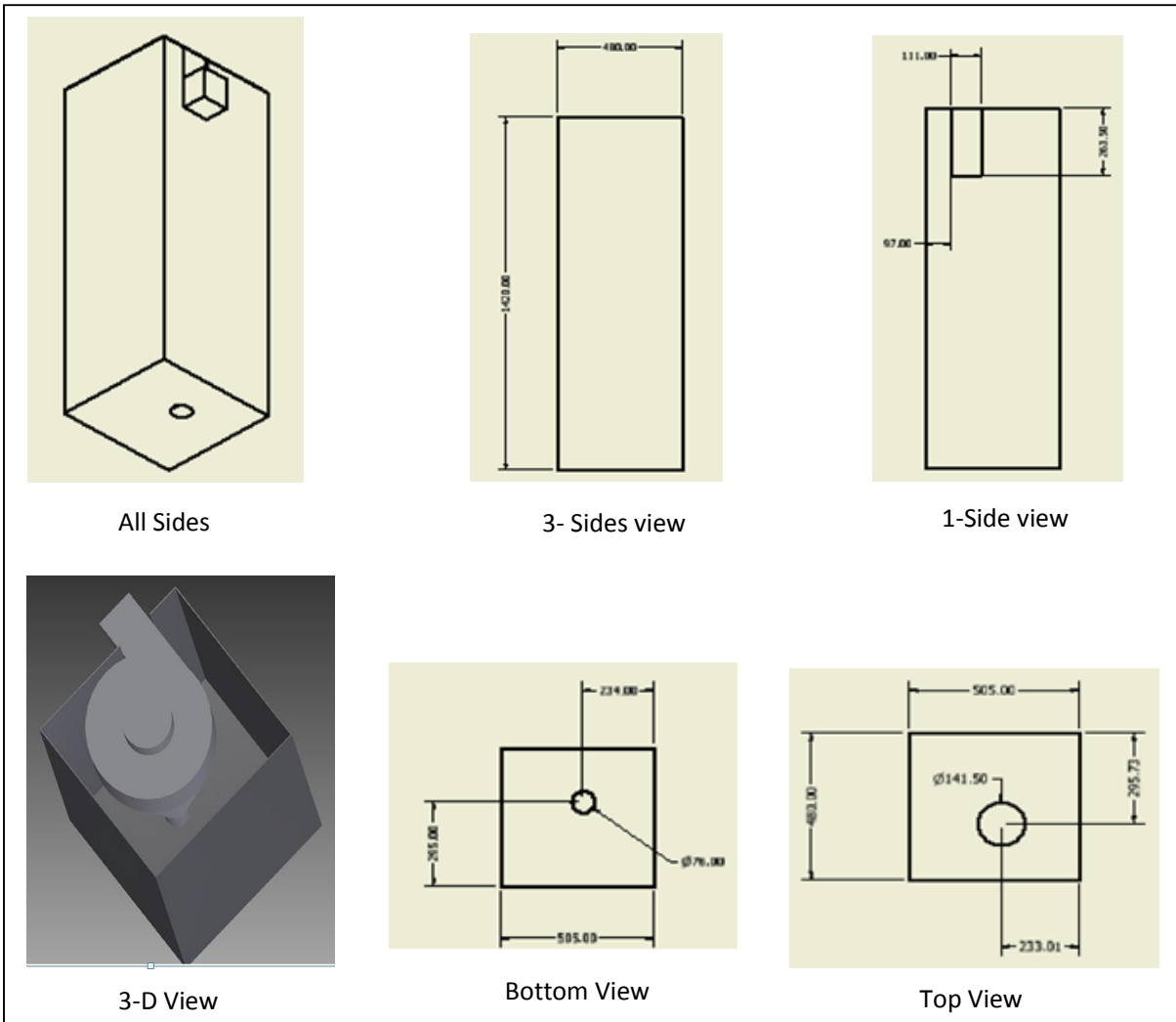

Figure 3.8: Dimensional view of WHRU

3.7.2 Materials of construction

Mild steel sheets were used in the construction of the waste heat recovery unit. Mild steel was chosen because is ductile, tough and malleable. It is less expensive when compared to stainless steel hence making it more suitable for local use. Mild steel has an excellent weldability due to low composition of carbon. The chemical composition of the mild steel material used is given in Table 3.4.

Table 3.4: Chemical compositions of mild steel

Element	**Composition**
Carbon	0.14 – 0.2%
Iron	98.81% - 99.26%
Manganese	0.6% - 0.9%
Phosphorus	≤ 0.04%
Sulfur	≤ 0.05%

As observed from Table 3.3, the mild steel material used was made by adding carbon and other elements in an iron. These elements attribute to the hardness, ductility and tensile strength of mild steel. Mild steel sheets with thicknesses of 3.0 mm, length of 2500 mm and width of 1225 mm were cut to get the different parts of the WHRU as shown in Figure 3.9. Angle irons were used to support the edges of WHRU and to allow for proper welding of the edges in order to prevent leakages.

Figure 3.9: Sections of the waste heat recovery unit

The parts shown in figure 3.9 were formed into a unit around the cyclone dust collector of the gasifier system. A drilling machine was used to create holes at the top and bottom section so as to fit at the vortex finder and collection chamber of the cyclone. More holes were also drilled at the sides where valves were fitted for water discharge and thermocouples for performance test. These parts were welded at the edges and onto the body of the cyclone using MAC-AFRIC™

200 Amp Inverter Arc welding machine and 2.5 mm mild steel arc welding rods. The feature of the arc welding machine is presented in Table 3.5.

Table 3.5: Welding Machine Configuration

Parameters	**Values**
Input current	23A – 32 A (AC)
Output current	200A (DC)
Input voltage	220V (AC)
Output voltage	21V – 28V (DC)
Duty Cycle	60%

After the welding together of the parts and onto the cyclone dust collector, the WHRU was filled with water to test for leakage. When the leakage test proved satisfactory, the WHRU was painted so as to prevent corrosion. The volume of water that the WHRU will hold was determined using equation (3.21)

$$V_{water} = V_{WHRU} - V_{cyclone}$$
$$\text{and} \qquad (3.21)$$
$$V_{cyclone} = V_{cylinder} + V_{cone}$$

where V_{WHRU} is the volume of waste heat recovery unit, $V_{cyclone}$ is the volume of cyclone, $V_{cylinder}$ is volume of cylinder and V_{cone} is volume of cone. Hence the volume of water in the WHRU was determined to be 0.267 m^3 which is equivalent to 267 litres.

The WHRU was insulated at a later stage when the system was under test using insulation blanket made of glass wool with 50 mm thickness and thermal conductivity of 0.039 W/mK. Figure 3.10a shows the cyclone before integration of WHRU, 3.10b shows the integrated WHRU and 3.10c show when the WHRU was insulated.

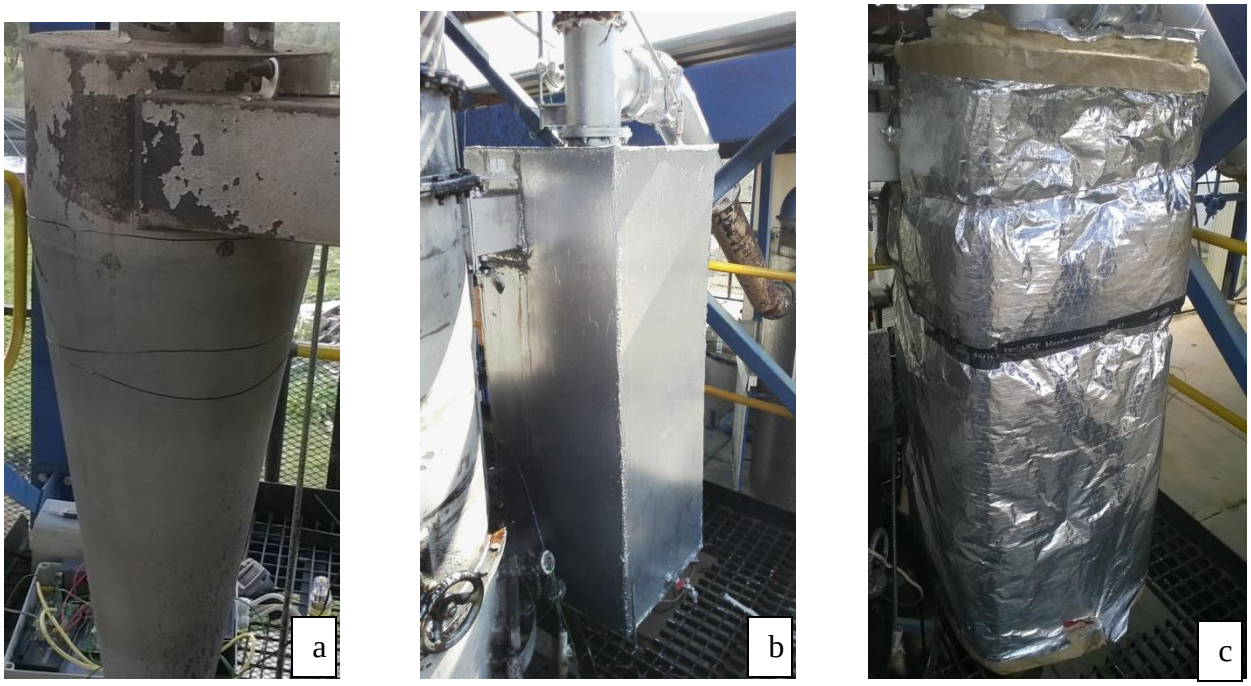

Figure 3.10: (a) Cyclone before integration of WHRU (b) Waste heat recovery unit after integration (c) insulated WHRU

3.8 PERFORMANCE TEST FOR WHRU

After the integration of the WHRU, the reactor section (gasifier) of the gasification system was loaded with about 424 kg of wood cut to sizes of 75 x 68 x 43mm. Air containing oxygen and some non-reactive gases such as nitrogen was blown into the oxidation zone through the air nozzles so as to enhance the combustion process. The waste heat recovery unit was filled with water to be heated before the ignition of the downdraft gasifier. The gasifer was then ignited through an opening at the reduction zone. Type-K thermocouples were inserted into the inlet duct and outlet duct of the cyclone so as to monitor the inlet and outlet temperature of the syngas as the gasification of the wood was in progress. Water temperature inside the WHRU was as

well monitored by inserting two thermocouples at the top and middle section of the WHRU because of the temperature difference that existed at the upper and lower section of the cyclone enclosed in the WHRU. This first set of experiment for the WHRU did not involve water flow as the aim at this stage was to monitor the water heating profile over an interval of time. In the second set water flow rate was varied using a control valve from 1litre/min – 4litre/min which corresponded to 0.02 kg/sec - 0.07 kg/sec.

3.8.1 Energy estimation for WHRU

In the determination of the energy balances for the hot fluid (syngas) and cold fluid (water) the following equations were used. At constant specific heat, the quantity of heat emitted by the syngas and absorbed by the water is shown in equation (3.22) and (3.23) respectively.

$$Q_e = \left(mC_p\right)_h \left(T_{h,i} - T_{h,o}\right) \tag{3.22}$$

$$Q_a = \left(mC_p\right)_c \left(T_{c,o} - T_{c,i}\right) \tag{3.23}$$

where m_h, m_c is Mass flow rate of syngas and water respectively, C_{ph}, C_{pc} is Specific heat capacity of syngas and water respectively, $T_{h,i}$, $T_{c,i}$ is Inlet temperature of syngas and water respectively, $T_{h,o}$, $T_{c,o}$ is Outlet temperature of syngas and water respectively.

Bearing in mind that the waste heat recovery unit was constructed using steel sheet, heat losses also called standing losses through the body of the WHRU were accounted for and determined using equation (3.24) [Delport, 2005].

$$Q_{loss} = \left[\frac{(T_h - T_{amb})}{\frac{\Delta x}{k} + \frac{1}{h}} \right] \tag{3.24}$$

where Q_{loss} is heat loss in W/m^2, T_h is water temperature inside the WHRUin °C, T_{amb} is air temperature outside the WHRU in °C, Δx is insulation layer thickness in m, k is thermal conductivity of the insulation layer in W/mK and h is Surface heat temperature coefficient in W/m^{2}K.

CHAPTER FOUR

RESULT AND DISCUSSION

4.1 INTRODUCTION

The gas leaving the reactor of a downdraft biomass gasifier contains large quantities of heat energy; this is due to the fact that the gas passes through a hot bed of charcoal before leaving the reactor. This heat is normally wasted in the gas scrubber/cooler that cools it from between 400°C -500 °C to ambient temperature (around 25 °C). The waste heat stream under consideration is the raw syngas that emanates from a gasification process in a downdraft gasifier situated at Melani village, Eastern Cape. This loss of heat is undesirable as it impacts on the thermal efficiency of the system. This chapter presents the result of the investigations carried out in order to determine the feasibility of recovering heat at the cyclone dust collector

4.2 BASELINE TEST

In assessing the potential of recovering heat from any system, one of the parameters of significance is temperature. The magnitude of the temperature difference between the heat source and heat sink determines the quality of heat to be recovered. In this study the heat source is the hot syngas stream and the aim is to recover the heat from the surface of the cyclone prior to the gas entering the scrubber. But prior to the actual heat recovery there is a need for baseline

study so as to determine the possible quantity of heat energy that could be recovered from the surface of the cyclone. Figure 4.1 presents the inlet gas temperature profile and cyclone surface temperature profile.

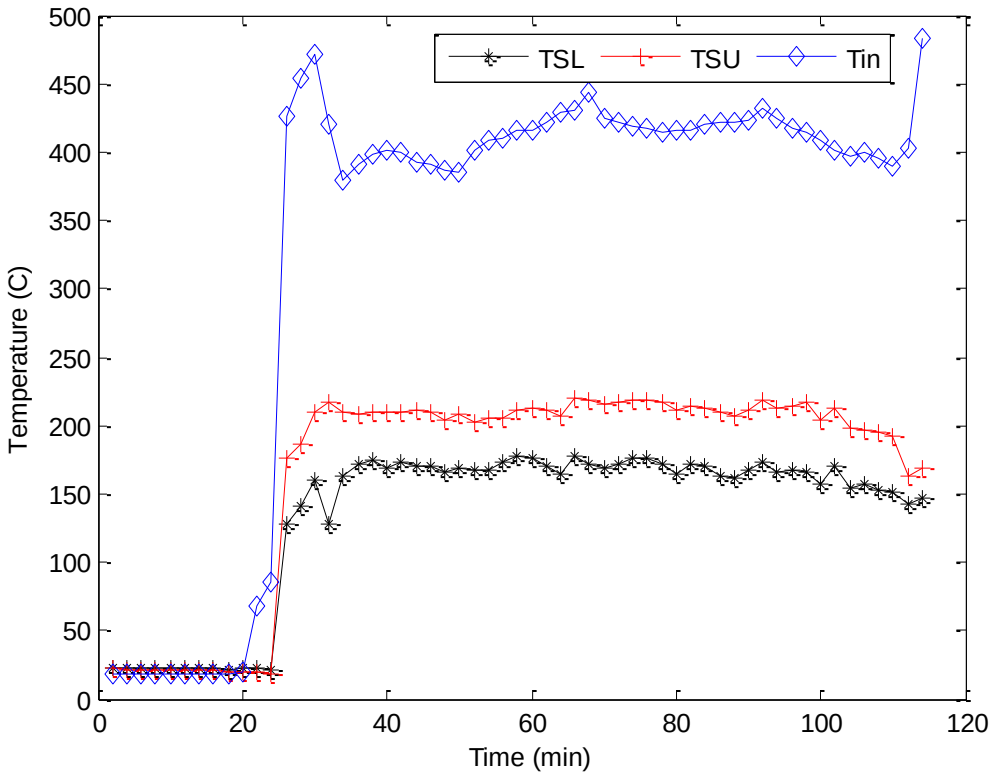

Figure 4.1: Gas inlet and cyclone surface temperature profile within the first 120mins

Prior to starting of the gasifier system the temperature of the syngas entering the cyclone (Tin) and cyclone surface temperatures (TSL and TSU) were 18.79 ºC, 22.59 °C and 21.31 ºC respectively. After the ignition of the gasifier the temperature of the gas entering the cyclone was the first to show an increase while the two surface temperatures followed after 5 minutes. This is because the syngas needs to first occupy the volume of the cyclone before heat dissipation

begins. A maximum temperature of 608.8°C was obtained from the syngas stream as it exits the reduction zone of the gasifier. This temperature obtained is due to the reduction reactions shown in equations (4.1) and (4.2) that take place at the reduction zone as the products of combustion go through a red hot charcoal.

$$C + CO_2 \leftrightarrow 2CO \ (+172.5\ kJ / mol) \tag{4.1}$$

$$C + H_2O \leftrightarrow CO + H_2 \ (+131.3\ kJ / mol) \tag{4.2}$$

These endothermic reactions: Boudouard (4.1) and water gas (4.2) reduces the gas temperature at the reduction zone because of the energy used in formation of their products. Guangul *et al* [2013] obtained a similar temperature profile for gas outlet temperature, the temperature increased from about 50 ºC to a maximum of 600 ºC. In addition, the obtained gas temperature of 608.8 ºC did not differ much from the temperature range (623 ºC - 700 ºC) obtained by Balas *et al* [2012]. This was the temperature range within which Balas *et al* [2012] obtained the individual gas components: H_2, CO_2, CH_4, N_2, CO.

As the gas stream approached the cyclone inlet duct, a decrease in temperature was observed as shown by Tin in Figure 4.1. This is as a result of the utilization of some of the sensible heat of the syngas in heating the air entering the gasifier through an internal heat exchanger. Hence there is no waste of heat in this regard. There were fluctuations in the temperature profiles, particularly the temperature of the gas entering the cyclone within the first 120mins of operation. Similarly the gas outlet temperature profile obtained by Guangul *et al* [2013] showed some fluctuation as it was increasing. This is also in agreement with the different zone temperature

profiles reported by Mamphweli and Meyer, [2013]. Afterwards, some stability was recorded as shown in Figure 4.2

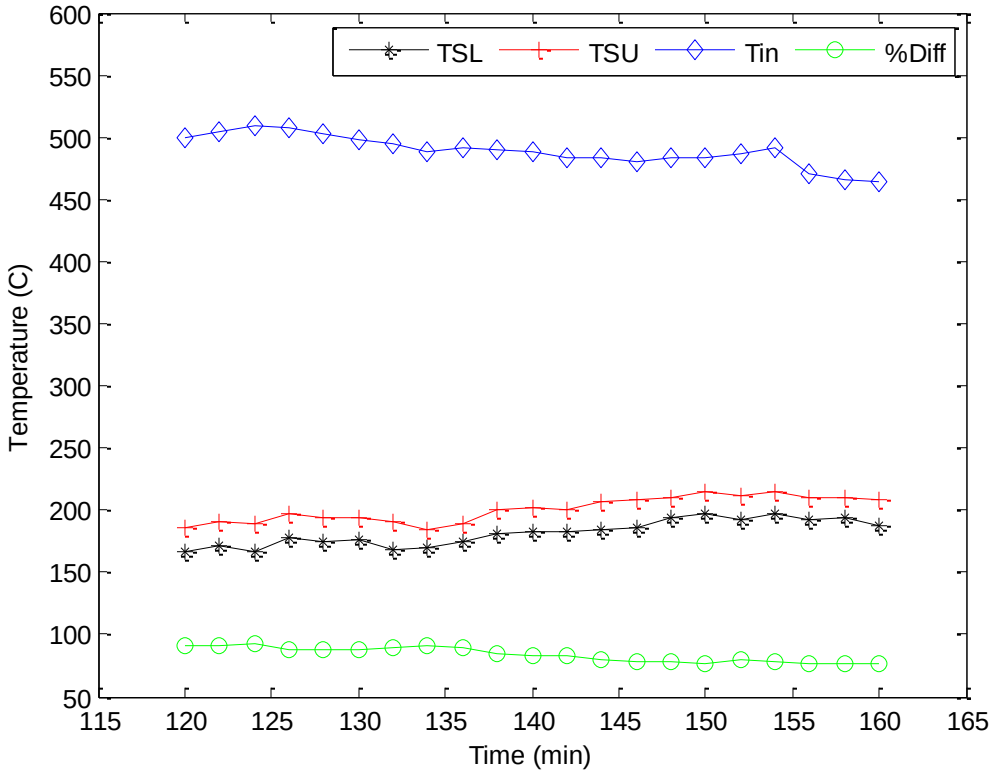

Figure 4.2: Gas inlet and cyclone surface temperature profile after the first 120mins

The percentage difference (%Diff) of 65% between the temperature of the syngas entering the cyclone and the surface temperature of the cyclone showed that not all the heat from the syngas is dissipated on the body of the cyclone. But some significant portion is still carried away by the syngas and eventually cooled at the gas scrubber which is the next point of entrance for the synags. This then suggests that there is more than one opportunity for heat recovery at the biomass gasification unit. From Figure 4.2, the syngas temperature was observed to be within a

temperature range of 450 ºC-500 ºC while the two surface temperatures ranged from about 150 ºC-220 ºC.

Comparing this result with that reported by Ma *et al* [2015] in which the temperature of the gasifier outlet was about 350 ºC-500 ºC and surface temperature of the catalytic reactor is approximately 200 ºC-360 ºC. The two gas temperatures compared very closely. The difference is that the heat recovery in Ma *et al* [2015] study occurred at the catalytic reactor while in the current study the heat recovery is intended to take place at the cyclone. However there are some similarities in terms of the position of the heat recovery unit, in both cases heat is recovered from the gas before entering the wet scrubber. For maximum heat recovery to occur the position of the heat recovery unit is important as well as the choice of the heat recovery equipment. In addition the surface temperature (TSU) at the upper part of the cyclone was found to be higher than the surface temperature (TSL) at the lower part of the cyclone as shown in figure 4.2. Hence a thermal image of the cyclone was taken for further analysis. The temperature gradient obtained from the thermal image is shown in Figure 4.3.

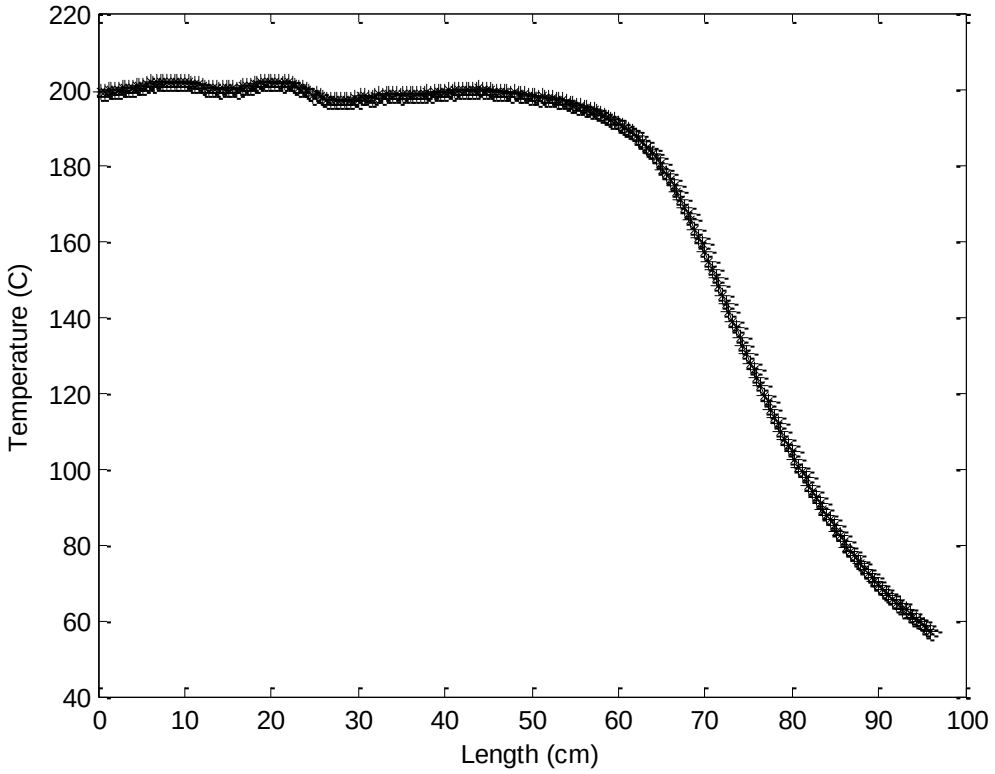

Figure 4.3: Temperature gradient along the length of the cyclone

The temperature gradient along the length of the cyclone shown in Figure 4.3 was obtained using a FLIR thermal camera. There is a downward decrease of temperature along the length of the cyclone as shown in Figure 4.3. As observed from Figure 4.3 the highest obtained temperature was around 200 ºC which compares closely to the surface temperatures measured using thermocouple shown in Figure 4.2. However the maximum cyclone surface temperature measured using thermocouple was 220 °C which is about 20 °C higher than that obtained from the thermal camera. This is attributed to the fact that thermocouple uses a direct contact measurement mechanism while FLIR thermal camera uses an indirect contact measurement

mechanism. Figure 4.3 shows that a larger part of the decrease in temperature occurred at the lowest part of the cyclone which is closer to the collection chamber of the particulates. This major decrease is represented between 59 cm to 97 cm which corresponds to the lowest part of the cyclone. The decrease in temperature could be attributed to more deposit of particulates from the syngas on the lower part of cyclone, thus, inhibiting the ease of heat transfer. Secondly, because the syngas enters from the top of the cyclone consequently, the upper part gets heated up first. The actual thermal image (Thermogram) is presented in Figure 4.4

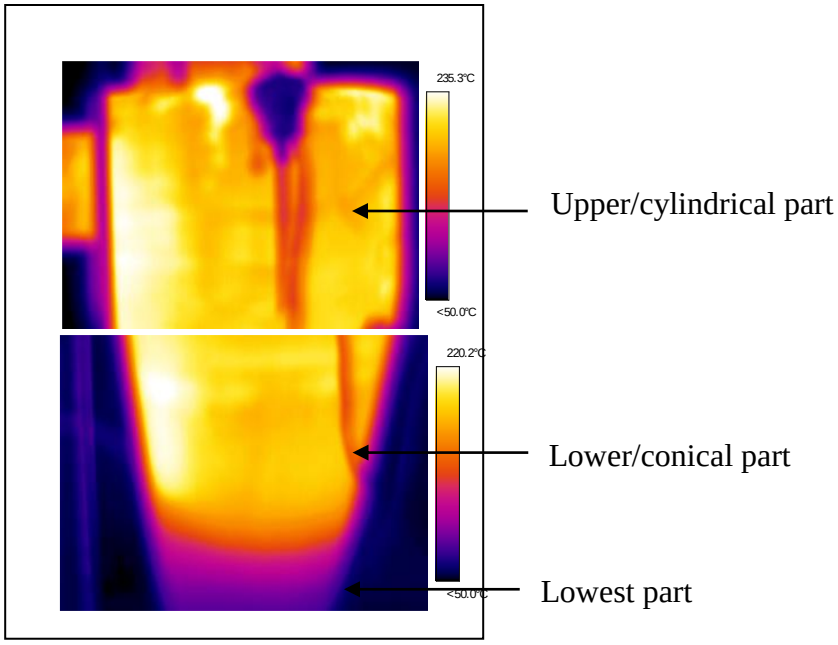

Figure 4.4: Thermal image of the cyclone

The two images shown in Figure 4.4 were taken within an interval of one minute so the time difference was assumed to be negligible. Figure 4.4 represents the thermal energy that is radiated through the surface of the cyclone. It provides the approximate surface temperature of the cyclone. The temperature of the syngas entering the cyclone falls within the medium temperature range while the surface temperature as detected from the thermal image is within low temperature range for waste heat temperature classification. Hence a heat recovery unit such as cold water jacket that can transform low level heat into valuable use has to be integrated. Basically there are three classifications of waste heat temperature (as shown in Table 4.1) for various waste heat recovery opportunities.

Table 4.1: Waste heat temperature classifications and some source examples [USDOE, 2008]

Type	**Temperature range**	**Example source**
High	1650ºC – 649°C	Hydrogen plant, Fume incinerator
Medium	650ºC – 230°C	Gas turbine exhaust, Catalytic crackers
Low	232ºC and lower	Welding machines, Annealing Furnaces

One basic advantage of the medium and low temperature range is in its compatibility with heat exchanger materials which is a good motivation for the present study. It was also essential to quantify the total heat that could be recovered from the syngas stream if it were to be cooled from about 500 °C to 25 °C. This is typical of the temperature to which it is cooled to at the gas scrubber/cooler. Hence the total quantity of heat contained in the syngas was determined using equation (4.3) and parameters presented in Table 4.2.

$$Q = V \times \rho \times C_p \times \Delta T \qquad (4.3)$$

where Q is the heat content in kcal, V is the flow rate of the substance in m^3/hr, ρ is density of the flue gas in kg/m^3, C_p is the specific heat of the substance in kcal/kg ºC and ΔT is the temperature difference in °C.

Table 4.2: Parameters for estimation of heat quantity

Item	**H_2**	**N_2**	**CH_4**	**CO**	**CO_2**	**Total**
Molar mass (g/mol)	2.02	28.01	16.04	28.01	44.01	118.09
% Composition of gas	22.30±0.1	42.90±0.7	1.90±0.1	22.30±1	10.70±0.4	100.10
Mass (g)	2.01	53.65	1.36	27.89	21.02	105.93
Specific heat capacity(J/g °C)	3.19	0.44	0.04	0.23	0.09	3.99

The volumetric flow rate of the syngas was assumed to be 300 Nm^3/h based on the specifications of the gasification system. A total gas density of 0.9734 kg/m^3 was determined from the molar mass, mass percentage composition of gases presented in Table 4.2. The specific heat capacity (at constant pressure) presented in Table 4.2 was converted to kcal/kg °C for consistency in units. The initial temperature of 25 °C was subtracted from the maximum temperature attained by the syngas entering the cyclone to obtain the temperature difference. The estimated quantity of heat would inform on the best heat recovery method to adopt. Some typical heat recovery methods include water heating, combustion air preheating, steam generation, feed water preheating and transfer to a low temperature process [US DOE, 2008].

4.3 CARBON PARTICLE CHARACTERIZATION

4.3.1 Morphology and elemental composition of carbon particles

Although the presence of carbon particles in the syngas does not affect the quality and quantity of heat contained in the syngas, it does influence the heat recovery process and choice of materials to be used for the recovery. Hence the carbon particles collected at the collection chamber of the cyclone dust collector were characterized. The morphology and elemental composition of carbon particles are of great importance due to possible deposition of these particles on heat recovery unit surfaces when extracting heat from particle laden syngas. Figure 4.5 presents the SEM image and EDS spectrum of the carbon particles investigated.

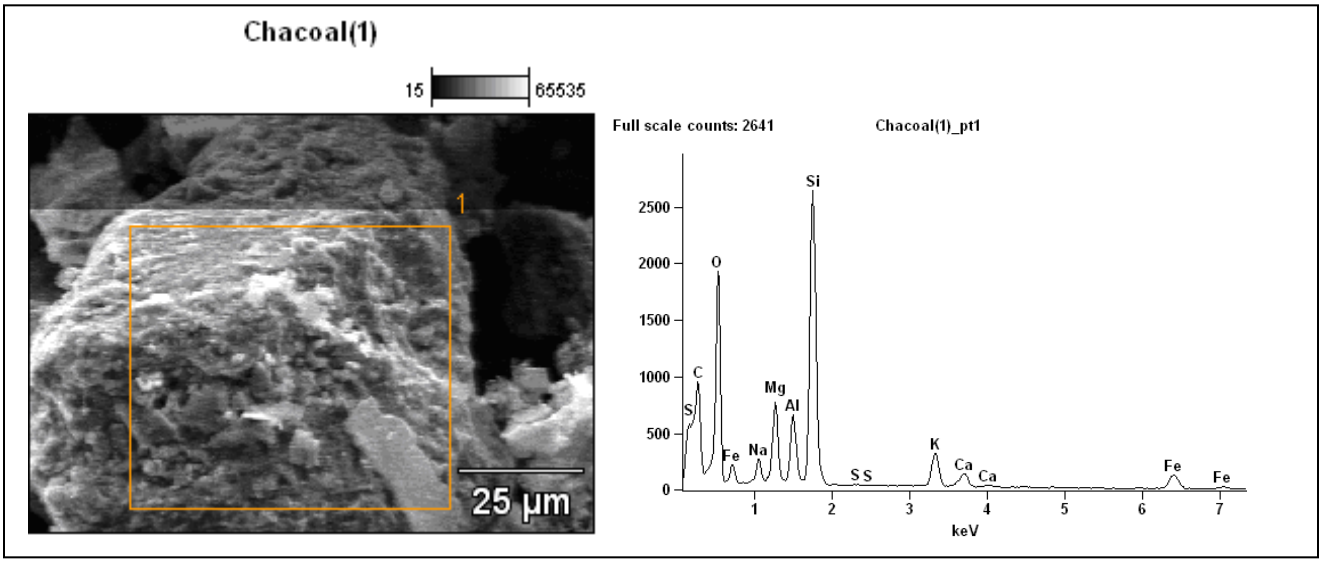

Figure 4.5: SEM image with EDS spectrum of carbon particles

The morphological structure of carbon particle sample presented in Figure 4.5 show that they consist of different elements at varying concentration in a lumped form. The lump of elements could be as a result of condensation of gaseous organic molecules during gasification. The particle size of 25 µm obtained for the carbon particles exceeds the size reported by world health organization that poses a threat to public health due to the ease with which it can readily reach the respiratory tracts when inhaled [San Miguel *et al*, 2012]. Table 4.3 presents the elemental compositions of the carbon particle analyzed using EDS in combination with SEM.

Table 4.3: EDS analysis of carbon particles

	Element (wt %)									
PS (µm)	C	O	Na	Mg	Al	Si	S	K	Ca	Fe
25	20.35	34.38	1.56	4.96	3.98	19.68	0.13	4.19	2.09	8.67

From table 4.3 it can be observed that carbon (C) and oxygen (O) are the only light elements that were detected from the sample. This is expected, bearing in mind that EDS has a low accuracy in detection of light elements. Carbon and oxygen are significantly higher than the rest of the elements with exception of silicon. High concentration of oxygen and some other ions such as iron (Fe) and sulphate can lead to corrosion of heat recovery equipments when carbon particles are deposited on them over time. Although it is also reported that oxygen can play a protective role sometimes by creating a passive film. But at high temperature this protective film is more likely to break due to lower rate of oxygen solubility [Addepalli, *et al*, 2015]. Silicon (Si) was found in significant concentration (19 wt %) as compared to sulphur (S) that was the least in concentration (0.13 wt %). This compares very closely with 16.1 wt% of Si and 0.2 wt% of S

reported for large spherical particles of fine slag. However the other classifications of fine slag, adhesive spherical fines, floccules, porous irregular particles and coarse slag differed in the concentration of Si and S [Pan *et al*, 2015]. Silicon at present is reported to have no negative effect on heat recovery equipment but sulphur does as sulphate is listed as one of the ions that cause corrosion. However sulphur concentration in the carbon particle is very minimal.

The presence of alkali and alkaline earth metals potassium (K), sodium (Na), magnesium (Mg) and calcium (Ca) could lead to formation of deposits on heat recovery equipment surface when used in direct contact heat transfer mechanism. In addition to these alkali and alkaline earth metals, chlorine is also identified as an important fouling facilitator on heat transfer surfaces [Lund *et al*, 2015]. Fouling leads to scale formation on heat transfer surface which consequently causes a decrease in heat flux and an increase in temperature of fluid that supposed to be cooled [Demadis, 2003]. Corrosion and fouling are the two identified failure mechanism that could occur if direct contact heat recovery equipment is used for recovery heat from the syngas due to the presence of carbon particles in the syngas. Hence an indirect contact heat transfer mechanism was adopted for this study.

4.3.2 Thermal characteristics

Figure 4.6 presents the weight loss underwent by the carbon particle sample when it was heated in a TGA from a temperature of 20°C to 900°C and the derivative of the sample weight with

respect to time. The heating temperature range represents a typical gasification temperature and the heating occurred under an inert atmosphere.

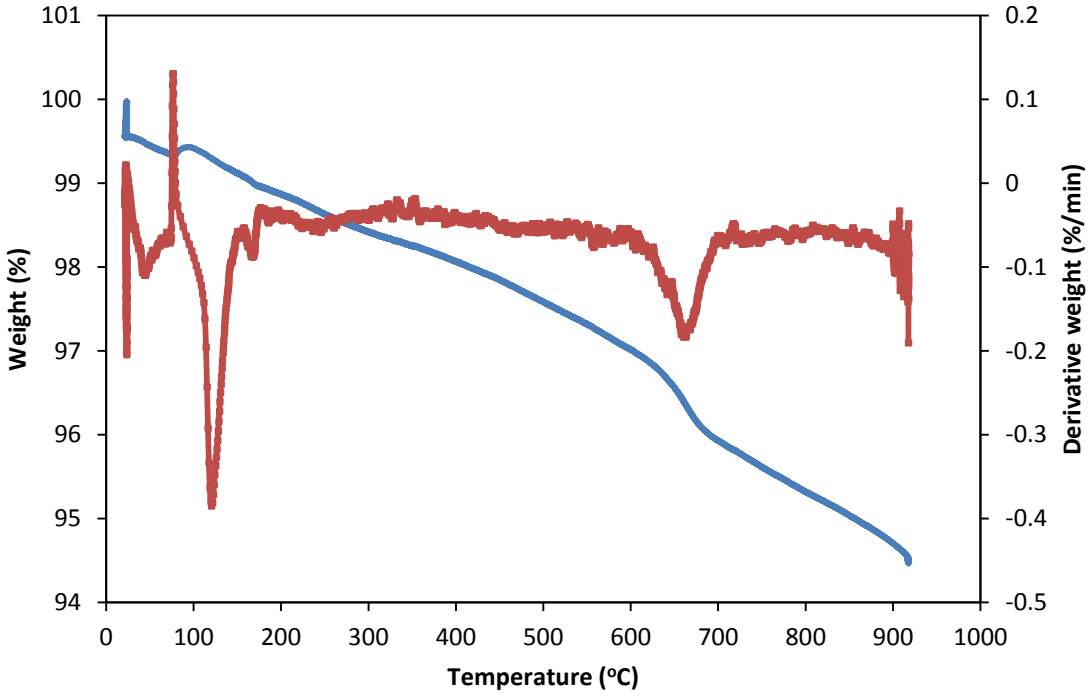

Figure 4.6: TGA and DTG plot of carbon particle in nitrogen atmosphere

It is observed from Figure 4.6 that there was a slight change in the weight of the sample over the heating temperature range of 20 °C – 900 °C. On average, a weight loss of approximately 5.4 wt% was recorded at the maximum temperature of 900 °C. The 5.4 wt% weight loss observed is slightly lower compared to 9.06 wt% recorded at a temperature of 750 °C [San Miguel *et al*, 2012]. This indicates the high thermal stable nature of the sample (carbon particles). In addition, the moisture content of the sample was evaluated from TGA residual weight as 0.4%. The obtained moisture content was very insignificant implying that nearly all the moisture in the

pine wood (feedstock) was driven off during the gasification that led to generation of the carbon particles. The low moisture content is very beneficial in terms of reduced energy utilization when reused as a feedstock in the gasification plant. Considering the temperature range (250 °C – 600 °C) within which volatiles are usually released, it could be deduced from Figure 4.6 that the volatile matter content of the carbon particles are low. This is comparable to commercial carbon black with volatile matter content of < 1-5 wt% [Miller *et al*, 2010]. The differential thermogravimetric curve in Figure 4.6 show four distinct peak, the first three peaks were observed at a temperature range of 40 °C – 200 °C and the third peak occurred within 600 °C – 700 °C. From the thermal degradation of the carbon particles shown in Figure 4.6, one can deduce that the fear of the carbon particles undergoing further degradation inside the heat recovery unit is less.

4.4 COMPUTER SIMULATION OF SYNGAS

Previous studies show that the final composition of syngas produced during gasification is influenced by a number of factors. Prior to actual gasification of pine wood for the present study, the percentage compositions of syngas produced during gasification were predicted using a downdraft gasifier model developed by Jayah *et al* [2003]. Jayah *et al* [2003] model incorporates Milligan flaming pyrolysis sub-model and gasification zone sub-model. This model is a very useful tool as it allows changes to be made easily without going through expensive experimental test. In the simulation, the feedstock considered was pine wood with a bulk density of 0.4g/cm^3 which is exactly the feedstock used in the biomass downdraft gasifier. The input parameters for the gasification simulation are presented in Table 4.4

Table 4.4: Parameters for the gasification simulation

Parameters	**Values**	**Parameters**	**Values**
Bulk density	0.4 g/cm^3	Throat angle	30 °C
Particle diameter	2.5 cm	Insulation Thickness	10 cm
Moisture content	10%	Thermal conductivity	2.8 W/cmK
Fixed carbon	32%	Air input temperature	300 K
Feed input	40 kg/hr	Air input	44.5 kg/hr
Throat diameter	10 cm	Heat loss	12.8%

The values presented in Table 4.4 are the optimum values for the various input parameters used for the gasification simulation. The elemental composition of the feedstock (pine wood) was also factored in, during the simulation. Figure 4.7 show the simulated percentage composition of syngas obtained.

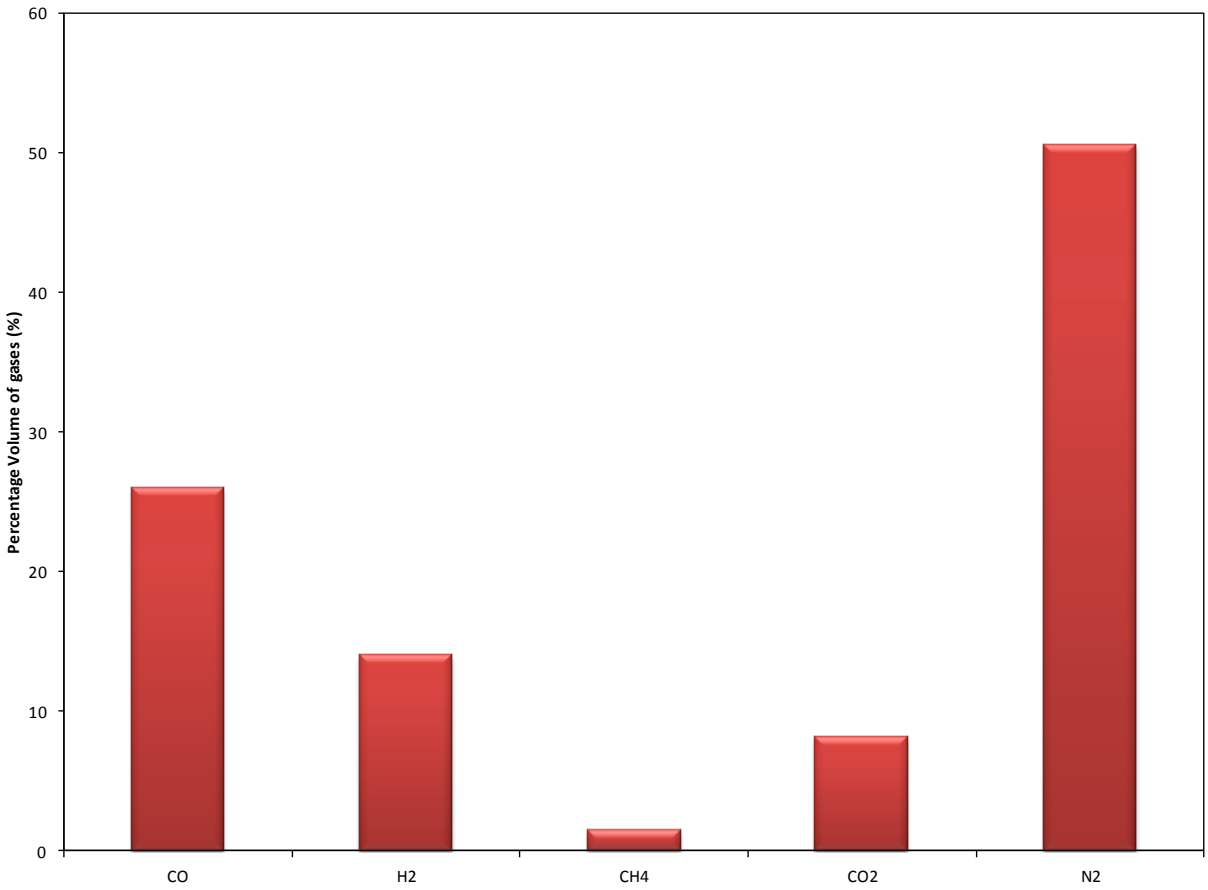

Figure 4.7: Simulated percentage volume of syngas components

The percentage volume of gases produced is a key parameter in determining the quality of a gasification product. As observed from Figure 4.7, the predicted percentage volume of the combustible component of syngas; carbon monoxide (CO), hydrogen (H_2) and methane (CH_4) are approximately 26.0%, 14.0% and 1.5% respectively. These combustible components are the main factors that influence the lower heating value (LHV) of syngas. Their individual heating values which are 12.75 MJ/Nm^2 for H_2, 12.63 MJ/Nm^2 for CO and 38.82 MJ/Nm^2 for CH_4 were used to calculate the LHV of the syngas. The calculated LHV of 5.18 MJ/Nm^3 obtained is very close to a LHV of 5.01 MJ/Nm^2 recorded for experimental gasification of Japanese cedar [Ma *et*

al, 2015]. In addition, it also compares very well with the maximum LHV of 5.4 MJ/Nm^3 recorded in Ran and Li [2012] experimental study. The calculated LHV of this study falls within the net LHV of 4-6 MJ/Nm^3 usually reported for air blown fixed bed gasifier [Mckendry, 2002, Laurence and Ashenafi, 2012]. A syngas with LHV of 5 MJ/Nm^3 and above indicates high flammability of such gas. Decrease in concentration of CO, H_2, CH_4 will result in reduction in the flammability of syngas and this decrease can be caused by increase in nitrogen (N_2) concentration. Hence during the actual gasification, the aim will be to keep the nitrogen concentration at a minimal level by controlling the air input (equivalence ratio). The predicted percentage volume of gases was compared with experimental data as well as simulated result obtained from literature as shown in Table 4.5.

Table 4.5: Comparison of syngas composition with literature

Type	**Percentage volume of gases (%Vol)**					**Ref**
	CO	H_2	CH_4	CO_2	N_2	
Sim	26.0	14.0	1.5	8.1	50.6	Present study
Sim	22.3	15.9	3.1	11.0	47.7	Di Blasi & Branca [2013]
Exp	23.2-26.6	14.3-16.7	1.3-1.8	8.6-11.3	46.2-49.4	Barrio *et al* [2001]
Sim	20.0	14.0	0.3	10.4	56.6	Barman *et al* [2012]
Exp	19.0	12.5	1.2	8.5	59.1	Jayah *et al* [2003]

As observed from Table 4.5, the composition of syngas obtained from a combination of Milligan flaming pyrolysis sub-model and gasification zone sub-model were compared with model results from Di Blasi and Branca, [2013] and Barman *et al*, [2012] and the experimental data they used for their model validation. The composition of H_2 (14.0%) from the present model is equal to the composition obtained from the model of Barman *et al*, [2012] but is 1.9% lesser than that

obtained by Di Blasi & Branca, [2013] model. Carbon monoxide (CO) composition is higher in the present model compared to the model results of Di Blasi & Branca, [2013] and Barman *et al*, [2012] but CO_2 composition is lesser as compared to their models. Hydrogen and carbon monoxide yield are enhanced by water-gas reaction, Boudouard reaction and steam reforming reaction.

The percentage volume of CO_2 (8.1%) and CH_4 (1.5%) in the present model agreed well with Jayah *et al*, [2003] experimentally obtained CO_2 (8.5%) and CH_4 (1.2%) composition. Increase in the rate of Boudouard reaction which is endothermic in nature causes a decrease in CO_2 yield. This is as a result of CO_2 reacting with carbon to yield CO [Emami Taba *et al*, 2012]. Nitrogen composition (50.6%) in the present model is higher than that obtained by Barrio *et al* [2001] and Di Blasi & Branca [2013] but lesser than the composition recorded by Barman *et al* [2012] and Jayah *et al* [2003]. Note that the higher the composition of N_2 the lesser the combustible gases and this translates to syngas dilution and also increases the downstream cleaning requirement.

4.5 COMPUTATIONAL FLUID DYNAMICS ANALYSIS OF WHRU

Computation fluid dynamics (CFD) uses sets of algebraic equations in place of partial differential equations (PDE) that govern gas and liquid (fluid) flows. Computational fluid dynamics simulation tool was employed to predict the effect; variation in mass flow rate of water will have on outlet temperature of syngas (heat source) and water (heat sink). A waste heat recovery unit (WHRU) was modeled around a cyclone dust collector attached to a gasifier

system so as to harness the heat lost through the surface of the cyclone. The model was developed with inventor and imported into CFD so as to simulate its performance at varying conditions. The basic input parameters and boundary conditions used in the simulation are shown in Table 4.6.

Table 4.6: Input parameters and boundary conditions for the CFD simulation

Parameters	**Syngas**	**Water**
Density (kg/m^3)	0.97	1000
Viscosity (kg/ms)	1.04×10^{-5}	8.9×10^{-4}
Specific heat Capacity (C_p) (kJ/kg °C)	3.99	4.187
Volume flow rate (kg/s)	0.037	Variable
Inlet temperature (°C)	350	20

The density of syngas was obtained from the density of each of the components of syngas and the volume share of each component. The assigned inlet temperatures are the typical obtainable values for syngas and water. Figure 4.8 shows the simulation result of the performance of the waste heat recovery unit as generated from Autodesk simulation CFD.

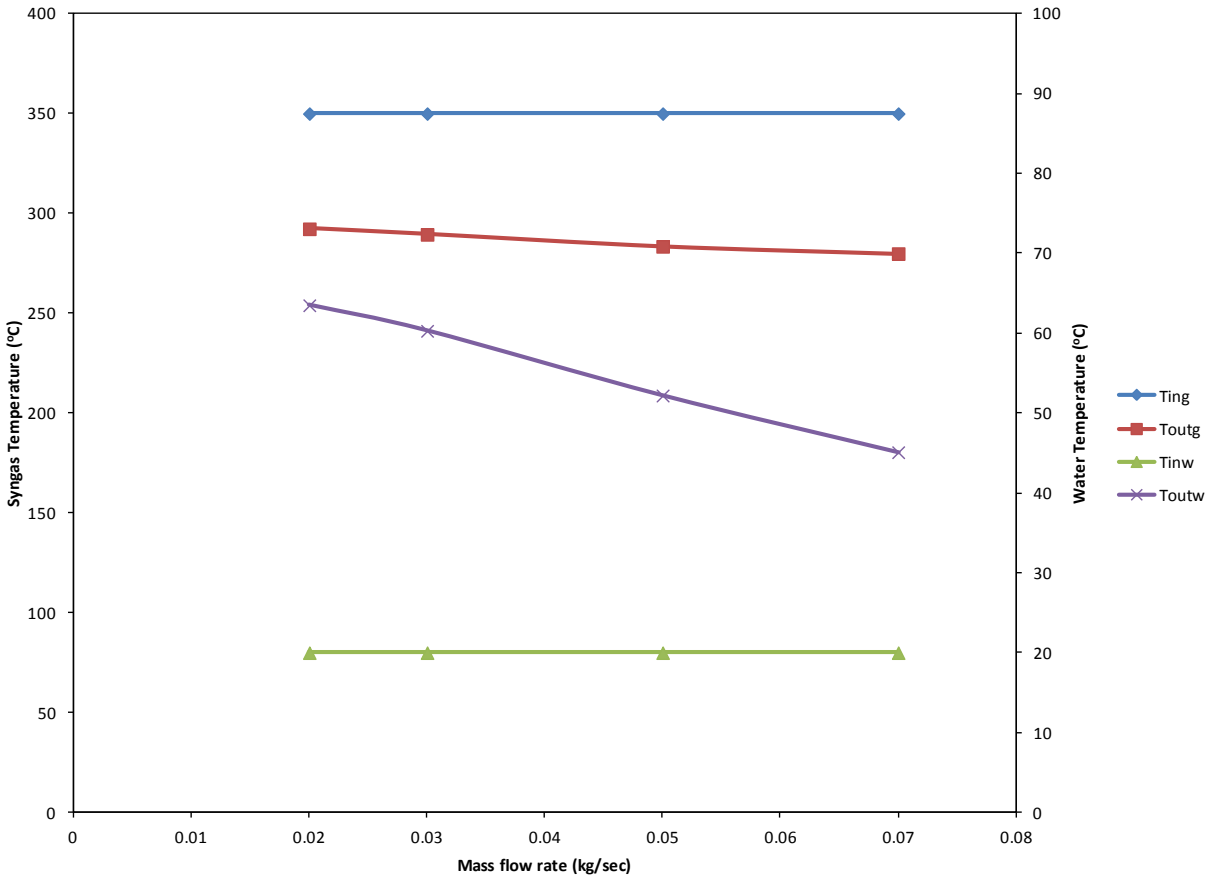

Figure 4.8: Simulation of the performance of a water waste heat recovery unit

The inlet temperature for the syngas (Ting) and water (Tinw) was assumed to be 350 °C and 20 °C respectively. The 350 °C is typical of the inlet temperature of the syngas into the cyclone inlet duct from the gasifier. Mass flow rate of water was varied from 0.02 kg/sec - 0.07 kg/sec which is equivalent to 1litre/min – 4litre/min while, the mass flow rate of syngas was kept constant. As observed from Figure 4.8 the outlet temperature of water (Toutw) reached a maximum value of 63.5 °C at the least mass flow rate of 0.02 kg/sec. Similarly, in an experimental study that evaluated the drying of biomass using waste heat from flue gas, the maximum temperature of flue gas exiting the process industry plant was recorded at the least

volumetric flow rate [Li *et al*, 2012]. Furthermore a continuous decrease in outlet temperature of water was observed in Figure 4.8 with an increase in mass flow rate of water. Li *et al* [2012] recorded a similar trend for flue gas exit temperature as against volumetric flow rate. In a numerical study of heat transfer in an unfinned double pipe heat exchanger, a continuous drop in cold water outlet temperature was recorded as mass flow rate varied from 0.02 kg/sec – 0.1 kg/sec [Kumar *et al*, 2014]. The drop in outlet temperature of water is attributed to displacement of hot water by cold water as the volume of water is increased. A similar trend was observed for the outlet temperature of syngas (Toutg) as there was a continuous decrease in outlet temperature of syngas with increase in mass flow of water at constant mass flow rate of syngas. An overall decrease of 67 °C approximately was recorded. In this case the drop in temperature of the syngas is due to heat transfer from the syngas to the water. Table 4.7 shows the determination of the energy utilized from the syngas in heating the water.

Table 4.7: Determination of emitted and absorbed heat energy

M_{frg} (kg/sec)	M_{frw} (kg/sec)	ΔT_g (°C)	ΔT_w (°C)	Q_g (kJ/sec)	Q_w (kJ/sec)
0.037	0.02	57.70	43.50	8.57	3.64
0.037	0.03	60.50	40.30	8.98	5.06
0.037	0.05	66.50	32.20	9.88	6.74
0.037	0.07	70.10	25.10	10.41	7.35

The heat energy available in the syngas and the quantity of heat energy gained by the water was determined from their mass flow rates, specific heat capacities and temperature difference between the inlets and the outlets. As observed from Table 4.7, the heat energy emitted (Q_g) from syngas experienced a continuous increase from 8.57 kJ/sec – 10.41 kJ/sec with increase in mass flow rate of water (M_{frw}). This is attributed to the continuous increase in temperature difference (ΔT_g) between the inlet temperature and outlet temperature of syngas. As expected the maximum syngas temperature difference of 70 °C resulted in maximum emitted heat energy of approximately 10.41 kJ/sec. Furthermore there was a continuous drop in the temperature difference between the inlet and outlet water temperature but the quantity of heat energy gained by water showed a continuous increase. Heat energy gained by water increased from 3.64 kJ/sec – 7.35 kJ/sec, with maximum heat gain corresponding with the highest flow rate of 0.07 kg/sec. It then implies that an increase in water flow results in a decrease in temperature which now requires more energy for the water to get heated. Calculating the efficiency based on the heat energy emitted from the syngas and heat energy absorbed by water in the WHRU, we obtained a minimum and maximum conversion efficiency of approximately 43% and 71% respectively. The CFD simulated results were then compared in terms of heat energy absorbed by water and outlet temperature of water. Figures 4.9 and 4.10 presents the comparisons.

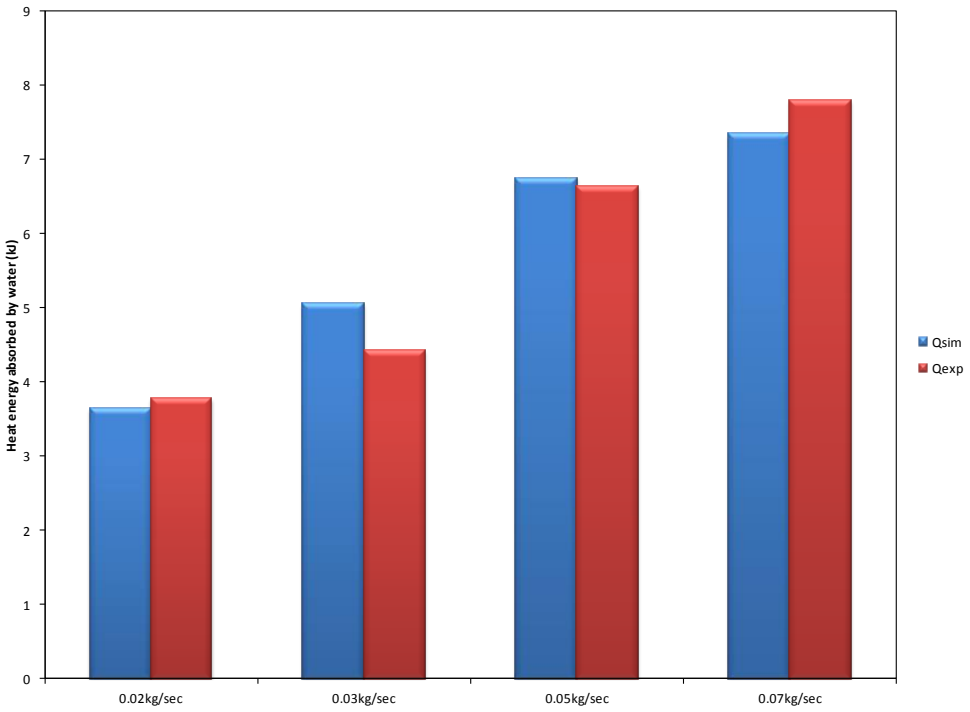

Figure 4.9: Comparison of experimental and CFD result for heat quantity

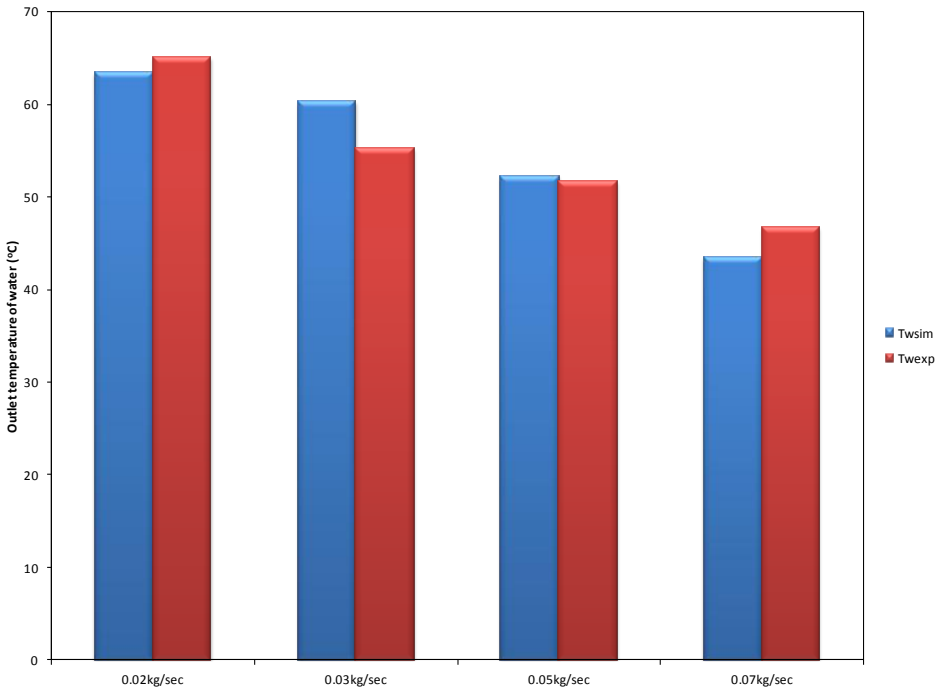

Figure 4.10: Comparison of experimental and CFD result for water outlet temperature

The simulated result for the quantity of heat energy absorbed by the water and outlet temperature of the water were compared with experimental data as shown in Figures 4.9 and 4.10. In overall as observed from figure 4.9 and 4.10, there was a good agreement between the simulated result and experimental result. The relative error varied from 1.66% - 14. 47% and 0.97% - 9.24% for heat energy absorbed by water and outlet water temperature respectively. Mass flow rate of 0.05 kg/sec showed the least error in both cases and 0.03 kg/sec showed the highest error in both cases. The heat energy absorbed by the water in the WHRU at 0.05kg/sec mass flow is 6.74 kJ for simulation and 6.63 kJ for experiment. For 0.03kg/sec mass flow the heat energy absorbed are 5.06 kJ and 4.42 kJ for simulation and experiment respectively. The CFD simulation has successfully shown that variation in mass flow rate does affect the outlet temperature of water and consequently the heat absorbed by the water. More also the close agreement between the simulation result and experiment proves the authenticity of the model used.

4.6 PERFORMANCE OF WASTE HEAT RECOVERY UNIT

Johansson biomass gasification system is a standalone power generation system as it utilizes the syngas produced from the downdraft gasifier in an internal combustion gas engine for power generation. The syngas exiting the gasifier and entering the cyclone dissipates heat on the body of the cyclone due to the high temperature at which it exits. In addition this same syngas undergoes some cooling process at the gas scrubber before reaching the gas engine. As the gas engine drives the synchronous generator for power generation, some of the un-combusted gases exit through the exhaust pipe at high temperatures. All these add-up as waste heat within the

gasification system, hence there is a significant opportunity for waste heat recovery in Johansson biomass gasification system.

As a result a waste heat recovery unit (WHRU) was designed, constructed and integrated around the cyclone dust collector of the gasification system. The WHRU was constructed using H R sheet commercial quality of dimensions 3 x 2,500 x 1,225 mm and angle equal commercial quality of dimension 30 x 30 x 2.5 mm. The experimental performance of the WHRU was conducted at different conditions and presented in this chapter. More also the temperature profile of the engine exhaust pipe is presented.

4.6.1 Syngas and water temperature profile

The waste heat recovery unit was filled with 267L of water which is heated indirectly by the heat from the surface of the cyclone as the syngas passes through the cyclone for purification purposes. The temperature profiles for syngas and water were recorded using type K thermocouples as the downdraft gasifier was in operation. The gasifier was operated over a time period of 230 minutes. There was no withdrawal of water from the WHRU as the test was on as well as no water flow. The obtained temperature profiles are presented in Figure 4.11

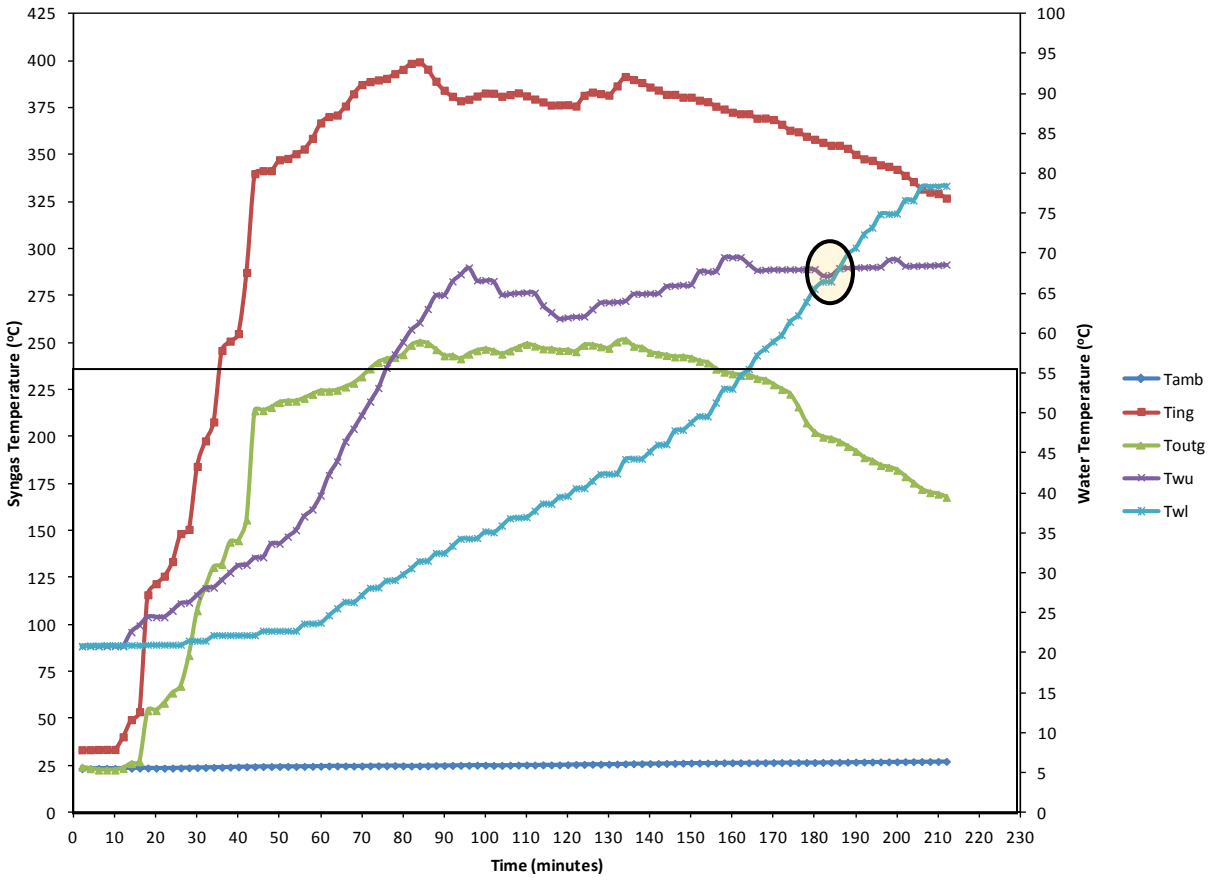

Figure 4.11: Waste heat recovery unit performance without insulation

From Figure 4.11 Ting represents the syngas inlet temperature to the cyclone, Toutg represent the syngas outlet temperature from the cyclone, Tamb is the ambient temperature of the surrounding in which measurements were taken, Twu represent the water temperature at the top section (cylindrical part of the cyclone) of the waste heat recovery unit (WHRU) and Twl is the water temperature at the middle section (conical part of the cyclone) of the WHRU. Figure 4.11 demonstrated that there was no significant change in ambient temperature. The first 12 minutes of the gasifier operation represents the initialization of the gasification process which is why the inlet and outlet temperature of syngas were both constant within this time period. Downdraft gasifier start-up time is usually reported to be between 20-30 minutes. This is the time needed to

ignite and bring the gasifier to a working temperature. It is shorter than that of updraft gasifier but longer than that of crossdraft which is usually between 5-10 minutes [Basu, 2010]. Syngas inlet temperature then picked up at the end of the 12 minutes initialization but syngas outlet temperature followed after 6 minutes.

A maximum syngas inlet temperature of 399.4 °C was recorded and this corresponded to an outlet syngas temperature of 250.3 °C. This is comparable to the syngas temperature prediction that was reported to range from 25 °C to a maximum of 425 °C [Mikulandric *et al*, 2014]. Furthermore the water temperature at the top section of the WHRU was the first to experience an increase in temperature compared to the water temperature at the middle section. This is attributed to existence of temperature gradient along the length of the cyclone. The temperature recorded at the cylindrical section (upper section of WHRU) of the cyclone is higher than the temperature at conical section (middle section of WHRU). The water temperature at the upper and middle section of the WHRU reached a temperature of 55 °C within 76 minutes and 162 minutes respectively. This is within the thermostat set temperature range of 50 °C- 60 °C for most electric water heaters and solar water heaters in South Africa. In addition this is the ideal storage temperature so as to prevent the risk of scalding [Kakaza and Folly, 2015]. Table 4.8 further shows the time it took the water at the top and middle section of the WHRU to experience a temperature rise.

Table 4.8: Water temperature rise by section

Temperature Rise (°C)	**Time taken for the rise (minutes)**	
	Cylindrical section (Twu)	Conical section (Twl)
30	40	80
40	60	120
50	71	150
60	80	172

As observed from Table 4.8 it took longer time in all cases for the water temperature at the middle section (conical section of cyclone) to experience a 10 °C rise than the top section. This is because of the same reason highlighted earlier and in addition the cylindrical section of the cyclone is the first point of entrance for the syngas so more heat is dissipated at the top than the middle. Recalling also that heat transfer is aided by temperature difference meaning that the more the temperature difference the more the heat is transferred. Over time the two water temperatures then attained equilibrium at a temperature of 67 °C and at a time period of 184 minutes. The top water temperature then experienced some stability after the equilibrium point but the middle water temperature continued to increase and stabilized at 73 °C. An estimation of the total quantity of heat utilized in raising the temperature of the water in the WHRU from 22 °C to 60 °C was made using equation (4.4).

$$Q = mc_p\Delta T \tag{4.4}$$

Using the total mass (m) of water in the WHRU which is 267 kg and specific heat (c_p) of water 4.186 kJ/kg°C, we obtained a total heat quantity of 42471.16 kJ. This quantity of heat is equivalent to 11.80 kWh of electricity hence it implies that 11.80 kWh of electricity is required to generate 42471.16 kJ of heat. In comparison to another study in which the waste heat from an air conditioning system was used in raising the temperature of a 350 kg of water from 20 °C to 55 °C, about 14 kWh of electricity was needed to generate the 51728 kJ of heat used in heating the water [Stalin *et al*, 2012].

Having established that the water temperature at the top section increases at a faster rate than the middle section, the WHRU was then insulated with a glass wool so as to compare the rate at which the water in the WHRU is heated when insulated and when not insulated. Figure 4.12 presents a comparison between insulated and non-insulated WHRU in terms of temperature attained within 30 minutes interval.

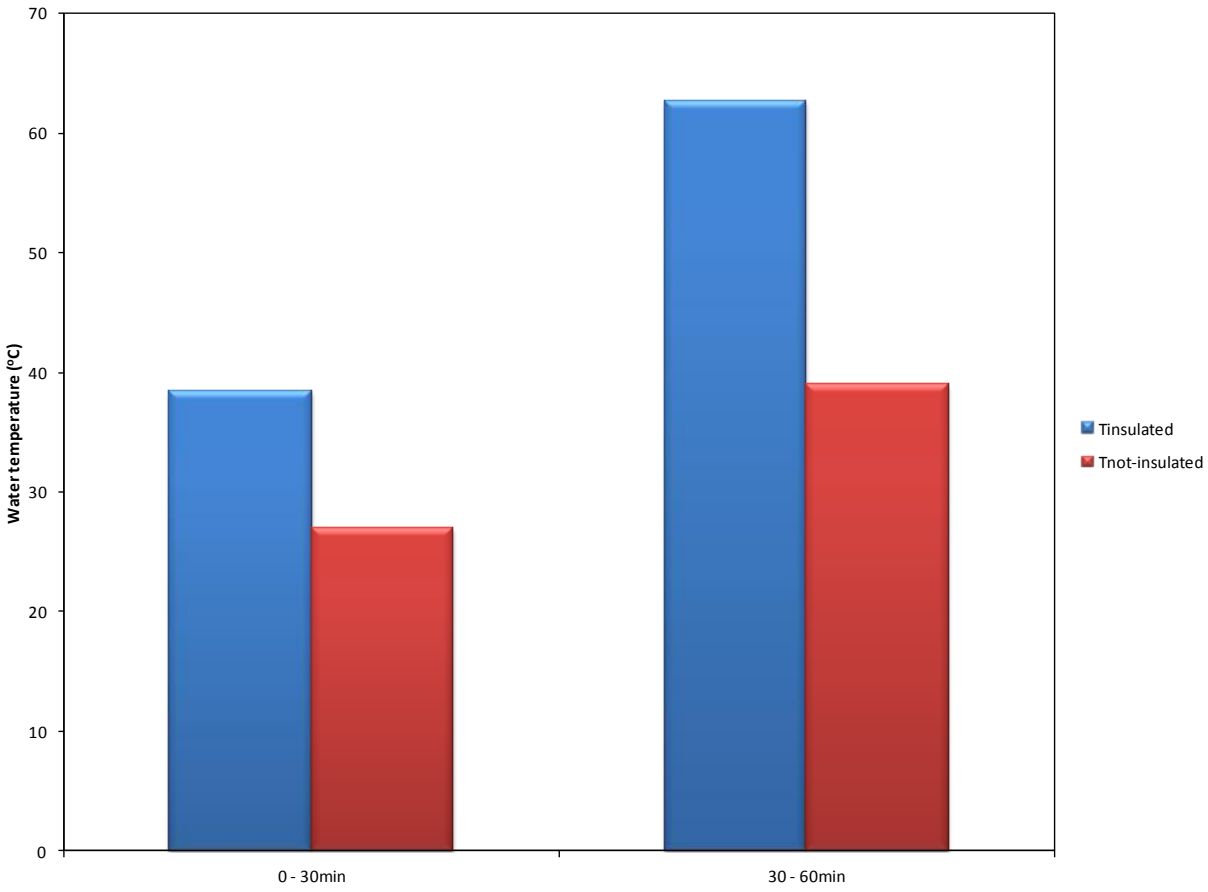

Figure 4.12: Comparison between insulated and non-insulated WHRU

In Figure 4.12 the temperature attainable by water in the WHRU when insulated and not insulated was compared for a 30min increase in time. The start-off temperature for the water in the WHRU when it is insulated and not-insulated which is 20.8 °C for both cases. It is observed from Figure 4.12 that after 30 minutes of heating the water in the WHRU, Tinsulated reached a temperature of approximately 38 °C while Tnot-insulated attained a temperature of 27 °C. More also at 60 minutes of heating Tinsulated and Tnot-insulated were at temperatures of 62 °C and 39 °C respectively. This then implies that it takes a shorter time for the water in the WHRU to experience an increase in temperature when it is insulated than when it is not. The insulation

material (glass wool) caused a reduction in heat loss as well as preservation of heat in the water. In general proper insulation provides good heat retention for water heaters and in turn results in improved efficiency [Varghese *et al*, 2015].

The standing losses Q_{loss} for the 267 l WHRU was then calculated according to equation (3.24) in chapter three and by using the thickness of the insulating material (glass wool) as 0.05 m, its thermal conductivity as 0.039 W/mK, heat transfer coefficient as 6.3 W/m^2K and ambient temperature of 25 °C as recorded in the experiment. The standing loss realized at a water temperature of 60 °C is 24.29 W/m^2. The Q_{loss} was then multiplied with the area of the WHRU in order to determine the dissipated energy. Hence the standing losses and corresponding dissipated energy are tabulated in Table 4.9

Table 4.9: Estimation of standing losses at different temperature

Water Temperature (°C)	**Standing loss (W/m^2)**	**Energy dissipated (kWh/day)**
65	27.76	2.11
60	24.29	1.84
55	20.82	1.58
50	17.35	1.32
45	13.88	1.05
40	10.41	0.79
35	6.94	0.53

It is evident from Table 5.2 that the lower the temperature of the water, the lower the standing losses as well as the energy dissipated. Hence heat losses can be minimized by heating the water

to a lower temperature. At 65 °C, the energy dissipated equals 2.11kWh. This compares very well with the experimentally measured result of 2.3kWh recorded at a geyser thermostat set temperature of 65 °C and ambient of 19 °C [Catherin *et al*, 2012]. In another study with a set point temperature of 65 °C and ambient temperature of 18.5 °C, the calculated standing loss obtained was 1.77 kWh [Harris *et al*, 2007] which is 0.34 kWh lesser than what was obtained in the present study. The typical average daily standing losses for a 200litre capacity of electric geyser and solar water heater are 3.02 kWh and 2.27 kWh respectively. This is in accordance to Kwikot geyser ratings.

The energy requirement for heating water in the WHRU was then compared with other water heating technology. A 40 °C rise in temperature was chosen for ease of comparison among the technologies. The comparison is presented in Table 4.10.

Table 4.10: Energy requirement comparison by technology

Technology type	**Energy required to heat water (kWh)**	**Capacity (litre)**
Gasification WHRU (present system)	11.80	267
Electric geyser	12.38	267
Solar water heater	6.19	250

As depicted in Table 4.10, the energy requirement for the electric heater exceeded that of the WHRU and solar water heater by 0.58 kWh and 6.19 kWh respectively. The solar water heater energy requirement is 50% lesser than that of the electric geyser. However the water capacity in the solar water heater is lesser compared to WHRU and electric geyser. The solar water heater

used 28% of energy from electricity and 72% from the sun. Using the cost of electricity at R1.30 per kWh, the cost of 11.80 kWh will be R15.34. This is how much that can be saved daily by the use of waste heat that is ordinarily disregarded. The cost of building the WHRU and insulation is presented as shown in table 4.11.

Table 4.11: Cost of waste heat recovery unit integration

Item	**Cost (R)**
Materials for WHRU construction	1949.40
Workmanship	2000.00
Insulation material	901.25
Total	4850.65

4.6.2 Variation in water flow rate

The flow rate of water was then varied from 1litre/min – 4litre/min (1 kg/min – 4 kg/min) which is the maximum that could be attained. At constant specific heat of syngas and water, the quantity of heat emitted ($Q_{emitted}$) by the syngas and quantity of heat absorbed ($Q_{absorbed}$) by the water was determined at the varying mass flow rates according to equations (3.22) and (3.23) in chapter three and presented in Table 4.12.

Table 4.12: Energy estimation for syngas and water

Mfrg (kg/sec)	**Mfrw (kg/sec)**	**ΔT_{syngas} (°C)**	**ΔT_{water} (°C)**	**$Q_{emitted}$ (kJ/sec)**	**$Q_{absorbed}$ (kJ/sec)**
0.037	0.02	80.6	45.10	11.97	3.78
0.037	0.03	89.6	35.20	13.31	4.42
0.037	0.05	94.10	31.70	13.97	6.63
0.037	0.07	101.70	26.60	15.10	7.80

Mfrg and Mfrw is the mass flow rate of syngas and water

As the flow rate of water increased from 0.02 kg/sec - 0.07 kg/sec, the outlet water temperature decreased from approximately 65 °C - 47 °C. Hence increase in water flow rate caused a decrease in outlet water temperature which translated to the decrease recorded in the water temperature difference (ΔT_{water}) shown in Table 5.5. This is similar to the case recorded by Varghese *et al* [2015] where an increase in mass flow rate from 16 kg/hr to 18 kg/hr caused a drop in outlet temperature from 49.75 °C to 41.5 °C. The heat energy absorbed by the water showed a continuous increase as mass flow rate of water was increasing.

This is in agreement with Dong *et al* [2015] study in which a continuous increase in energy consumption was recorded as water flow rate increased from 4 kg/min – 6 kg/min. This is attributed to the direct proportionality relationship that exists between mass flow rate and quantity (Q) of heat. According to equation (3.22) and (3.23), the quantity of heat is both dependent on mass flow rate and temperature difference hence at constant mass flow rate, the quantity of heat will follow exactly the trend of temperature difference but at varying mass flow rate and temperature difference the quantity of heat will then follow the trend of mass flow rate. As expected maximum energy of 7.80 kJ/sec was absorbed at the highest mass flow rate of 0.05

kg/sec (3kg/min). Furthermore the emitted heat energy from the syngas showed a similar trend with the absorbed heat energy. This implies that the more the energy of the syngas is emitted the more readily available the energy is to be absorbed, hence increasing the flow of the water leads to more energy being absorbed by the water. From the heat energy emitted by the syngas it is indicative that much energy is still available for recovery as the waste heat recovery unit only absorbed a small portion. Evaluating the efficiency of conversion based on the heat emitted and heat absorbed, an efficiency range of 32% -52% were obtained with mass flow rate variation of 0.02 kg/sec – 0.07 kg/sec. This implies that above 50% of efficiency can be obtained in the waste heat recovery unit with a mass flow rate of 0.07 kg/sec and higher.

4.7 ENGINE EXHAUST HEAT RECOVERY OPPORTUNITY

The quantity of heat energy lost through exhaust gases depend greatly on engine load. A study stated that as much as 35% of thermal energy generated from combustion of fuel in a gas engine is lost to the environment through the exhaust gas. The temperature and mass flow rate of the exhaust gas aid in quantify the heat content of an exhaust gas [Jadhao and Thombare, 2013]. The exhaust temperature of the gas engine was measured while under operation using thermocouples so as to ascertain the available heat recovery potential as well as a suitable technology for its recovery. Figure 4.13 presents the gas engine exhaust temperature recorded over a period of 30 minutes.

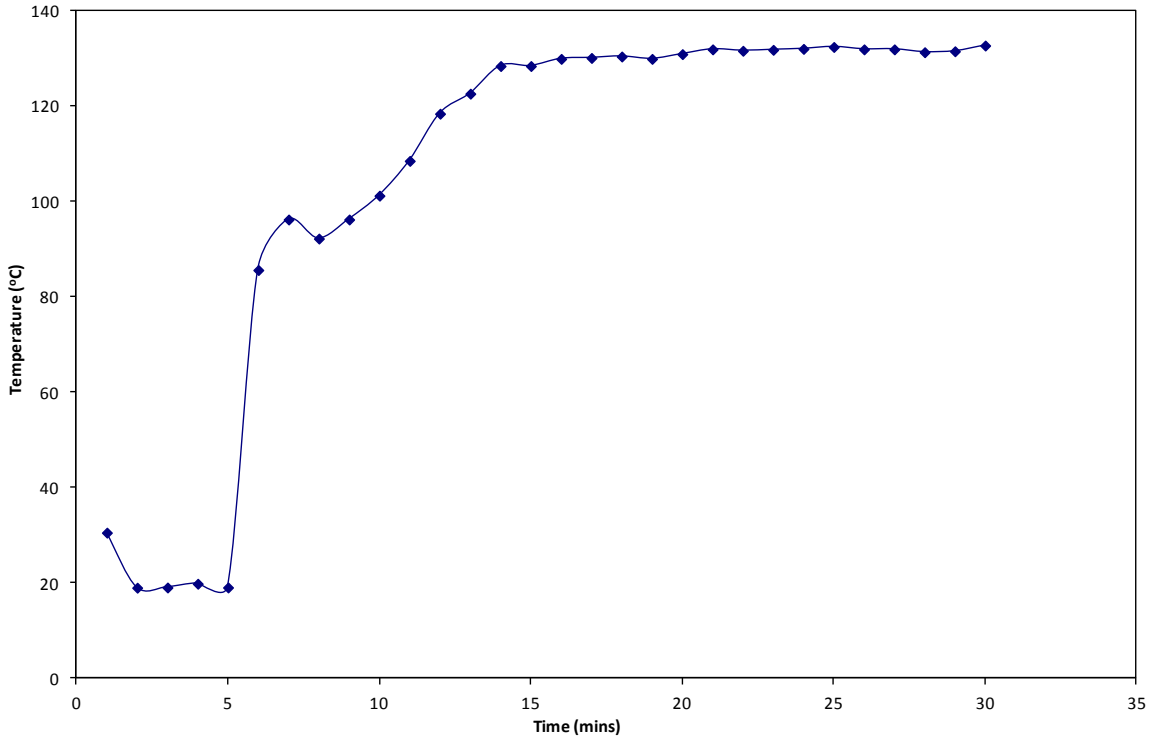

Figure 4.13: Gas engine exhaust temperature

In Figure 4.13, a significant increase in exhaust gas temperature was observed between 5mins and 8mins when the temperature rose from 20 °C to approximately 97 °C. A further 35 °C rise in temperature was record between 10 minutes – 15 minutes before attaining stability at about 130 °C. The obtained maximum temperature (130 °C) of gas engine is low compared to the temperature range (370 °C – 540 °C) reported for gas turbine exhaust [Bruckner *et al*, 2015]. The low temperature obtained is attributed to the fact that the gas engine was not operated at full load capacity of 120 kW. The engine was only powering a 40 kW bakery when the entire oven elements are switched on which is not always the case. The waste energy from the gas engine can serve as an important heat source in a number of ways such biomass drying before its utilization in a gasifier and generation of additional power with a thermoelectric generator.

Hence the recovery and utilization of this waste heat will not only conserve heat but will as well reduce the waste heat and carbon dioxide emissions dumped to the environment.

CHAPTER FIVE

SUMMARY, CONCLUSION AND RECOMMENDATIONS

5.1 SUMMARY OF FINDINGS

A number of heat recovery opportunities exist at the Johansson biomass downdraft gasifier system. This is attributed to the cleanup process that syngas have to go through before further utilization at the gas engine. Syngas cleanup is a necessity due to the presence of contaminants such as carbon particles that can cause operational challenges in the gas engine when syngas is used in its raw nature. However this syngas cleanup process impacts on the thermal efficiency of the gasifier system.

Therefore this present study first investigated the feasibility of recovering heat at the cyclone dust collector with an overall aim of designing and constructing a custom-built waste heat recovery unit that could harness the heat dissipated on the body of the cyclone by the syngas during cleanup.

From the initial investigation conducted before the integration of the waste heat recovery unit around the cyclone, the cyclone surface temperature was found to be in the range of 150 °C– 200 °C. A temperature difference was also found to exist between the cylindrical and conical part of the cyclone. This was evident from the temperature gradient obtained from the thermal image of the cyclone taken while in operation. More also it was found that the syngas still carried away some portion of the heat energy after dissipating some portion at the cyclone.

The carbon particle analysis conducted showed the presence of oxygen, iron, sulphur, alkali and alkaline earth metals potassium (K), sodium (Na), magnesium (Mg) in different concentration with oxygen (34.38%) topping the list. The thermal degradation of the carbon particles only showed a 5.4% weight loss.

From simulation of syngas composition the percentage volume of gases recorded for the individual components of syngas, carbon monoxide was found to be 26%, hydrogen 14%, methane 1.5%, carbon dioxide 8.1% and nitrogen 50.6%. In the computational fluid dynamic simulation of the waste heat recovery unit, the outlet temperature of the water reached a maximum value of 63.5 °C at a mass flow rate of 0.02 kg/sec. This rise in temperature resulted in a heat energy absorption of 3.64 kJ. Comparing the computational fluid dynamic simulation with experimental result, it was found that the relative error varied from 1.66% - 14. 47% and 0.97% - 9.24% for heat energy absorbed by water and outlet water temperature respectively.

The performance test conducted after the construction and integration of the waste heat recovery unit. The result obtained showed that the water temperature could be raised from 20 °C to a maximum of 78 °C without water flow and without withdrawal. The total quantity of heat energy used in raising the temperature of the water by 40 °C was found to be 42471.16 kJ which is equivalent to 11.80 kWh of energy. In addition the standing loss was estimated at 2.11 kwh which when added will give a total energy requirement of 13.9 kWh.

5.2 SUMMARY OF CONTRIBUTION

Gasification being a high temperature process, results in generation of hot syngas, hence providing an opportunity for heat recovery. A custom built waste heat recovery unit integrated into the biomass downdraft gasifier system is a major contribution of this study. The biomass gasification system was producing power only before the integration of the waste heat recovery unit; this intervention turned the gasification system into a combined heat and power system. The WHRU designed is the first of its kind and it performs very well in terms of heat recovery and water heating.

5.3 CONCLUSION

The cyclone surface temperature range of 150 °C – 220 °C recorded from the initial investigation showed the viability of heat recovery at the cyclone dust collector. The choice of an indirect heating mechanism adopted was based on the analysis of carbon particles present in the syngas. The high concentration of oxygen (O) and some other ions such as iron (Fe) and sulphate can lead to corrosion of heat recovery equipments when carbon particles are deposited on them over time. Corrosion and fouling are the two identified failure mechanism that could occur if direct contact heat recovery equipment is used for recovery heat from the syngas due to the presence of carbon particles in the syngas. Hence an indirect contact heat transfer mechanism was adopted for this study.

From the performance test conducted it is evident that the custom-built waste heat recovery unit can deliver hot water up to a temperature of 60 °C. The quantity of heat used in raising this water temperature was equivalent to 11.80 kWh of electricity. Using the cost of electricity at R1.30 per kWh, the cost of 11.80 kWh will be R15.34. This is how much that can be saved daily by the use of waste heat at the cyclone that is ordinarily disregarded. This study have successfully proved that the existing Johansson biomass gasifier system which current generates power using an internal combustion engine powered by syngas can also meet some heat applications need such as water heating as proven and biomass drying as suggested. This approach will effectively improve the overall efficiency of the biomass gasification system.

5.4 RECOMMENDATIONS

The developed heat recovery system can also add value in other biomass gasifiers. It is therefore recommended that other biomass gasifiers that have cyclone dust collector are also fitted with the designed heat recovery system. A maximum temperature of about 130 °C was recorded at the engine exhaust pipe which represents a significant opportunity for heat recovery. Hence this study recommends a further investigation into the recovery of heat at the exhaust pipe using a thermoelectric generator. The inlet temperature of syngas to the cyclone and outlet temperature of syngas from cyclone also showed that significant quantity of heat is still carried away by the syngas to the gas scrubber. Therefore this study recommends that heat recovery equipment should also be integrated between the cyclone and gas scrubber.

REFERENCE

Adams, T. N. (1980), 'A simple fuel bed model for predicting particulate emissions from a wood waste boiler', Combustion and Flame, vol. 39, pp. 225-239.

Addepalli, S., Eiroa, D., Lieotrakool, S., Francois, A.L., Guisset, J', Sanjaime, D., Kazarian, M., Duda, J., Roy, R., phillips, P. (2015) Degradation study of heat exchangers, Procedia CIRP, Vol 38, pp. 137-142.

Ahrenfeldt, J. (2007) *Characterization of Biomass Producer Gas as Fuel for Stationary Gas Engines in Combined Heat and Power Production*, Ph.D. Thesis, Technical University of Denmark.

Arafat, H.A. and Jijakli, K. (2013) Modeling and comparative assessment of municipal solid waste gasification for energy production, *Waste Management*, Vol 33, pp. 1704–1713.

Ashgriz, N., Mostaghimi, J. (2012) *An Introduction to Computational Fluid Dynamics*, Chapter 20 in Fluis Flow Handbook, University of Toronto, Ontario.

Babu BV, Sheth PN. Modeling and simulation of reduction zone of downdraft biomass gasifier: effect of char reactivity factor, *Energy Conversion Management*, Vol 47, pp. 2602–2611.

Bahng, M. K., Mukarakate, C., Robichaud, D.J., Nimlos, M.R. (2009) *Analytica Chimica Acta*, Vol 651, pp.117–138.

Balas, M., Lisy, M., Stelcl, O. (2012) The Effect of Temperature on the Gasification Process, Acta Polytechnica Vol. 52 No. 4.

Barman, N. S., Ghosh, S., De, S. (2012) Gasification of biomass in a fixed bed downdraft gasifier – A realistic model including tar, *Bioresource Technology*, Vol 107, pp. 505 - 511.

Barrio, M., Fossum, M., Hustad J.E. (2001) Operational characteristics of a small-scale stratified downdraft gasifier. In: Sixth International conference on technologies and combustion for a clean environment, Vol. 3, Porto, Portugal, pp. 1269–1276.

Basu, P. (2010) "Chapter 5 - gasification theory and modeling of gasifiers," in Biomass Gasification and Pyrolysis Anonymous Boston: Academic Press, pp. 117-165.

Basu, P. (2010) Biomass Gasification and Pyrolysis: Practical Design and Theory, Elsevier, The Boulevard, Langford lane Kidlington, Oxford, UK IsBN: 978-0-12-374988-8.

Bhattachary, S.C., Hla, S.S., Pham, H.L. (2001)A study on a multi-stage hybrid gasifier engine.

Bhavanam, A. and Sastry, R. C.(2011) Biomass Gasification Processes in Downdraft Fixed Bed Reactors: A Review, International Journal of Chemical Engineering and Applications, Vol. 2, No. 6.

Blocken, B. (2004) "Wind-driven rain on buildings"; Ph.D. thesis, Leuven: K.U. Leuven.

Bruckner, S., Liu, L., Miro, L., Radspieler, M., Cabeza, L.F., Lavemann, E. (2015) Industrial waste heat recovery technologies: An economic analysis of heat transformation technologies, *Applied Energy*, Vol 151, Pp. 157-167.

Catherine, Q., Wheeler, J., Wilkinson, R., de Jager, G. (2012) Hot water usage profiling to improve geyser efficiency,Journal of Energy in Southern Africa, Vol 23 No 1.

Centeno, F., Mahkamov, K., Silva Lora, E.E., Andrade, R. V. (2012) Theoretical and experimental investigations of a downdraft biomass gasifier-spark ignition engine power system, Renewable Energy, Vol 37, pp. 97-108.

Channiwala, S. A. (1992), quoted in Gaur, S. & Reed, T. B. (1998), Thermal Data for Natural and Synthetic Fuels, Marcel Dekker Inc, NY.

Chaurasia, A. (2016) Modeling, simulation and optimization of downdraft gasifier: Studies on chemical kinetics and operating conditions on the performance of the biomass gasification process, Energy, Vol 116, pp. 1065-1076.

Chawdhury, M.A. and Mahkamov, K. (2011) Development of a Small Downdraft Biomass Gasifier for Developing Countries, *Journal of Scientific Research*, Vol 3, pp. 51-64.

Chen, H., Zhang, X., Wu, B., Bao, D., Zhang, S., Li, J., Lin, W. (2016) Analysis of dual fluidized bed gasification integrated system with liquid fuel and electricity products, *International Journal of Hydrogen Energy*, Vol 41, pp. 11062-11071. combustion in grate furnaces and comparison with measurements. Energy & Fuels, Vol 19, (1), pp. 311-323.

Coronado, C. R., Yoshioka, J.T., Silveira, J.L. (2011) Electricity, hot water and cold water production from biomass. Energetic and economical analysis of the compact system of cogeneration run with woodgas from a small downdraft gasifier, *Renewable Energy*, Vol 36, pp.1861-1868.

Couto, N., Rouboa, A., Silva, V., Monteiro, E., Bouziane, K. (2013) Influence of the biomass gasification processes on the final composition of syngas, *Energy Procedia*, Vol 36, pp.596 – 606.

Couto, N., Rouboa, A., Silva, V., Monteiro, E., Bouziane, K. (2013) Influence of the biomass gasification processes on the final composition of syngas, Energy Procedia, Vol 36, pp. 596 – 606.

Damartzis, T., Zabaniotou, A. (2011) Thermochemical conversion of biomass to second generation biofuels through integrated process design—A review, *Renewable and Sustainable Energy Reviews*, Vol 15, pp. 366–378.

Damartzis, Th., Michailos, S., Zabaniotou, A. (2012) Energetic assessment of a combined heat and power integrated biomass gasification–internal combustion engine system by using Aspen Plus®, *Fuel Processing Technology*, Vol 95, pp. 37–44.

Delport, G.J. (2005). The Geyser Gadgets that work/donot work. Proceedings of the 13th Domestic Use of Energy Conference, Cape Town, March 2005, Cape Peninsula University of Technology: pp. 139 – 144.

Demadis, K. D. (2003), "Combating heat exchanger fouling and corrosion phenomena in process waters", Compact Heat Exchangers and Enhancement Technology for the Process Industries, pp. 483-490.

Demirbas, M.F., Balat, M., Balat, H. (2009) Potential contribution of biomass to the sustainable energy development, *Energy Conversion and Management*, Vol 50, pp. 1746–1760.

Desrosiers, R. (1979) Thermodynamics of gas–char reactions. In: Reed TB, editor. A survey of biomass gasification. Colorado: Solar Energy Research Institute.

Di Blasi, C. and Branca, C. (2013) Modeling a stratified downdraft wood gasifier with primary and secondary air entry, *Fuel*, Vol 104, pp. 847–860.

Dogru, M., Midilli, A., Akay, G., Howarth, C.R. (2004) Gasification of leather residue part 1 Experimental study via a pilot scale air blown downdraft gasifier, Energy Sources, Vol 26, pp. 35-44.

Dong, J., Zhang, Z., Yaho, Y., Jiang, Y., Lei, B. (2015) Experimental performance evaluation of a novel heat pump water heater assisted with shower drain water, Applied Energy, Vol 154, Pp. 842-850.

Duan, W., Yu, Q., Wang, K., Qin, Q., Hou, L., Yao, X., Wu, T. (2015) ASPEN Plus simulation of coal integrated gasification combined blast furnace slag waste heat recovery system, *Energy Conversion and Management*, Vol 100, pp. 30–36.

Emami Taba, L., Faisal Irfan, M., Wan Daud, W.A.M, Harun Chakrabarti, M.(2012) The effect of temperature on various parameters in coal, biomass and CO-gasification: A review, *Renewable and Sustainable Energy Reviews* Vol 16, pp.5584–5596.

EPA, Air and Pollution Technology Fact Sheet: Venturi scrubbers. Provides information about venturi scrubbers. http://www.epa.gov/ttn/catc/dir1/fventuri.pdfrs.

Fernandopulle, M. and Amadoru, I. (2012) Coconut Shell Biomass Gasification with waste heat recovery technology to dry pulverized kernel for virgin coconut oil extraction.

Francois, J., Abdelouahed, L., Mauviel, G., Patisson, F., Mirgaux, O., Rogaume, C., Rogaume, Y., Feidt, M., Dufour, A. (2013) Detailed process modeling of a wood gasification combined heat and power plant, *Biomass and Bioenergy*, Vol 51, pp. 68-82.

Giltrap, D.L., McKibbin, R., Barnes, G.R.G. (2003) A steady state model of gas-char reactions in a downdraft biomass gasifier, *Solar Energy*, vol. 74, pp. 85-91.

Guangul, F.M., Sulaiman, S.A., Ramli, A. (2013) Temperature profile and producer gas composition of high temperature air gasification of oil palm fronds, 4th International Conference on Energy and Environment 2013, Earth and Environmental Science 16, 012067.

Gumz. W. G. (1950), Gas Producers and Blast Furnaces, Theory and Method of Calculation, John Wiley and Sons, New York.

Harris, A., Kilfoil, M. & Uken, E-A. (2007). Domestic energy savings with geyser blankets, Proceedings of the 15th Domestic Use of Energy Conference, Cape Town, 2007, Cape Peninsula University of Technology: pp. 153-158.

Herguido, J., Corella, J., Gonzalez-Saiz, J. (1992) Steam gasification of lignocellulosic residues in a fluidized bed at a small pilot scale, Industrial & Engineering Chemistry Research, Vol 31, pp. 1274 -82.

Hernández, J.J., Aranda-Almansa, G., Bula, A. (2010) Gasification of biomass wastes in an entrained flow gasifier: Effect of the particle size and the residence time, *Fuel Processing Technology*, Vol 91, pp. 681–692.

Hesham, G. I. (2014) Experimental and CFD analysis of turbulent flow heat transfer in tubular exchanger, International Journal of Engineering and Applied Sciences, Vol 5, ISSN 2305-8269.
Hinds, W. C., (1999) Aerosol technology: properties, behavior, and measurement of airborne particles 2nd. ed.; Wiley: New York, 1999.

Hoffmann, A.C. and Stein, L.E. (2008) Gas cyclones and swirl tubes: principles, design, and operation. 2nd ed., Vol. 26, Berlin, New York: Springer, pp. 422.

Jadhao, J.S., Thombare, D.G. (2013) Review on Exhaust Gas Heat Recovery for I.C. Engine, *International Journal of Engineering and Innovative Technology* (IJEIT), ISSN: 2277-3754.

Janajreh, I. and Al Shrah, M. (2013) Numerical and experimental investigation of downdraft gasification of wood chips, *Energy Conversion and Management*, Vol. 65, pp. 783-792.

Jarungthammachote S., Dutta A., 2007, Thermodynamic equilibrium model and second law analysis of a downdraft waste gasifier, *Energy*, Vol 32, Pp. 1600–1669.

Javier, G., José, C., María, A., Miguel, C. (1999) Biomass gasification in atmospheric and bubbling fluidized bed: Effect of the type of gasifying agent on the product distribution, *Biomass and Bioenergy*, Vol 17, pp. 389-403.

Jayah, T.H. (2002) *Evaluation of a downdraft wood gasifier for tea manufacturing in Sri Lanka*, A thesis submitted in total fulfilment of the requirements of the degree of Masters by Research, The University of Melbourne.

Jayah, T.H., Aye, L., Fuller, R.J., Stewart, D.F., (2003) Computer simulation of a downdraft wood gasifier for tea drying, *Biomass Bioenergy*, Vol 25, 459–469.

Jeya Singh, V.C., Sekhar, S.J. (2016) Performance studies on a downdraft biomass gasifier with blends of coconut shell and rubber seed shell as feedstock, Applied Thermal Engineering, Vol 97, pp. 22-27.

Jöller, M.; Brunner, T.; Obernberger, I. (2005) Modeling of aerosol formation during biomass

Kakaza, M. and Folly, K.A. (2015) Effect of solar water heating system in reducing household energy consumption, IFAC-PapersOnline 48-30, pp. 468-472.

Kanti, P.K., Karithika, U.P., Ali, S., Kumar, S.N., Shyam, C.C. (2016) CFD analysis of shell and tube heat exchanger, International Journal of Engineering Research, Vol 5, pp. 1129-1254.

Kirkels, A.F., Verbong, G.P.J. (2011) Biomass gasification: Still promising? A 30-year global overview, *Renewable and Sustainable Energy Reviews*, Vol 15, pp. 471–481.

Kumar, S., Karanth, K.V., Murthy, K. (2015) Numerical study of heat transfer in a finned double pipe heat exchanger, World Journal of Modelling and Simulation, ISSN 1 746-7233, Vol 11, pp. 43-54.

Kumar, S., Karanth, K.V., Murthy, K. (2015) Numerical study of heat transfer in a finned double pipe heat exchanger, World Journal of Modelling and Simulation, ISSN 1 746-7233, Vol 11, pp. 43-54.

Kuo, P-C., Wu, W. (2015) Design of co-gasification from coal and biomass combined heat and power generation system, *Energy Procedia*, Vol 75, pp. 1120 – 1125.

Kuzmin, D. (2013) Introduction to Computational Fluid Dynamics [online]. Last accessed 10 October 2016 at http://www.mathematik.uni-dortmund.de/~kuzmin/cfdintro/lecture1.pdf.

Laohalidanond, K., Chaiyawong, P., Kerdsuwan, S. (2015) Status of Using Biomass Gasification for Heat and Power in Thailand, Energy Procedia, Vol 79. pp. 385-390.

Laurence, L.C and Ashenafi, D. (2012) Syngas Treatment Unit for Small Scale Gasification-Application to IC Engine Gas Quality Requirement, *Journal of Applied Fluid Mechanics*, Vol. 5, pp. 95-103.

Li, H., Chen, Q., Zhang, X., Finney, K.N., Sharifi, V.N., Swithenbank, J. (2012) Evaluation of a biomass drying process using waste heat from process industries: A case study, *Applied Thermal Engineering*, 35, pp. 71-80.

Lund, P., Byrne, J.A., Berndes, G., Vasalos, I. (2015) *Advances in Bioenergy: The Sustainability Challenge*, John Wiley & Sons, ISBN-1118957865, 9781118957868.

Ma, H-K., Lin, C-P., Wu, H-P., Peng, C-H., Hsu, C-C. (2015) Waste heat recovery using a thermoelectric power generation system in a biomass gasifier, *Applied Thermal Engineering*, Vol 88, pp.274-279.

Ma, H-K., Lin, C-P., Wu, H-P., Peng, C-H., Hsu, C-C. (2015) Waste heat recovery using a thermoelectric power generation system in a biomass gasifier, *Applied Thermal Engineering*, Vol 88, pp.274-279.

Mamphweli, N. S. and Meyer, E. L. (2012) Components and operation of the fixed bed downdraft system Johansson Biomass Gasifier, Nova Science Publisher, ISBN: 978-1-61209-681-0.

Mamphweli, N. S. and Meyer, E. L. (2013) Performance monitoring system for a biomass gasifier, *Journal of Engineering, Design and Technology*, 11, (1), pp. 7-18.

Maniatisa, K., and Beenackers A.A.C.M. (2000) Tar Protocols. IEA Bioenergy Gasification Task, *Biomass and Bioenergy*, Vol 18, pp. 1-4.

Manickam, M., Schwarz, M.P., Perry, J. (1998) CFD modelling of waste heat recovery boiler, Applied Mathematical Modelling, Vol 2, pp. 823 - 840.

Martínez, J.D., Mahkamov, K., Andrade, R.V., Silva Lora, E.E. (2012) Syngas production in downdraft biomass gasifiers and its application using internal combustion engines, *Renewable Energy*, Vol 38, pp. 1-9.

Mathieu, P., Dubuisson, R. (2002) Performance analysis of a biomass gasifier, *Energy Conversion Management*, Vol 43, 1291–1299.

McKendry, P. (2002) Energy production from biomass (part 3): gasification technologies *Bioresource Technology*, Vol 83, pp. 55–63.

Melapi, A., Mamphweli, S., Katwire, D. M., Meyer, E.L. (2015) The Physical and Chemical Properties of Fine Carbon Particles-Pinewood Resin Blends and Their Possible Utilization, *Journal of Chemistry*, Article ID 137580 http://dx.doi.org/10.1155/2015/137580.

Melgar, A., Pe´rez, J.F., Laget, H., Horillo, A. (2007) Thermochemical equilibrium modeling of a gasifying process, *Energy Conversation Management*, Vol 48, pp. 59–67.

Melvinraj, C.R., Varghese, V.C., Wilson, V., Thazhatha, T.J., Mithun, K., Kakkassery, S.J. (2014) Comparative Study of Heat Exchangers Using CFD, International Journal of Engineering Research and Applications, www.ijera.com, ISSN:22489622, vOL 4, pp. 118-120.

Miller FP, Vandome AF, McBrewster J. Carbon black. VDM Publishing House Ltd; 2010. ISBN 6130702493.

Mondal, P., Dang, G.S., Garg, M.O (2011) Syngas production through gasification and cleanup for downstream applications — Recent developments, *Fuel Processing Technology*, Vol 92, 1395–1410.

Morgalla, M., Lin, L., Seemann, M., Strand, M. (2015) Characterization of particulate matter formed during wood pellet gasification in an indirect bubbling fluidized bed gasifier using aerosol measurement techniques, *Fuel Processing Technology*, Vol 138, pp. 578–587.

Narváez I., Grio A., Aznar M.P., Corella J. (1996) Biomass gasification with air in an atmospheric bubbling fluidized bed, Effect of six operational variables on the quality of the produced raw gas. *Industrial & Engineering Chemistry Research*, Vol 35 (7), pp. 2110-20.

Nazaroff, W.W. and Alvarez-Cohen, L. (2000) Gaseous Emission-Control Technologies Air-Quality Technology, http://engineering.dartmouth.edu /~d30345d/courses/engs37/Cyclones.pdf.

Pan, C., Liang, Q., Guo, X., Dai, Z., Liu, H. and Gong, X. (2015) Characteristics of Different Sized Slag Particles from Entrained-Flow Coal Gasification, Energy Fuels, Vol 30, pp. 1487−1495.

Pandey, S., Baral, B., Karki, S., Upreti, A. (2013) Prediction of Syngas Composition from Biomass Gasification using Thermodynamics Equilibrium Model, Rentech Symposium Compendium, Vol 3.

Park, S.-H and Lee, B.-K (2009) Development and application of a novel swirl cyclone scrubber(2) Theoretical, *Journal of Hazardous Materials*, Vol 164, pp. 315–321.

Patra, T.K., Nimisha, K.R., Sheth, P.N. (2016) A comprehensive dynamic model for downdraft gasifier using heat and mass transport coupled with reaction kinetics, *Energy*, Vol 116, pp. 1230 -1242.

Pavlas, M., Stehlík, P., Oral, J., Klemeš, J., Kim, J-K., Firth, B. (2010) Heat integrated heat pumping for biomass gasification processing, *Applied Thermal Engineering*, Vol 30, pp. 30–35.

Pepiot, P., Dibble, C.J. Foust, T.D. (2010) Computational fluid dynamics modeling of biomass gasification and pyrolysis, in Anonymous American Chemical Society, pp. 273-298.

Prins, M.J., Ptasinski, K.J., Janssen, F.J.J.G. (2003) Thermodynamics of gas–char reactions: first and second law analysis. *Chemical Engineering Science*, Vol 58, pp. 1003–1011.

Puig-Arnavat, M., Bruno, J.C., Coronas, A. (2010) Review and analysis of biomass gasification models, *Renewable and Sustainable Energy Reviews*, 14, pp. 2841–2851.

San Miguel, G., Domı´nguez, M.P., Herna´ndez, M., Sanz-Pe´rez, F. (2012) Characterization and potential applications of solid particles produced at a biomass gasification plant, *Biomass and Bioenergy*, 47, pp. 134-144.

Santhanam, S., Schilt, C., Turker, B., Woudstra, T., Aravind, P.V. (2016) Thermodynamic modeling and evaluation of high efficiency heat pipe integrated biomass GasifiereSolid Oxide Fuel CellseGas Turbine systems, *Energy* 109 (2016), pp. 751-764.

Sevvel, P., Nirmalkannan, V., Thennarasu, P. (2015) Experimental Method on Cyclone Heat Exchanger, *International Journal of Innovative Research in Science, Engineering and Technology*, Vol 4, ISSN:2347-6710.

Shafie, S.M, Mahlia, T.M.I., Masjuki, H.H., Ahmad-Yazid, A. (2012) A review on electricity generation based on biomass residue in Malaysia. *Renewable and Sustainable Energy Reviews*, Vol 16, pp. 5879–89.

Sharma, A.K. (2008) Equilibrium and kinetic modelling of char reduction reactions in a downdraft biomass gasifier: a comparison, *Solar Energy*, Vol 52, pp. 918–28.

Sharma, A.K. (2011) Modeling and simulation of a downdraft biomass gasifier 1, Model development and validation, *Energy Conversion and Management*, vol. 52, pp. 1386-1396.

Skorek-Osikowska, A., Bartela, L., Kotowicz, J., Sobolewski, A., Iluk, T., Remiorz, L. (2014) The influence of the size of the CHP (combined heat and power) system integrated with a biomass fueled gas generator and piston engine on the thermodynamic and economic effectiveness of electricity and heat generation, *Energy*, Vol 67, pp. 328-340.

Smith, K., Thornton, M. (2009) Feasibility of thermoelectrics for waste heat recovery in conventinal vehicles, National Renewable Energy Laboratory, Technical report NREL/TP-54044247.

Stalin, J. M., Krishnan, S. M., Kumar, G.V. (2012) Efficient usage of waste heat from air conditioner, *International Journal of Advances in Engineering & Technology*, ISSN: 2231-1963.

System, *Biomass and Bioenergy*, Vol 21, pp.445-460.

Tremel, A., Becherer, D., Fendt, S., Gaderer,M., Spliethoff, H. (2013) Performance of entrained flow and fluidised bed biomass gasifiers on different scales, Energy Conversion and Management, Vol 69, pp. 95–106.

Varghese, J., Samsher, Manjunath, K. (2017) A parametric study of a concentrating integral storage solar water heater for domestic uses, *Applied Thermal Engineering*, Vol 111, Pp. 734–744.

Várhegyi, G., Antal Jr., M. J., Jakab, E., Szabó, P. (1997) Kinetic modeling of biomass pyrolysis, *Journal of Analytical and Applied Pyrolysis*, Vol. 42, pp. 73-87.

Vera, D., de Mena, B., Jurado, F., Schories, G. (2013) Study of a downdraft gasifier and gas engine fueled with olive oil industry waste, Applied thermal engineering, Vol 51, pp. 119-129.

Villanueva, A.L., Gomez-Barea, A., Revuelta, E., Campoy, M., Ollero, P. (2008) Guidelines for selection of gasifiers modelling strategies. In: 16th European biomass conference and exhibition.

Wang, H., Yan, J., Dong, L. (2016) Simulation and economic evaluation of biomass gasification with sets for heating, cooling and power production, *Renewable Energy*, Vol 99, pp. 360-368.

Wang, L. (2004) *Theoritical study of cyclone design*, A thesis submitted in partial fulfillment of the requirements for the degree of Doctor of Philosophy, Graduate Studies of Texas A&M University.

Wang, L. (2004) *Theoritical study of cyclone design*, A thesis submitted in partial fulfillment of the requirements for the degree of Doctor of Philosophy, Graduate Studies of Texas A&M University.

Woolcock, P.J. and Brown, R.C. (2013) A review of cleaning technologies for biomass-derived syngas, *Biomass and Bioenergy*, Vol 52, pp.54 – 84.

Zainal ZA, Ali R, Lean CH, Seetharamu KN. Prediction of performance of a downdraft gasifier using equilibrium modeling for different biomass materials, *Energy Conversion Management*, Vol 42, pp. 1499–1515.

Zainal, Z.A., Rifau, A., Quadir, G.A., Seetharamu, K.N. (2002) Experimental investigation of a downdraft biomass gasi-er, *Biomass and Bioenergy*, Vol 23, pp. 283-289.

Zie ̨bik, A., Malik, T., Liszka, M. (2015) Thermodynamic evaluation of CHP (combined heat and power) plants integrated with installations of coal gasification, *Energy*, Vol 92, pp.179-188.

APPENDIX A

Research output associated with this research

A1. Research article published in Journal

i. Nwokolo, N., Mamphweli, S., Makaka, G. (2016) An investigation into heat recovery from the surface of a cyclone dust collector attached to a downdraft biomass gasifier, Applied Thermal Engineering, Vol 98, pp. 1158–1164.

A2. Research articles submitted for publication

i. Nwokolo, N., Mamphweli, S., Makaka, G. (2016) Performance evaluation of a custom built waste heat recovery unit in a gasification plant, Applied Energy.

ii. Nwokolo, N., Mamphweli, S., Makaka, G. George, T. (2016) Computational fluid dynamics simulation of a waste heat recovery unit and prediction of syngas composition. Energy conservation and Management.

iii. Nwokolo, N., Mamphweli, S., Makaka, G. (2016) Analytical and thermal evaluation of carbon particles recovered at the cyclone of a downdraft biomass gasification system, Sustainability Journal.

A3. Research articles presented at conferences

i. Nwokolo, N., Mamphweli, S., Makaka, G. Computation fluid dynamic simulation of the performance of a waste heat recovery unit in a gasification plant, 3rd DST/NRF National conference on Global Change 2016 at the University of Kwazulu Natal Durban..

ii. Nwokolo, N., Mamphweli, S., Makaka, G. Design, manufacture and performance monitoring of a waste heat recovery unit in a gasification plant, The 61st annual

conference of the South African Institute of Physics jointly hosted by the departments of Astronomy and Physics, University of Cape Town.